Probing Adhesion GPCR Mechanisms via High Throughput Screening for Novel GPR56 Modulatory Compounds

by
Alexander Vizurraga

A dissertation submitted in partial fulfillment
of the requirements for the degree of
Doctor of Philosophy
(Cellular and Molecular Biology)
in the University of Michigan
2023

Doctoral Committee:

Associate Professor Gregory Tall, Chair
Assistant Research Scientist Andrew Alt
Associate Professor Michael Holinstat
Professor Alan Smrcka

Alexander L. Vizurraga

alvizurr@umich.edu

ORCID iD: 0000-0001-7167-1686

Dedication

For my mother, who has always supported

my endeavors through thick and thin

Acknowledgements

This work is the culmination of over a decade of guidance and support from a seemingly endless cast of friends and mentors for whom I cannot thank enough. First, I'd like to thank my undergraduate research advisor Dr. Tarun Dam. Tarun, you took my early appreciation for chemistry and biology, and molded it into a fascination for biochemistry research. I am forever thankful for your guidance throughout my undergraduate career, and your hands-on mentoring at the bench. Next, of course, I cannot express enough gratitude for the mentorship and guidance from Dr. Greg Tall during my time at the Tall Lab. I am truly privileged to have been able to train as a scientist under you. I came into graduate school as a naïve kid who thought he was in over his head. You took me in, trained me, guided me, and challenged me to become a better scientist. Your mentorship bolstered my love for science and is something I will always cherish. For everything that you've done – be it the late-night texts helping me with protein purifications, or the editing of my manuscripts, or even just the casual conversations at my bench – thank you. I would also like to thank my dissertation committee members, Drs. Alan Smrcka, Michael Holinstat, and Andy Alt for their continual guidance and support throughout my research. Your input was instrumental for the research presented here.

A deserved thanks goes out to all the members of the Tall Lab, past and present, who helped me throughout my time in the lab, and served as comrades on our little "island" of tranquility amid the chaos of AGPCR research. To the post-docs Drs. Jennifer Yeung, Wenxi Yu, Luciana Rosselli-Murai, and Charu Gupta, thank you for making the lab such a friendly place. You all have taught

me so much – not just about research, but about life and career goals as well. To the research specialists Drs. Yukiko Maeda and Frank Kwarcinski, thank you for all the tireless work you have done with protein purifications, membrane preparations, and GPCR assays. To the current graduate students, Tingzhen Shen, Xinyi Lu, and Tyler Bernadyn, thank you for being such great friends in the lab. Although it's early in your careers, I see immense potential in your projects and foresee you all becoming exceptional scientists.

Next, I would be remiss to not mention the friends I made outside the lab. Thank you to all of those within my PIBS cohort who I befriended for the hilarious memories we've created. Ajay Larkin, Eric Bell, Amanda Photenhauer, Cyrina Ostgaard, Veerin Sirihorachai, and Brian Peterson, thank you all for making such a fun and exciting Dungeons and Dragons campaign to relieve the stress of grad school. I'd like to especially thank Ajay and Eric for being such close friends and always finding the time to hang out, even during the mayhem of the pandemic.

I'd also like to thank everyone in the Ann Arbor Smash Ultimate group. Four years ago, I decided on a whim to attend a Super Smash Bros tournament, not realizing you guys would quickly become some of my closest friends in grad school. To Kyle, Isley, Andres, Ryan, Jonathan, Ethan, and all others that manage and attend MISU tournaments, thank you for fostering such an awesome and friendly community that I am proud to be a part of (and for tolerating my awful character choices of Yoshi and Banjo).

And finally, thank you to my family, especially my mother, who has always been supportive of me through the good times and the bad times. No matter how complicated and convoluted my research became, you were always willing to listen and provide support. Thank you, and I promise I will visit more!

Table of Contents

List of Figures

List of Abbreviations

Abbreviation	Definition
3-α-DOG:	3-α-acetoxy-dihydrodeoxygedunin
1,4-DHP:	1,4-Dihydropyridine
7TM:	Seven-Transmembrane Domain
ADGR:	Adhesion G Protein-Coupled Receptor
AGPCR:	Adhesion G Protein-Coupled Receptor
B2AR:	β2 Adrenergic Receptor
BAI:	Brain Angiogenesis Inhibitor
BFPP:	Bilateral Frontoparietal Polymicrogyria
cAMP:	Cyclic AMP
CCh:	Carbachol
CRE:	cAMP Response Element
CTF:	C-terminal Fragment
DHM:	Dihydromunduletone
ECD:	Extracellular Domain
ECL:	Extracellular Loop
ECM:	Extracellular Matrix
ER:	Endoplasmic Reticulum
FLRT:	Fibronectin Leucine-Rich Repeat Transmembrane Proteins

GAIN:	GPCR Autoproteolysis Inducing
GDP:	Guanosine Diphosphate
GPCR:	G Protein-Coupled Receptor
GPS:	GPCR Proteolysis Site
GTP:	Guanosine Triphosphate
HHQ:	Hexahydroquinoline
HTS:	High Throughput Screen(ing)
ICL:	Intracellular Loop
ISO:	Isoproterenol
LPHN:	Latrophilin
M1R:	Muscarinic Acetylcholine Receptor 1
NTF:	N-terminal Fragment
PAR:	Protease-Activator Receptor
SAR	Structure Activity Relationship
SRE:	Serum Response Element
TG2:	Tissue Transglutaminase-2
TM:	Transmembrane Domain

Abstract

Adhesion G Protein-Coupled receptors (AGPCRs) are a poorly understood subset of class B GPCRs that comprises 33 members across nine subfamilies. These GPCRs are unique in their possession of large extracellular regions that include a highly conserved GPCR autoproteolysis inducing (GAIN) domain that cleaves the receptor into two fragments that remain noncovalently attached in the inactive, holoreceptor form. These fragments, deemed the extracellular N-terminal fragment (NTF) and the membrane-embedded C-terminal fragment (CTF), can dissociate from one another to expose a small stalk region on the CTF termed the tethered-peptide-agonist (tethered agonist, or TA). Exposure of the TA allows it to bind to the orthosteric site of the receptor to maximally activate G protein signaling. AGPCRs play critical roles in several cellular processes, including but not limited to the regulation of cell migration, shape, polarity, differentiation, and immune response. AGPCRs are also notable oncogenes and biomarkers for a wide array of different cancers. However, despite holding enormous therapeutic potential, most AGPCRs are classified as orphans with few molecular tools to study their activation *in vivo*. This has confounded the study of their activation in endogenous tissue systems, and significantly impeded the development of AGPCR-targeted therapeutics. This issue is further exacerbated by a clear lack of AGPCR structures that showcase the receptor in its active, TA-bound form.

Here, we highlight the first cryo-EM structures of the activated forms of two model AGPCRs, GPR56 and LPHN3. High-resolution maps allowed for us to detail the exact mechanism of orthosteric TA activation: Following exposure to the extracellular environment, the tethered agonist bends 180° to adopt a partial helix conformation deep within the orthosteric site.

Mutational analysis revealed that the TA forms critical interactions with conserved residues on TMs 1, 2, 6, 7, and extracellular loop 2. TA binding also introduces breaks in TMs 6 and 7 that open the intracellular side of the receptor to enhance G protein signaling. Following this, active and inactive forms of GPR56 were used in a modified cell-based luciferase gene reporter assay to screen novel agonists and antagonists from a collection of over 200,000 compounds. Our agonist screen revealed that hexahydroquinoline (HHQ) derivatives are potent, selective full agonists for GPR56 that are predicted via *in silico* docking to bind to the orthosteric site in a manner similar to the TA. Structure activity relationship (SAR) analysis resulted in the identification of an optimized structure, Compound 36.40, with a twenty-fold improvement in potency over synthetic peptides that typically used to study AGPCRs. Additionally, our antagonist screen allowed for the early-stage characterization of two novel GPR56 inhibitors that robustly attenuated GPR56-depndent aggregation of human platelets. Taken together, we have elucidated the tethered agonist mechanism of activation for AGPCRs while also discovering novel, potent GPR56 activators and inhibitors that will prove useful as pharmacological tools, or as leads for AGPCRs-targeted therapeutics.

Chapter 1 Introduction to Adhesion GPCRs: Structures, Activation Mechanisms, and Ligands

This chapter was adapted from the publication, Vizurraga, A., Adhikari, R., Yeung, J., Yu, M., Tall, GG., *Mechanisms of adhesion G protein-coupled receptor activation.* J Biol Chem, 2020. **295**(41): p. 14065-14083 [15]

1.1 Abstract

Adhesion G protein coupled receptors (AGPCRs) are a thirty-three-member subfamily of Class B GPCRs that control a wide array of physiological processes and are implicated in many diseases. All AGPCRs possess large, self-proteolyzing extracellular regions that range from hundreds to thousands of residues in length. AGPCR autoproteolysis occurs within a highly conserved GPCR Autoproteolysis-Inducing (GAIN) domain that is proximal to the N-terminus of the G protein-coupling seven transmembrane spanning (7TM) bundle. GAIN domain-mediated self-cleavage is constitutive and produces two-fragment holoreceptors that remain intact at the cell surface. Dissociation of the AGPCR fragments stimulates G protein signaling through the action of the tethered-peptide-agonist stalk region that is occluded within the GAIN domain in the holoreceptor form. AGPCRs can also signal independently of fragment dissociation, and a few receptors possess GAIN domains incapable of self-proteolysis. This has resulted in complex theories as to how these receptors are activated *in vivo,* complicating pharmacological advances. Currently there is no existing structure of an activated AGPCR to support any of the theories. Ligand identification for AGPCRs is emerging, yet many of the receptors remain classified as orphans. Here, we provide a detailed layout of the currently accepted modes of AGPCR activation,

and provide a classification means for the ligands that have been identified and discuss how these ligands may activate AGPCRs in physiological contexts.

1.2 Introduction

G protein coupled receptors (GPCRs) are the largest class of membrane receptors, comprising over 800 members in humans. The GPCR seven-transmembrane helical bundle (7TM) allows for regulation of distinct G protein signaling cascades in response to diverse extracellular stimuli. Due to a broad influence on health and disease, GPCRs are heavily investigated for pharmacological intervention and are the targets of many approved drugs [16]. Consequently, study of each individual GPCR subclass will provide unique angles that are beneficial for the development of therapeutics. GPCR signaling is initiated by agonist binding to its orthosteric site, which results in rearrangements of the transmembrane helices of the 7TM bundle to allow efficient heterotrimeric G protein coupling and activation. G protein α subunits exchange GDP for GTP, allowing for functional dissociation of $G\beta\gamma$ and activation of downstream effectors. GPCRs are divided into 6 classes - Class A (Rhodopsin-like), Class B (Secretin), Class C (Metabotropic Glutamate), Class D (Pheromone), Class E (Cyclic AMP) and Class F (Frizzled) [17-19]. Within this naming system, the adhesion GPCRs (AGPCRs) are Family B members, but have been more aptly termed subfamily B2, while the traditional Class B peptide hormone binding GPCRs comprise subfamily B1.

AGPCRs are distinguished not only by their large extracellular regions (ECRs) that contain a wide variety of adhesive sub-domains, but also by the highly-conserved GPCR autoproteolysis inducing (GAIN) domain that constitutively self-cleaves the receptors into two fragments [10]. While extensive work has been done to characterize AGPCRs, it is largely uncertain how AGPCRs are activated in endogenous tissues. How ligand binding to the adhesion sub-domains in the ECR

regulates the activation state of the 7TM bundle is arguably the most intensely studied problem in current AGPCR research. To date, mechanisms involving AGPCR fragment dissociation and modes of allosteric modulation in response to endogenous ligands have been proposed. Here, we sought to provide clarity to these activation mechanisms by detailing the structural topologies of AGPCRs, while examining the prospective actions of endogenous ligands. Select aspects of AGPCR physiological regulation will also be discussed as routes to receptor activation.

1.3 Structural Topology of Adhesion GPCRs

The thirty-three human adhesion GPCRs are divided among 9 subfamilies, ADGR: A-G, L, and V based on sequence similarity (Also referred to as Group I – IX) [20, 21]. As with other classes of GPCRs, adhesion GPCRs possess 7TM domains that are known to signal through heterotrimeric G proteins in many cases. Unique to AGPCRs, however, is their possession of ECRs that typically consist of three main components: N-terminal adhesion domains, an autoproteolytic GAIN domain, and a conserved stalk region proximal to the 7TM termed the tethered agonist.

1.3.1 Extracellular "Adhesive" Domains

The N-terminal ECRs range from hundreds to thousands of residues and share characteristics with other receptor sub-family members. The ECRs contain a variety of adhesive-related subdomains that are often repeated (**Figure 1.1A**). For example, group E AGPCRs, contain Epidermal Growth Factor-like repeats that are found in many types of proteins that mediate cell adhesive interactions [22, 23]. Twelve AGPCRs contain a ~70 residue hormone binding (HormR), located N-terminally to their GAIN domain. There has yet to be a report of a hormone that binds to an AGPCR, leading many to believe that the HormR domain has additional functions beyond hormone binding (**Figure 1.1E**) [24]. Another interesting motif found in select adhesion GPCR

ECRs is the Sperm protein, Enterokinase and Agrin (SEA) domain. This domain is found in ADGRF1 (GPR110), ADGRF5 (GPR116), and ADGRG6 (GPR126) [25-27]. SEA domains mediate a second autoproteolytic cleavage event that is distinct from GAIN domain self-cleavage. Not much is known about the role of the SEA domain, but its function leaves open the possibility that these particular receptors have alternative modes of signaling regulation.

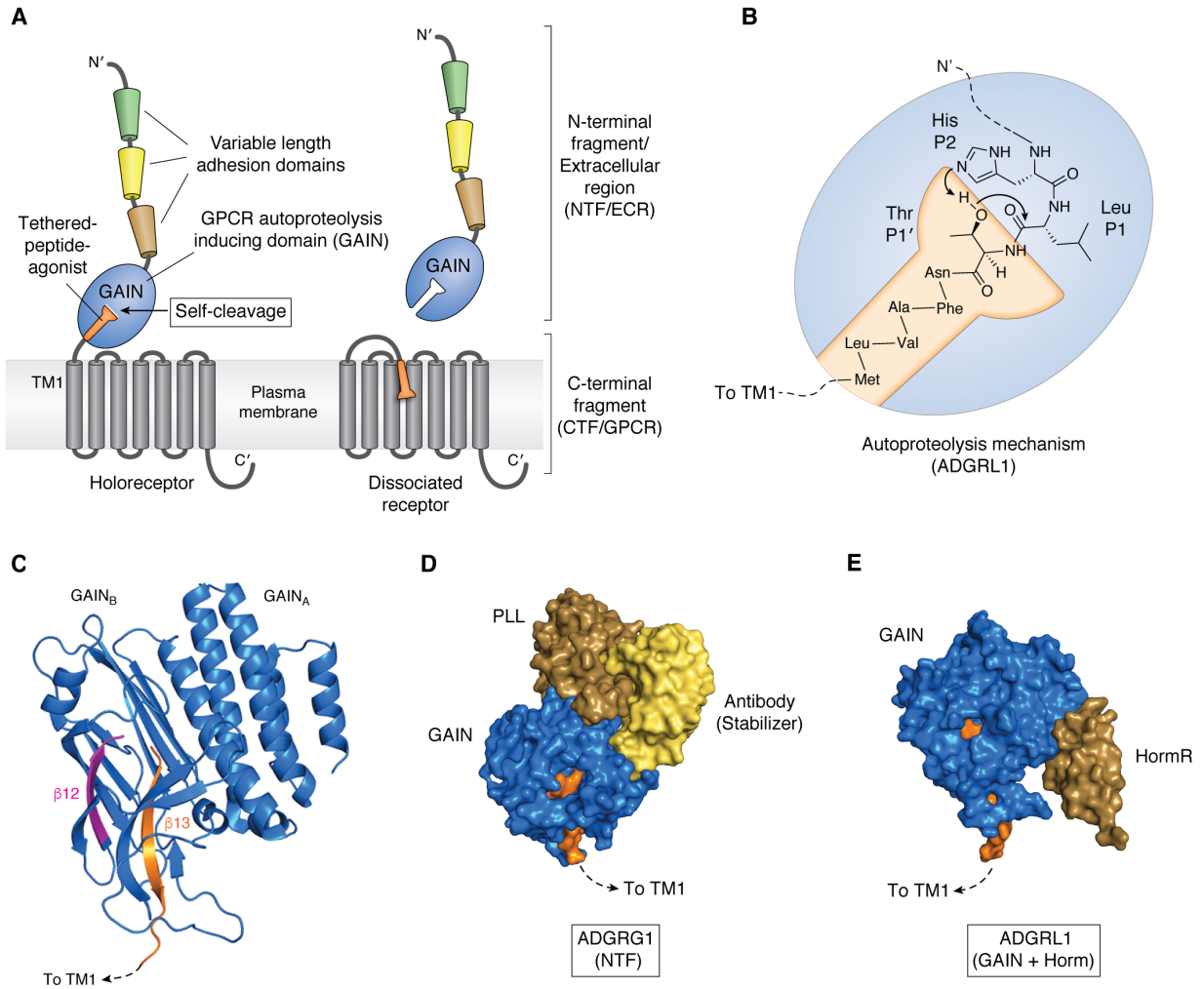

Figure 1.1 Structural Topology of Adhesion GPCRs. A. General structural outline of Adhesion GPCRs. Adhesion GPCRs exist as two-fragment receptors following constitutive autoproteolysis via the GAIN domain. In the holoreceptor form, the two AGPCR fragments are non-covalently bound. In the dissociated form, the N-terminal fragment (NTF) or extracellular region (ECR) is released extracellularly, while the freed C-terminal fragment (CTF) or GPCR domain remains in the plasma membrane. The ~20 residue stalk (orange) that is exposed following NTF / CTF dissociation is termed the tethered-peptide-agonist. **B.** The autoproteolysis mechanism of the GAIN domain, as shown for ADGRL1 (Latrophilin-1) [10]. **C.** Ribbon representation of the β-strand 12 - GPS proteolyzed loop - β-strand-13 orientation within the GAIN domain in the holoreceptor state. **D. and E.** Space-filled models of the ADGRG1 (GPR56) NTF (PDB: 5KVM) with stabilizer antibody and the GAIN domain plus adjacent HormR domain from ADGRL1 (PDB: 4DLQ). The residues of the tethered-peptide-agonists and remainder of the stalks are colored

1.3.2 The GAIN Domain and Autoproteolysis

At the C-terminal end of nearly every AGPCR ECR, ending 7-18 residues prior to the start of the first transmembrane span of the 7TM bundle, is the GPCR Autoproteolysis-Inducing (GAIN) domain [10] (**Figure 1.1A**). A seminal finding in the AGPCR field was the X-ray crystallographic solution of GAIN domain structures [10]. GAIN domains are divided into two sub-domains: an alpha-helical-rich $GAIN_A$, and beta-sandwich $GAIN_B$. Complete GAIN domains are ~320 amino acids with variability typically observed within the $GAIN_A$ subdomain. The GAIN domain is a fully self-sufficient protease that catalyzes constitutive, unregulated autoproteolysis that splits the receptor into two fragments. The receptor fragments remaining after self-cleavage are the extracellular N-terminal fragment (NTF) and the membrane-intercalated C-terminal fragment (CTF), which is also referred to as the GPCR- or 7TM domain. The NTF and CTF remain non-covalently bound after self-proteolysis, which is considered to occur early during receptor biosynthesis in an intracellular compartment [28]. The two-fragment holoreceptor is trafficked to the plasma membrane where it resides, poised for signaling.

The AGPCR self-proteolysis reaction requires proper folding of the GAIN domain and occurs within $GAIN_B$ when a conserved basic residue at the P2 position of the cleavage site abstracts a hydrogen from the side chain of the conserved, polar threonine (or serine) at the P1' position (**Figure 1.1B**) [29]. AGPCR P2 site basic residues are most commonly histidines, such as His836 in ADGRL1 (LPHN1), but can be arginine, such as Arg855 in ADGRB5 (BAI3) [10]. The proton abstraction initiates a nucleophilic attack of the carbonyl group of the P1 residue, which is most commonly leucine. The resulting ester intermediate is resolved by a final nucleophilic attack of a water molecule. The consensus self-cleavage site within the GAIN domains of most AGPCRs is HL/T. Prior to solution of the GAIN domain structure, the HL/T site and surrounding

sequence was termed the GPCR Proteolysis Site (GPS), reflecting the idea that the minimal sequence was sufficient for proteolysis, rather than the larger structure of the GAIN domain [30-32]. Given that this original definition has changed, GPS has now commonly come to mean the HL/T consensus site within the GAIN domain.

The GPS is located 14-25 residues N-terminal to the start of the first transmembrane span (TM1). The start of the CTF, the P1' threonine, is also immediately N-terminal to the first residue of the final (13^{th}) β-strand of the β-sandwich structure that comprises the $GAIN_B$ subdomain. Therefore, β-strand 13 is part of the CTF, but it is embedded within $GAIN_B$, and the GPS (*i.e.* HL/T) is essentially the loop that links β-strands 12 and 13 (**Figure 1.1C**). β-strand 13 sequences of adhesion GPCRs are highly conserved and very hydrophobic, which aligns with their location within the interior core of $GAIN_B$ subdomain (**Figure 1.1C-E, Figure 1.2**). β-strand-13 is non-covalently bound by a dense network of ~20 hydrogen bonds that hold it firmly within the $GAIN_B$ subdomain [10].

1.3.3 The Tethered-Peptide Agonist

Within recent years the stalk that connects TM1 to the GAIN domain, and includes β-strand 13, has been named the adhesion GPCR tethered-peptide-agonist (also referred to as the tethered agonist, or TA). This conserved sequence within multiple AGPCRs was shown independently by two groups to play a pivotal role in mediating receptor activation [33, 34]. One feature that seems to be an obvious requirement for tethered-peptide agonism is that the NTF and CTF of the receptor must become dissociated to liberate the agonist peptide from the interior core of the GAIN domain. Interestingly, not all AGPCRs undergo autoproteolysis; some receptors including ADGRC1 (CELSR1), ADGRA2 (GPR124), ADGRF2 (GPR111), ADGRA3 (GPR125) and ADGRF4 (GPR115) may be activated by alternative modes that do not involve fragment dissociation and

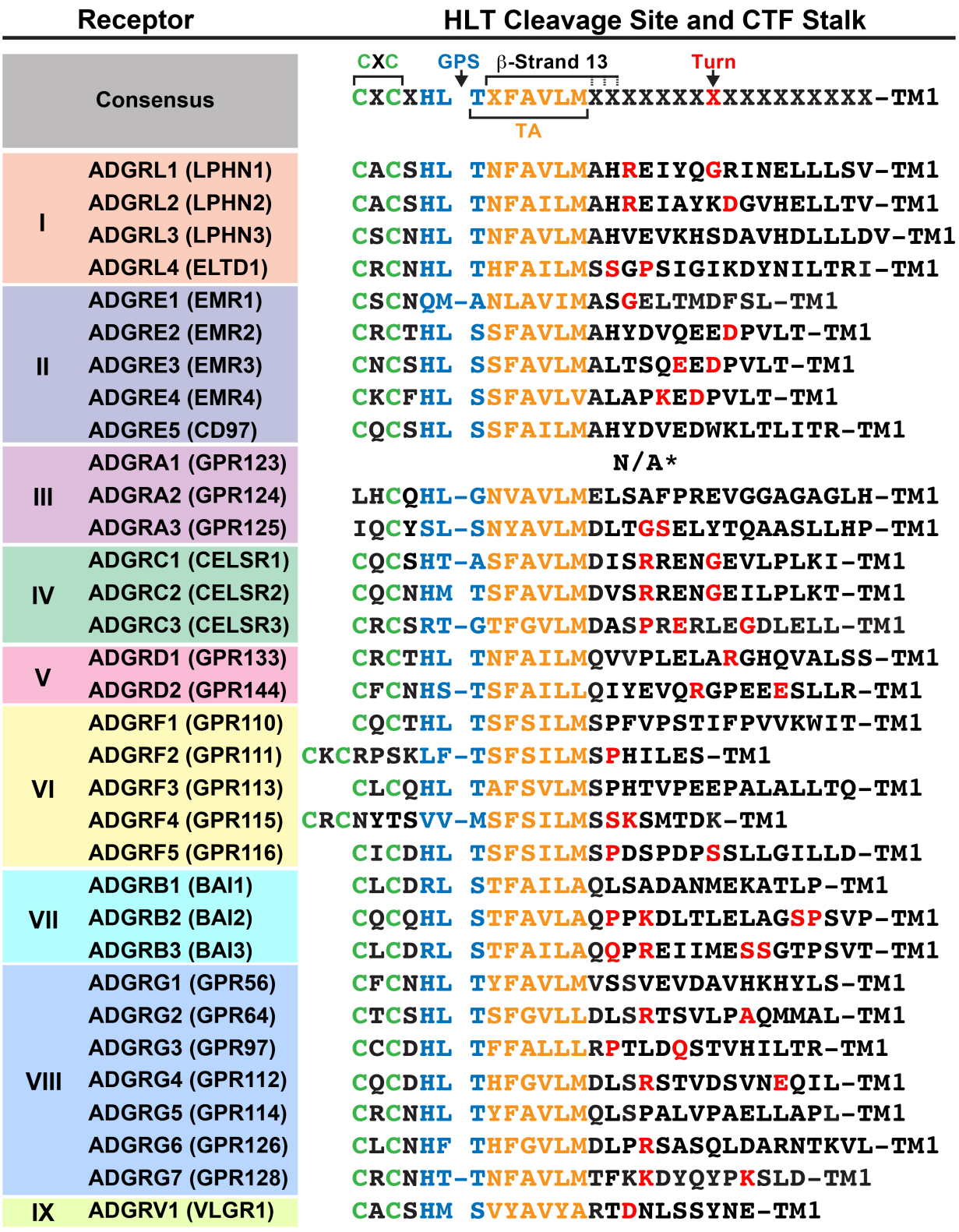

Figure 1.2 Adhesion GPCR GPS and Tethered Agonist / β-Strand 13 Sequences. Receptors are grouped by the recently adopted IUPHAR naming scheme, with previous names in parentheses. CTF stalk lengths are based on transmembrane span boundary predictions via TMHMM 2.0 [1, 2]. Turn elements were predicted using the Chou & Fasman Secondary Structure Prediction Server (CFSSP) [9].

tethered-peptide agonism [35-37]. Impaired self-cleavage is typically attributed to alterations of the GPS; receptors lacking a basic residue at the P2 position (*e.g.,* ADGRF2 or ADGRF4) or a polar residue at the P1' position. (*e.g.* ADGRC1) demonstrate minimal or no autoproteolysis (**Figure 1.2**) [35-37]. Differences in post-translational modifications have also been proposed to regulate GAIN-mediated cleavage, such as N-linked glycosylation events within the GAIN domain [10, 38, 39]. However, observations of inefficient cleavage in these instances may more likely be manifestations of experimental receptor overexpression that impart improper receptor trafficking or processing. Non-cleaved AGPCRs are still capable of signaling, leaving open the question of how these receptors become activated.

1.4 Adhesion GPCR Activation Mechanisms

GPCRs exhibit different basal activity levels that depend on the individual characteristics of each receptor. Basal activity is one state that GPCRs occupy within a dynamic energy landscape of active and inactive conformations [40-42]. **Figure 1.3** depicts four proposed activity states of adhesion GPCRs with cartoon diagrams that the field has used with representation of G protein binding site dynamism as a function of receptor activation. Accompanying the diagrams are activity profiles of relative signaling strength. An understanding of the ways that AGPCRs become activated is emerging. There have been a broad and imaginative variety of proposed AGPCR activation schemes [24, 43-48]. The current evidence supports two fundamental modes of AGPCR modulation: orthosteric agonism (*i.e.* tethered-peptide agonism), in which NTF/CTF dissociation is required, and allosteric regulation, which has also been termed the tunable model and does not require receptor subunit dissociation [33, 44, 45, 47, 49]. Both fundamental activation modes are supported through several lines of evidence, and it is likely that individual AGPCRs can be activated in both manners.

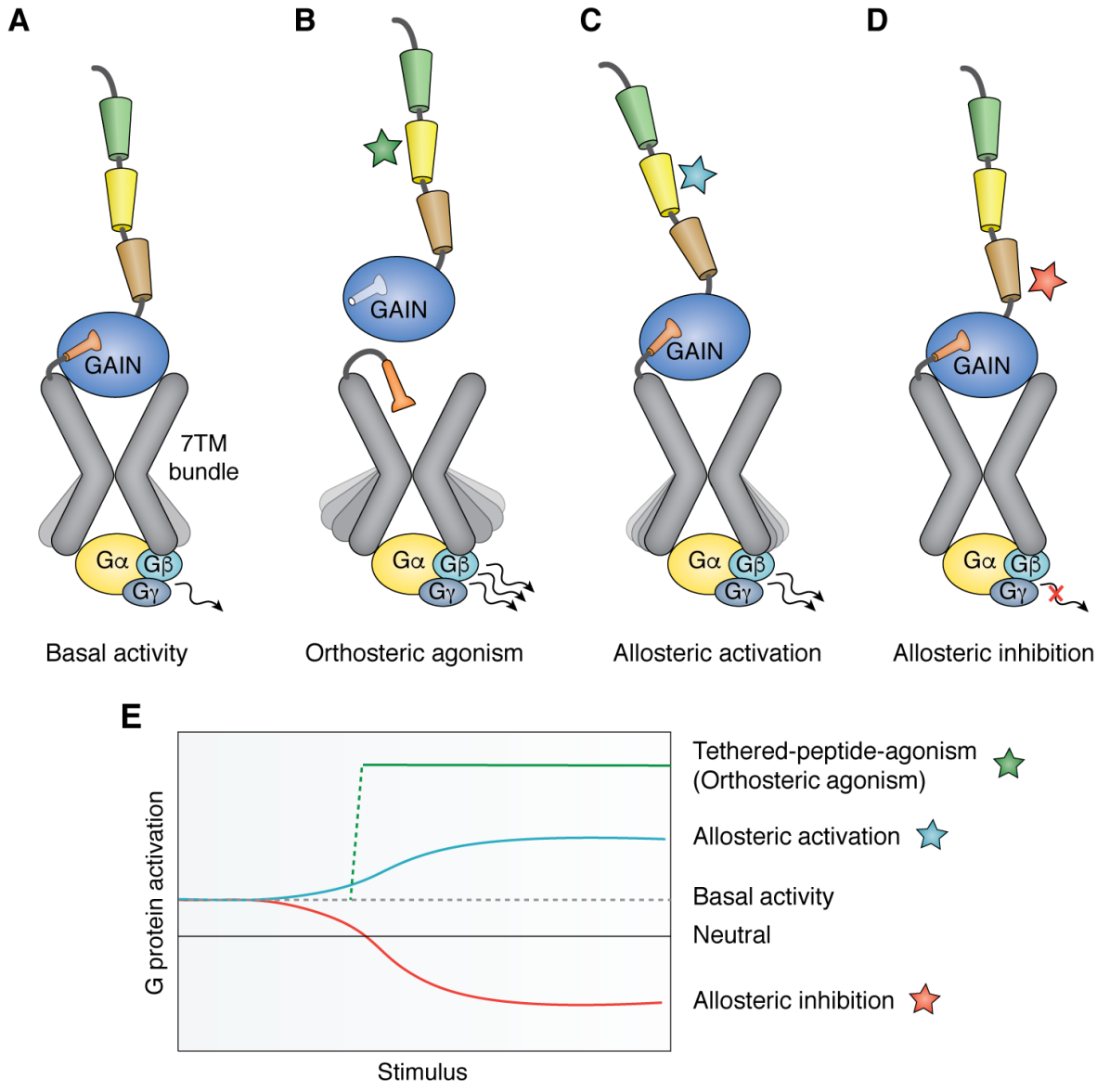

Figure 1.3 Models of Adhesion GPCR Activation. **A.** Adhesion GPCRs, as with other GPCRs, occupy a range of activated and inhibited states. Consequently, AGPCRs possess varying levels of basal G protein signaling. The adhesion GPCR N-terminal sub-domains (dark green, yellow, and brown modules) are portrayed to reflect the potential variety within adhesion GPCR ECRs. **B.** In the orthosteric agonism model of activation, NTF / CTF dissociation via an anchored ligand (depicted by the green star) results in exposure of the tethered-peptide-agonist (orange), allowing it to bind to an orthosteric site that is predicted to lie within the 7TM helical bundle. Orthosteric agonism is proposed to be a threshold response (all or none) due to forced NTF dissociation, which results in stabilization of highly active states of the receptors and maximal signaling. **C and D.** In allosteric modes of AGPCR regulation, ligands (denoted as a blue or red star) can interact with various AGPCR N-terminal adhesive motifs to stabilize active (activation, **C**) or inactive states (inhibition, **D**), respectively. Allosteric activation and inhibition mechanisms are unknown but may be mediated by GAIN-7TM interactions that favor stabilization of specific receptor conformations. **E.** Relative signaling strength outputs in response to stimulus for each of the receptor modulation modes.

1.4.1 Orthosteric Agonism (Tethered-Peptide Agonism)

Orthosteric agonism is a receptor activation model that is dependent on the action of the highly conserved AGPCR tethered agonist. The most important residues, or the core of the tethered agonist, are the seven residues located immediately C-terminal to the GPS. These residues mostly overlap with β-strand 13, the conformation the sequence adopts in the holoreceptor form. The core residues share the consensus sequence TXFAVLM with the T, F, and M residues showing the highest conversation across all AGPCRs (**Figure 1.2**). Pre-dating understanding that this sequence was a tethered-peptide-agonist, a study by Hall and colleagues compared the signaling strength of ADGRG1 (GPR56) to an engineered ADGRG1 construct in which the entirety of the NTF was deleted (ΔNTF, or CTF). The ΔNTF receptor exhibited substantially higher G protein-dependent signaling than the full-length receptor [50]. Since then, ΔNTF variants of several AGPCRs were found to have increased signaling capacity [33, 50-53]. A subsequent study used urea to operationally dissociate the two fragments of AGDRG1 in membrane homogenates and found that the isolated CTF was markedly more efficacious at activating G proteins than the holoreceptor [33]. It was consequently found that the TM1 N-terminal stalk sequence consisting of ~20 residues behaved as a tethered-peptide-agonist and dramatically activated AGPCRs. Deletion of tethered agonist residues dramatically lowered receptor activities *in vitro,* as shown for ADGRG1, ADGRG2 (GPR64), ADGRG6, and ADGRD1 (GPR133), and ADGRF1 [11, 33, 34, 54]. Partial deletion of the zebrafish ADGRG6 tethered agonist resulted in a puffy ear phenotype and impairment of nerve cell myelination, essentially phenocopying the fish model deletion of the ADGRG6 CTF [34, 55]. Sequential N-terminal truncations to the first residues of ΔNTF AGDGRG1 and ADGRF1 receptors resulted in incremental loss of G protein signaling activity *in vitro* [33]. AGPCRs with substitution mutations to critical residues within the tethered

agonist also had reduced activities [33, 34, 56, 57]. By contrast, deletion of the entire stalk of a ΔNTF version of ADGRB1 surprisingly had little impact on signaling compared to a version with an intact stalk [11]. This led to the proposal of stalk-independent signaling which may align with the concept that GPCRs are diverse and have a broad range of basal signaling capacity, and that it is clear that AGPCRs can be activated by means that do not rely on the tethered agonist [11, 58]. ADGRB1 did respond in vivo to synthetic peptide agonists, indicating the probability of bimodal ADGRB1 activation [3].

Further evidence supporting AGPCR tethered agonism was demonstrated via synthetic tethered agonist-mimetic peptides that activated their corresponding receptors *in vitro,* and in some cases *in vivo.* ADGRG1, ADGRG2, ADGRG5 (GPR114), ADGRG6, ADGRD1, ADGRF1, ADGRF4, and ADGRF5 all demonstrated increases in signaling when exposed to these synthetic activating peptides [33, 34, 56, 57, 59, 60]. As with the tethered agonist stalks from which they are derived, synthetic peptide agonists have a critical dependence on their N-terminal residues. Differences as small as single residue substitutions or deletions at the N-terminus can severely abrogate the agonistic properties of the peptides [33, 34]. Receptor specificity of synthetic peptide agonists also depends on the sequence similarities shared among the tethered agonists. For example, synthetic peptide agonist cross-reactivity was exhibited among members of the Group VI AGPCR subfamily that share a highly conserved tethered-peptide-agonist, and include ADGRF1, ADGRF4, and ADGRF5 (**Figure 1.2**) [59].

The conformation that tethered-peptide-agonists adopt once released from the GAIN domain core is not known, but many seven-residue tethered-peptide-agonist sequences contain β-turn elements within the middle of the stalk regions [33]. Performing turn element predictions on all tethered agonist-containing AGPCRs via the Chou & Fasman Secondary Structure Prediction

(CFSSP) server revealed that turn elements are often conserved among receptors within the same subfamily (**are**, red) [9]. These turn elements may serve as flexible point to allow the tethered agonist to bind intramolecularly back towards its orthosteric site within the CTF. Mutations to synthetic peptide agonists near the prospective turn points alters their capacity to stimulate signaling. For example, a 13-residue synthetic peptide that was derived from the ADGRF4 tethered agonist, a non-cleaved receptor with an unusually small CTF stalk (**Figure 1.2**), was incapable of promoting signaling [59]. However, mutating 2-3 residues around the predicted turn element, so that the peptide now matched the ADGRF5 sequence, restored its ability to activate ADGRF4. This suggests that the turn regions of AGPCR tethered-peptide-agonists may be critical for their ability to activate their receptors.

The presence of the turn elements may also help to account for the sprawling evidence that synthetic peptides modeled after AGPCR tethered agonists critically depend upon length. Most studies found that longer peptides with lengths of 12-20 residues, which in most cases includes the predicted turn motifs, exhibit the highest efficacies [33, 34, 59, 60]. The lone reported exception to this is the 7-mer peptide derived from the ADGRG1 tethered agonist, which is the only ADGRG1-modeled peptide capable of activating the receptor *in vitro* [33]. Intriguingly, the ADGRG1 7-mer peptide does not activate ADGRG5, even though ADGRG5 has an identical tethered agonist sequence (**Figure 1.2**). However, longer ADGRG5-mimetic peptides (18-20 residues, comprising the complete stalk) will activate both ADGRG1 and G5 *in vitro* and in cells, even though the sequences share no similarities beyond the first seven residues [34, 61]. The C-terminal ends of longer peptides may be necessary for proper folding or bending about the predicted turn element to accommodate binding to the AGPCR orthosteric site, while the 7-mer ADGRG1 peptide may be a rare perfect fit that requires only the core tethered agonist sequence.

It is also plausible that the C-terminal ends of activating peptides help stabilize them in solution, as the C-termini are far more hydrophilic than the hydrophobic 7-mer N-termini.

The current leading model of adhesion GPCR activation is that the tethered-peptide-agonist binds intramolecularly to its orthosteric site following receptor NTF / CTF dissociation. Upon NTF dissociation, the hydrophobic agonist residues are exposed to the aqueous extracellular environment, resulting in a thermodynamically unfavored condition. Hydrophobic effects may be the driving force for the tethered agonist to rapidly bind to its orthosteric binding pocket within the 7TM bundle (**Figure 1.3B**). Given that the core seven residues comprising the tethered agonist are completely embedded within the GAIN domain in the holo-receptor form, it is likely that orthosteric agonism is an abrupt, threshold-like response; receptor fragment dissociation is a binary off/on switch and results in full agonist-driven signaling once the NTF is removed (**Figure 1.3E**). The rapid onset of signaling is predicted because tethered agonist binding to its orthosteric site is a first order event; the ligand and receptor are tethered together in extreme proximity, and binding of the tethered agonist within the 7TM may be driven to overcome the disfavored hydrophilic environment. This mechanism has some parallels and distinctions to Protease-Activated-Receptor (PAR) activation. PARs are Class A GPCRs that are activated when exogenous proteases (*e.g.,* thrombin or trypsin) cleave their N-terminal stalk leader sequences. PARs are distinguished from AGPCRs in that they are proteolyzed *in trans*, rather than autoproteolytically. Following proteolysis, the new N-terminus of the TM1 stalk is proposed to bind to an orthosteric site that includes extracellular loop 2 (ECL2) [62-64]. A fundamental difference between PARs and AGPCRs is that PAR stalk sequences are typically longer, and the tethered agonists are less hydrophobic than those of AGPCRs. Consequently, while PAR tethered agonists are proposed to bind to PAR 7TM extracellular loops, it would make sense that AGPCR tethered agonists might

bind instead, deeper within the hydrophobic core of the 7TM bundle. However, it is currently unsolved precisely where the tethered agonists of both receptor classes bind to their respective 7TMs.

The means of force-mediated AGPCR fragment dissociation are largely unknown. Given the dense hydrogen-bonding interaction network that holds the tethered-peptide-agonist (β-strand 13) within the GAIN domain, it is expected that a substantial force would be needed to break those non-covalent bonds. Many adhesion GPCRs have been observed to undergo fragment dissociation, which has often been referred to as NTF shedding. Freed NTFs in various tissues or cell culture models were observed for ADGRG1, ADGRA2, ADGRB1 (BAI1), and ADGRE5 (CD97) [36, 65-68]. While shedding may imply spontaneous dissociation of the NTFs, these observations could also be remnants of ligand-induced NTF dissociation events [36, 69]. AGPCR fragment dissociation could be achieved by NTF binding to its ligands that are anchored to the extracellular matrix (ECM) or adjacent cells. Cell movement in relation to the anchored ligands would generate sufficient shear force to dissociate the fragments and initiate G protein signaling. In line with this, adhesion GPCRs were recently considered to be a group of metabotropic mechanosensors [44, 70-72]. Ligand-mediated shear force dissociation of the NTF is discussed further in the ligands section.

Tethered agonist activation of AGPCRs does not account for all means of AGPCR activation, with the most obvious examples being non-cleaved AGPCRs that are incapable of undergoing NTF/CTF dissociation. Non-cleaved receptors, and many engineered uncleavable mutants of cleaved receptors are still capable of signaling through G proteins [11, 57, 73, 74]. In these instances, it is unreasonable to predict that the tethered agonist directly regulates signaling as it is covalently bound to the NTF within the interior of the GAIN domain. Consequently, an

alternative model has been proposed whereby AGPCR CTFs may be activated allosterically via conformational changes through ligand-induced structural changes of the NTFs.

1.4.2 Allosteric Activation and Inhibition

In allosteric models of adhesion GPCR activation, the NTF and CTF remain bound, and changes in signaling may be induced by receptor conformational changes upon ligand binding to the NTF, rather than orthosteric engagement by the tethered-peptide-agonist. The exact mechanisms of allosteric activation or inhibition are not clear, as the N-terminal ligand binding domains and the G protein-coupling 7TM domain are distal, separated by hundreds or even thousands of residues. Binding of an allosteric ligand must somehow transmit an activation signal over a large structural space. The GAIN domain located immediately N-terminal to the 7TM domain, is the best candidate to transmit the allosteric signals. Following binding of an allosteric ligand or antagonist, the GAIN domain could help to stabilize active- or restricted-conformation states of the 7TM domain to promote or inhibit signaling, respectively (**Figure 1.3C-D**).

Beyond the β-strand 13 / tethered agonist linkage, interactions between the GAIN or other ECR elements and 7TM domains are not well characterized and have only been observed indirectly in a few isolated studies. In HEK293T cells co-expressing myc-tagged ADGRB1 NTF and a CTF ADGRB1 variant (ΔNTF), anti-myc was used to co-immunoprecipitate the ADGRB1 CTF [75]. ADGRG1 harbors two disease-causing mutations R565W and L640R that are present in ECLs 2 and 3, respectively, that lead to the pathogenesis of the neurodegenerative disease bilateral frontoparietal polymicrogyria (BFPP) [76]. Relative cell surface abundance of the mutant receptors was impaired, but not when the mutants were expressed as CTF variants, suggesting that the ECLs may provide critical contacts with the NTF that drive proper receptor trafficking [77]. Additional evidence comes from a study that purported that NTFs and CTFs of chimeric AGPCRs

had the ability to exchange or to swap via a "split personality" model [78]. Given the intricacies of how the tethered agonist is embedded within the GAIN domain, it is unlikely that AGPCRs are capable of NTF exchange that includes re-embedding of the tethered agonist, especially considering that GAIN domains are destabilized following NTF / CTF dissociation or when constructed recombinantly to lack β-strand 13. These observations of NTF swapping may, however, be evidence of additional, conserved GAIN-CTF contact points that are distinct from β-strand 13.

While additional GAIN or NTF direct interactions with the TM remain undefined, evidence for them would help explain how AGPCRs are allosterically activated by ligands to produce more modest signaling strength outputs than orthosteric agonism (**Figure 1.3E**). Several endogenous and engineered soluble binding partners of AGPCRs have been identified that bind to AGPCR NTFs and induce signaling changes. One example is the docosahexaenoic acid (DHA) metabolite, synaptamide that was identified as an ADGRF1 ligand and proposed to activate cAMP signaling to promote synaptogenesis and anti-neuroinflammatory responses [79-81]. Synaptamide binds directly to the GAIN domain and results in a modest increase in cAMP levels as shown by gene reporter assay [80]. Functional studies of ADGRG1 in neural progenitor cells demonstrated that ADGRG1 NTF-targeting antibodies could stimulate $G_{12/13}$ signaling [82]. Recent structural studies of the ADGRG1 NTF corroborated this, showing that NTF-targeted antibodies could induce small, antibody-specific decreases or increases in G protein signaling [58, 83]. The changes in signaling were modest and within 0.5-fold of basal levels as opposed to tethered agonist- or synthetic peptide agonist-activated receptors that exhibit many-fold increases in signaling over holoreceptors [11, 33, 34, 50, 57, 59]. It is difficult to envision how soluble antibody ligands alone could support the anchoring and force requirements that are proposed to be needed for NTF dissociation, and there

was no observation of NTF dissociation following the ADGRG1 antibody treatments. Therefore, AGPCR NTF-directed antibodies may be useful probes for understanding allosteric regulation of AGPCR activation that is independent of receptor fragment dissociation.

Allosteric modulation of AGPCRs also occurs through NTF interactions with ligands *in cis* (on the same cell) or *in trans* (from an adjacent cell). In these instances, the ligands or binding partners may convey conformational change to the 7TM via the NTF/GAIN. ADGRA2 interacts *in cis* with the protein RECK to regulate Wnt7/Frizzled receptor activation for modulation of central nervous system angiogenesis [84, 85]. ADGRA2 is predicted to be non-cleaved due to its atypical GPS (**Figure 1.2**), so it makes sense for the receptor to mediate signaling allosterically in a large "signalosome" complex rather than through tethered agonism. Additional *in cis* interactions with AGPCRs have been observed, directly or indirectly for ADGRB3 and Stabilin-2, ADGRC1 and Vangl-2 or Frizzled-6, and ADGRL1 and Contactin-6 [86-88]. Most ADGRL (Latrophilins) receptors interact *in trans* with Teneurin and FLRT ligands to form trans-synaptic signaling complexes, that in some contexts are implied to be stable due to their role in maintaining the architecture of the synapse [6-8, 70-72, 89, 90]. The stabilities of these *cis* or *trans* ligand / NTF complexes provide additional evidence for the idea that AGPCRs function in adhesion capacities and in doing so may allosterically regulate signaling in the absence of fragment dissociation.

1.5 Modulation of AGPCR Activity via Ligand Binding

Wide-ranging de-orphanization studies have uncovered endogenous ligands that target individual AGPCRs (reviewed in [43-45, 47, 49, 91, 92]). Efforts to decipher the action of the AGPCR ligand repertoire have provided useful clues for understanding receptor activation mechanisms in physiological contexts. **Table 1.1** details the currently known endogenous AGPCR

Table 1.1 Endogenous AGPCR Ligands

Class	Receptor	Extracellular Matrix Components	Lipids/Soluble Proteins/Small Molecules	Trans Presented Proteins	References
A	ADGRA1		*Orphan*		
	ADGRA2	Integrin-αVβ3, glycosaminoglycans, Syndecan-1,2			[5, 36]
	ADGRA3		*Orphan*		
B	ADGRB1	αVβ5 integrin	Phosphatidylserine, Lipopolysaccharide	RTN4R, CD36	[5, 93-96]
	ADGRB2		Glutaminase Interacting Protein (GIP)		[97]
	ADGRB3		C1ql1-C1ql4		[98, 99]
C	ADGRC1		*Orphan*		
	ADGRC2		*Orphan*		
	ADGRC3	Dystroglycan			[100]
D	ADGRD1		*Orphan*		
	ADGRD2		*Orphan*		
E	ADGRE1			Unknown NK Cell Receptor	[101]
	ADGRE2	Chondroitin sulfate, Integrins-αVβ3*, α5β1*		CD90*	[23, 102]
	ADGRE3			Unknown Ligand on Macrophages and Neutrophils	[103]
	ADGRE4			Unknown B cell Ligand	[104]
	ADGRE5	Chondroitin sulfate, Integrins-αVβ3, α5β1		CD55, CD90, LPA Receptor	[52, 102, 105-107]
F	ADGRF1		Synaptamide		[79, 80]
	ADGRF2		*Orphan*		
	ADGRF3		*Orphan*		
	ADGRF4		*Orphan*		
	ADGRF5		Surfactant Protein-D		[108, 109]
G	ADGRG1	Collagen III, Heparin, Transglutaminase-2, Laminin	Progastrin		[61, 74, 110-116]
	ADGRG2		*Orphan*		
	ADGRG3		*Orphan*		
	ADGRG4		*Orphan*		
	ADGRG5		*Orphan*		
	ADGRG6	Collagen IV, Laminin-211	Cellular Prion Protein		[53, 117, 118]
	ADGRG7		*Orphan*		
L	ADGRL1			Teneurin-2/4, Neurexin-1α, -1β, -2β, -3β, FLRT1/3,	[6, 119-121]
	ADGRL2			Teneurin-2, FLRT3	[6, 122]
	ADGRL3			Teneurin-3, FLRT1/3, UNC5A	[6, 89, 123]
	ADGRL4		*Orphan*		
V	ADGRV1		*Orphan*		

ligands and **Figure 1.4** proposes a means to classify adhesion GPCRs based on the type(s) of ligand that each receptor binds. Some AGPCRs have multiple ligands and span multiple categories of the classification system; 1. *trans*-cell presented proteins, 2. extracellular matrix components, and 3. soluble proteins, peptides, lipids, and small molecules. Cis-cell presented protein ligands is an emerging category with select examples.

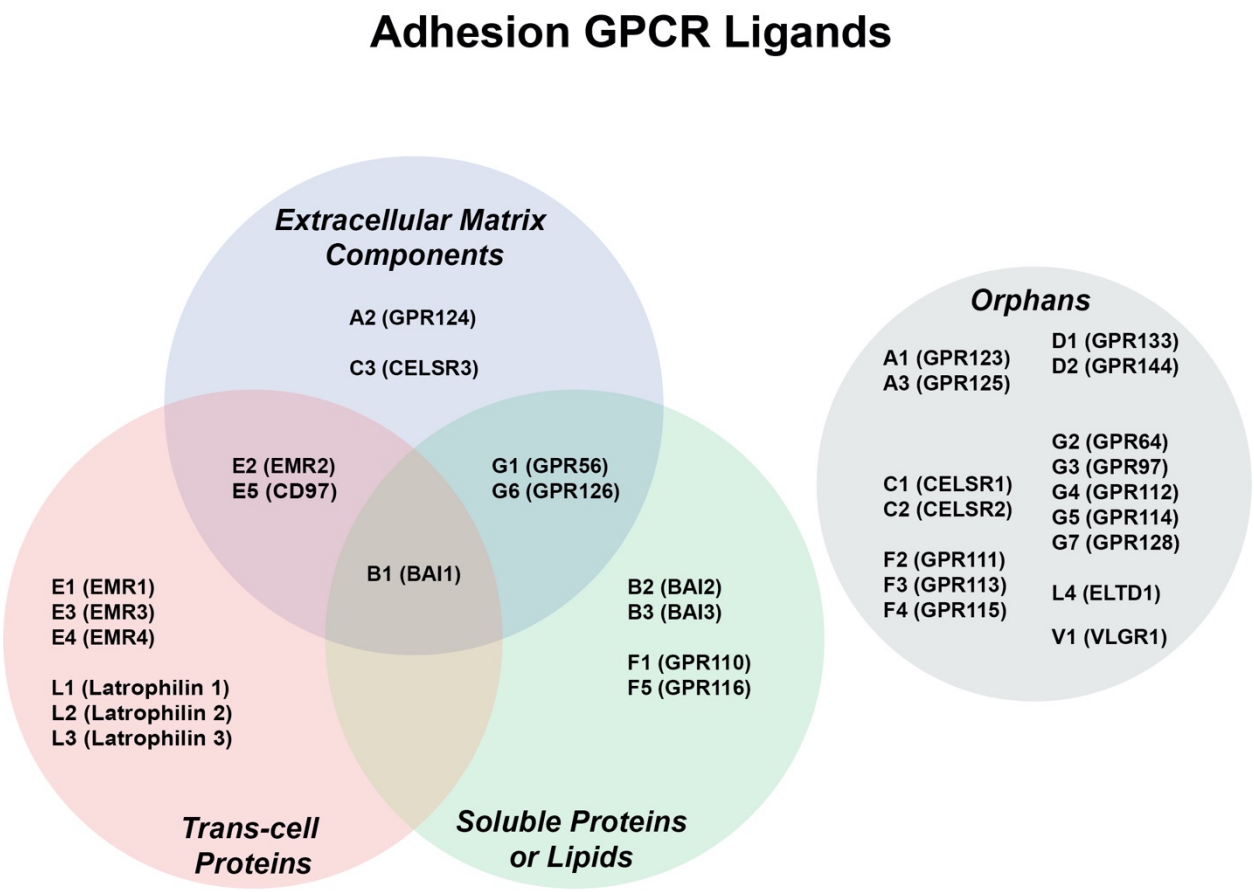

Figure 1.4 Classification of Adhesion GPCR Ligands. Adhesion GPCRs recognize three types of extracellular ligands that target the NTFs to regulate G protein signaling. Trans-cell presented proteins (red) are ligands that form inter-cell connections with AGPCRs. They allow for direct cell-to-cell messaging and are well characterized in ADGRE and ADGRL subfamilies in immune cells and neurons, respectively. They are predicted to activate AGPCRs via either allosteric modulation or tethered agonism (via forced dissociation of the NTF). Extracellular matrix components (blue) are anchored ligands that may also activate AGPCRs by tethered agonist and allosteric activation modes. Integrins and collagen subtypes are currently well characterized examples of ECM or ECM-associated ligands for specific receptors. Lipids, soluble proteins, and small molecules (green) are unanchored ligands that are expected to regulate signaling via allosteric modulation. 16 adhesion GPCRs have no reported ligand and thus remain classified as orphans (gray). This figure accompanies **Table 1.1** in which the specific ligands are referenced.

1.5.1 Trans-Cell Presented Proteins

Trans-signaling complexes are formed through interactions of the extracellular extensions of protein ligands presented by neighboring cells and the N-terminal adhesive modules of AGPCRs to provide modes of cell-to-cell adhesion and communication. Stable trans-cell AGPCR and ligand complexes may signal through both allosteric activation modes and/or tethered agonism. Tethered agonism imparted by trans-cell adhesive ligands is thought to occur by ligand binding to its AGPCR binding site(s) more tightly than the strength of the non-covalent contacts that β-strand 13 has within the GAIN domain. Shear force created by the two cells moving in relation to each other serves to dissociate the ligand-anchored NTF from the CTF to promote signaling. Multiple trans-cell ligands may bind simultaneously to AGPCR N-terminal adhesive modules, which is thought to provide strong multivalent binding that is sufficient to anchor the NTF. Prominent examples of AGPCRs that utilize trans-cell ligands are those present at synaptic junctions which bind to ligands spanning the synapse. ADGRL (Latrophilins) and ADGRB (BAI) receptors are both enriched in synaptic junctions and serve as models of trans-cell synaptic AGPCR signaling.

Most ADGRL receptors (ADGRL1-4), excluding ADGRL4, are localized on axons, axonal growth cones and nerve terminals [6, 92, 120, 121]. They are structurally distinguished from other AGPCRs by the presence of an N-terminal olfactomedin (Olf) domain and a lectin-like (Lec) domain. ADGRL receptors regulate inter-neuron adhesion and the migration of growth cones (actin-rich neuronal extensions), while promoting synapse formation and remodeling through control of cytoskeletal rearrangements [6, 7, 89, 90, 120]. Defects or variants in *ADGRL* genes are associated with neuronal disorders including attention deficit and hyperactivity disorder, autism spectrum disorder, schizophrenia, rhombencephalosynapsis, and microcephaly [124-129]. ADGRL receptors bind to three classes of single-membrane pass, trans-presented protein ligands:

teneurins, neurexins, and fibronectin leucine-rich repeat transmembrane proteins (FLRTs). Teneurins bind to the ADGRL Lec domain, while neurexins and FLRTs interact with the ADGRL Olf domain [10, 90, 130, 131]. These proteins interact in trans-synaptic signaling complexes and provide models for understanding how AGPCRs can be activated by trans-presented ligands. For instance, ADGRL1 interacts with both Teneurin-2 (also known as Lasso) and FLRT simultaneously to regulate dendrite arborization, axonal extension, and synaptogenesis [90, 130, 131]. These neuronal reshaping processes are thought to result from Rho / Rac-mediated actin cytoskeletal changes downstream of $G_{12/13}$ signaling, through which ADGRL3 was recently shown to signal [14, 132-137]. ADGRLs also couple to $G_{i/o}$ and G_q, which may influence neuronal migration and synaptogenesis, as asymmetric production of cAMP or Ca^{2+} within the cell influences growth cone guidance [12, 13, 92, 138, 139].

ADGRLs are self-cleaved receptors (**Figure 1.2**) and will activate signaling following NTF/CTF dissociation via tethered-peptide-agonism [10, 14, 140, 141]. The receptors can utilize both allosteric and/or tethered agonism modes of activation. For allosteric activation, teneurins and FLRTs may convey conformational modulation through the ADGRL NTF to elicit signaling (**Figure 1.5**, Left). Studies in *Drosophila* neurons showed that mechanically-induced ionotropic channel currents were dependent on the presence of the *Drosophila* homolog of ADGRL1, dCIRL [70]. Neurons were made to express a cleavage-deficient variant of dCIRL, and a normal response to the mechanical stimulus was observed, implying that allosteric modulation, and not tethered agonism was the primary means of receptor activation in this context. Ligand binding and shear force may dissociate the ADGRL NTF and CTF in other contexts, such as when a synapse breaks (**Figure 1.5**, Right). The strong tethered agonist-dependent $G_{12/13}$ signaling that would result upon synaptic breakage coincides with the known Rho / Rac dependent signaling events that drive actin-

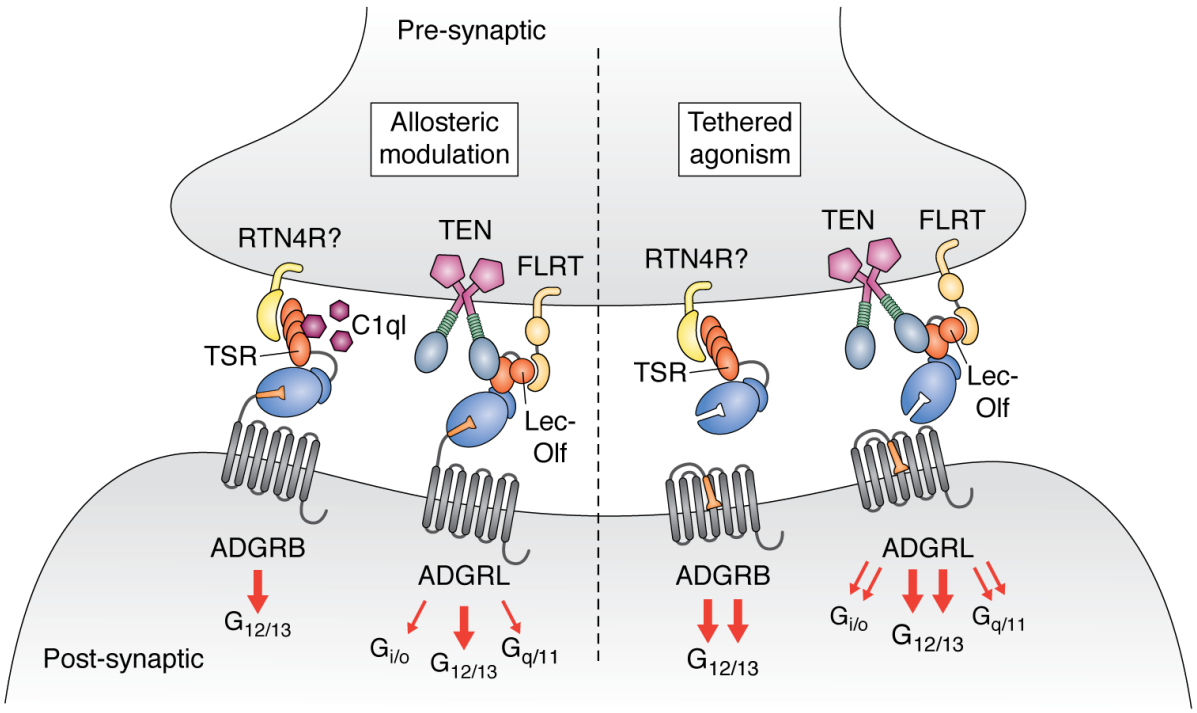

Figure 1.5 Trans-synaptic Adhesion GPCRs. ADGRL and ADGRB receptors are enriched in the central and peripheral nervous systems, and their activation is thought to induce synaptogenesis and axonal growth. ADGRB receptors are enriched in the post-synapse and bind secreted C1q-like proteins and an unknown trans-synaptic ligand (possibly the peripheral membrane-associated RTN4R) to regulate synapse formation and maintenance via the thrombospondin-like repeat (TSR) domains [3-5]. ADGRL is also enriched in the post-synapse and interacts with both FLRT and Teneurin (TEN) single-pass receptors simultaneously to form trans-synaptic links that promote synaptogenesis [6-8]. FLRT binds to the ADGRL2 N-terminal Olfactomedin (Olf) domain, while Teneurin2 binds the ADGRL2 Lectin-like (Lec) domain. In a fragment dissociation-independent model, a force-dependent signal may be transduced through the trans-synaptic junction to ADGRL and ADGRB receptors via allosteric modulation to induce $G_{12/13}$ signaling necessary for Rho activation and downstream cytoskeletal remodeling (Left) [11]. $G_{12/13}$ is coupled to both sub-classes of receptors, but ADGRL may also signal via $G_{i/o}$ and $G_{q/11}$ pathways [12-14]. ADGRL and ADGRB NTFs and CTFs may be dissociated when synapses absolve allowing for tethered agonist orthosteric activation of the receptors to induce synaptic remodeling (right).

dependent dendritic spine shape change programs [132-137]. Recent studies have also demonstrated that in migrating neurons, ADGRL1 interacts *in trans* with teneurin and FLRT to promote detachment and neurite retraction in repulsion processes [131]. The repulsive effects seem to contrast roles that ADGRL ligands such as teneurin have in mediating synaptogenesis [89, 120, 142]. It is possible that ADGRLs have dual roles in force-dependent axonal guidance. Migrating neurons may form transient FLRT/teneurin/ADGRL complexes that experience shear forces that elicit fragment dissociation and tethered agonist $G_{12/13}$ signaling for cytoskeletal-dependent neuron

repulsion. This is supported by the fact that strong $G_{12/13}$ signaling is associated with neurite retraction [132, 133]. In contrast, the synaptogenic effects attributed to FLRT and teneurin may be the consequences of formation of stable complexes with ADGRLs that allosterically signal through $G_{i/o}$ and G_q to regulate axonal growth and synapse formation. This is supported by studies demonstrating that ADGRL1/teneurin-2 promote calcium-dependent signaling and axonal growth [120, 142].

ADGRB receptors (ADGRB1-3) contain an N-terminal HormR domain and thrombospondin type 1 repeats (TSRs). Like ADGRLs, the ADGRB receptors are enriched in various brain tissues depending on the receptor subtype, including the cerebral cortex, hippocampus, basal ganglia, olfactory bulb, and thalamic nuclei [143-146]. ADGRBs signal through $G_{12/13}$ to activate Rho pathways and downstream cytoskeletal changes [11, 75]. Defined ligands for ADGRB receptors are the soluble C1q-like proteins (C1ql1-4) and phosphatidylserine, which both interact with the TSRs [93, 98]. BAI interaction with C1q-like proteins mediates synapse formation, while interactions with phosphatidylserine serves as an engulfment signal for apoptotic fibroblasts [93, 98, 99]. While the C1ql proteins and phosphatidylserine are the most studied ligands for ADGRBs, the trans-presented Reticulon 4 Receptor (RTN4R, or Nogo 66 receptor) was recently proposed to be an ADGRB1 ligand that also interacts through the TSRs [5]. RTN4R shares many functional features with ADGRB1: both are enriched in neurons and regulate axonal growth, axonal regeneration, and synaptic plasticity [147]. RTN4R was characterized as an ADGRB1 ligand in only one study, but it may account for the findings from another report that described an unknown ligand that was linked trans-synaptically to ADGRB1 [3]. The mechanism of activation by C1ql, phosphatidylserine, or RTN4R ligands is currently unknown, and downstream signaling outcomes have not been well characterized outside of microscopy-based

synaptic growth assays that monitor synaptic densities and dendrite growth [3, 98, 99]. Given that the ADGRB ligands bind to the same regions on the NTF, the binding may be mutually exclusive. For the ADGRB-RTN4R interaction, both allosteric and orthosteric tethered-agonist means of activation are plausible (**Figure 1.5**). In contrast, ADGRB binding to soluble C1ql proteins may only impart allosteric activation, as soluble proteins lack the anchoring properties that are necessary for force-mediated fragment dissociation. Interestingly, C1ql proteins can form higher order multimeric complexes [148]. Multimeric C1ql proteins could potentially link multiple ADGRB receptors to influence signaling activation in an unknown manner [98].

1.5.2 Extracellular Matrix Ligands

Select AGPCRs are involved in cell-to-extracellular matrix (ECM) adhesion events through direct interactions with protein or carbohydrate components of the ECM. In many cases, the ECM ligands are insoluble, for example, multiple collagen subtypes, and serve as anchor points for AGPCRs in several essential cell signaling processes [36, 53, 94, 100, 102, 115]. As with trans-cell AGPCR complexes, AGPCR-ECM complexes are most often formed by the AGPCR NTFs, depending on the specific adhesive subdomains of individual receptors. ECM and ECM-associated components that have been identified as ligands for AGPCRs include integrins, glycosaminoglycans, laminins, transglutaminase 2 (TG2) and collagens subtypes, which were identified for the ADGRA, ADGRB, ADGRE, and ADGRG receptor subfamilies (**Table 1.1**). Interactions between ADGRG-family receptors, particularly ADGRG1 and ADGRG6 with ECM components are perhaps the best characterized examples of ECM-AGPCR interactions and provide insight into how these ligands may activate AGPCRs.

ADGRG1 and ADGRG6 are widely expressed but are well-known for functions in the nervous system. ADGRG1 regulates oligodendrocyte development in the CNS and is also present

in skeletal muscle [110, 115, 149, 150], while ADGRG6 is a receptor used within Schwann cells of the peripheral nervous system to promote nerve myelination and repair [55, 151]. Collagen subtypes III and I, and tissue transglutaminase-2 (TG2) were identified as ECM interactors for ADGRG1, and collagen subtype IV and laminin-211 were identified to bind to ADGRG6 [53, 110, 111, 115, 117]. Addition of these ligands to both receptors resulted in signaling stimulation both *in vitro* and *in vivo,* but the exact mechanisms by which this occurs are not entirely known. Given the capability of multivalent interactions within the ECM, it is plausible that ECM ligands serve as an anchoring point for AGPCRs to allow for receptor fragment dissociation following a mechanical stimulus, leading to signaling via tethered agonism. Supporting this, HEK293 or COS-7 cells expressing ADGRG6 exhibited increased cAMP production when exposed to collagen IV or extracellular laminin-211 under a shaking or rotating force [53, 117]. ECM components may also activate AGPCR signaling via simultaneous binding of more than one ligand, as shown by the interaction of ADGRG1 with TG2 and laminin. ADGRG1 was only activated by simultaneous binding of TG2 and laminin; neither ECM component was incapable of activating the receptor alone [74]. Interestingly, activation by laminin and TG2 was receptor cleavage dependent, as the H381S cleavage-deficient ADGRG1 mutant was not activated by TG2 and laminin [74]. In each of these cases, details of the mechanism fell short of demonstrating ligand-dependent NTF / CTF dissociation that was commensurate with force and ligand action, but the cleavage-dependence of ADGRG1 activation provides reasonable evidence to support a tethered-agonist-based activation mechanism.

Multivalent ligand binding may also account for the ability of collagen to activate AGPCRs. Select subtypes of collagen activate both ADGRG1 and ADGRG6 receptors *in vitro* and *in vivo* by binding to the NTFs: collagen III interacts with the ADGRG1

pentraxin/laminin/neurexin/sex-hormone-binding-globulin-like domain (PLL domain, also referred to as its collagen-binding domain) while ADGRG6 interacts with collagen IV through its C1r/C1s / Uegf / Bmp1 (CUB) and pentraxin (PTX) domains [53, 69, 115]. These interactions are vital for function of the receptors in neurons as disruption of the collagen binding sites with point mutations or deletions resulted in myelination defects [53, 150]. ADGRG1 loss-of-function mutations also cause the neurological disease bilateral frontoparietal polymicrogyria (BFPP), a cortical brain malformation disorder [68]. Fibrillar collagen crosslinked within the ECM could have the capacity to serve as an anchored, multivalent ligand for both ADGRG1 and ADGRG6 and bind tightly to allow force-mediated NTF / CTF dissociation and tethered agonism. Addition of collagen III to HEK293 cells overexpressing ADGRG1 reduced the amount of NTF at the cell surface while enriching it in conditioned medium, suggesting that collagen was capable of allowing, or inducing AGPCR fragment dissociation [69]. Not all AGPCRs that interact with ECM components are self-cleaved, such as ADGRA2, which interacts with integrins and glycosaminoglycans (**Table 1.1**). These ligands may instead form a cell-to-ECM tethered-complex that regulates AGPCR signaling via allosteric modulation.

1.5.3 Soluble extracellular ligands

In comparison to trans-cell and ECM ligands, there is a markedly lower number of known soluble ligands that regulate AGPCR signaling, which is unconventional for most other GPCR classes. The ligands that have been identified consist of a few small molecules, peptides, and soluble proteins. This is perhaps indicative of how AGPCR signaling is manifested. Whereas most GPCRs are activated by orthosteric binding of a soluble ligand, AGPCRs are activated by their own tethered ligand. Thus, it makes sense that there are relatively no known endogenous AGPCR ligands that bind to the 7TM domain at sites akin to the orthosteric site of Class A GPCRs. The

soluble ligands that have been identified for AGPCRs instead target the NTF, similar to the other two classes of AGPCR ligands. However, given that diffusible ligands are not anchored, it is probable that they regulate activity by allosteric modulation rather than tethered agonism. Two receptors that best illustrate this are ADGRF1 and ADGRF5.

ADGRF5 is a $G_{q/11}$-coupled receptor enriched in the lung and kidney that regulates the levels of pulmonary surfactants – lipid-protein complexes produced by alveolar type II (AT-II) cells that reduce surface tension at the air-liquid interface in the alveoli [56, 109]. Pulmonary surfactants are essential to prevent lung collapse, and impairments to production are associated with neonatal respiratory distress syndrome (RDS), acute lung injury (ALI) and acute RDS (ARDS) [152]. The proposed function of ADGRF5 is to suppress production and stimulate uptake of pulmonary surfactants by binding surfactant protein D (Sp-D) [109]. Deletion of ADGRF5 in mice resulted in enlarged alveoli that contained an excess of surfactant, leading to hypertrophy of AT-II cells. Sp-D was proposed to be an ADGRF5 ligand by demonstration that the two proteins could be co-immunoprecipitated. The interaction between ADGRF5 and Sp-D is not fully characterized beyond knowledge that Sp-D binds the NTF of ADGRF5, which contains several Ig-like repeats. However, a separate study showed that overexpression of Sp-D did not decrease alveolar surfactant pools or cause respiratory distress, which would be expected if Sp-D was indeed a ligand for ADGRF5 [56, 153]. Given that alveolar cells undergo consistent expansion and compression in the ventilatory cycle, it was proposed that ADGRF5 may be activated by mechanical stretching of AT-II cells [56]. While mechanical stimulation in this context is reasonable, there have been no proposed ECM or trans-presented ligands that serve as the anchoring point. Such a ligand may exist, and would support a mechanical means of activation, but has not been described. It is also plausible that mechanical stimulation activates ADGRF5 via

an unknown receptor through Sp-D, where Sp-D acts to link two receptors that may allow for a transmission of a mechanical signal. In this instance, Sp-D is instead influencing the mechanical activation of ADGRF5 rather than serving as an activating ligand itself. ADGRF5 can also be activated by synthetic peptide agonists, leaving open the probability of tethered agonist regulation and necessitation of a ligand deorphanization effort [56].

ADGRF1 is enriched in neural stem cells (NSC) and was initially recognized as an oncogene in various cancers such as gliomas, osteosarcomas, and lung and prostate cancers. [25, 154, 155]. Recently, the brain-enriched lipid metabolite N-docosahexaenoylethanolamine (synaptamide) was found as an endogenous ADGRF1 ligand that mediates early neurodevelopment [79-81]. ADGRF1 interacts with synaptamide at nanomolar affinity and may increase neurite growth and neurogenesis in cortical neurons and NSCs [81]. Synaptamide binds at the $GAIN_A$ and $GAIN_B$ sub-domain junction and was predicted from crosslinking studies to induce conformational changes to the ECR and TM6 [80]. ADGRF1 is self-cleaved at its GPS, it responded to synthetic agonist peptides, and urea treatment of the full-length receptor resulted in increased G_q signaling, showing that the receptor can be activated by tethered agonism [33, 59]. As with other soluble AGPCR ligands, synaptamide is unanchored, which leaves open the question of whether it can induce NTF / CTF dissociation. It seems probable that synaptamide may work through allosteric means to activate ADGRF1.

Besides endogenous soluble ligands, small molecule AGPCR probe compounds were identified from high throughput screens based on the ability to activate or inhibit select receptors, for example, for the ADGRG sub-family. Cell-based gene reporter assays showed that ADGRG1 could be activated by the small molecule partial agonist 3-α-acetoxydihydrodeoxygedunin (3-α-DOG) or inhibited by the antagonist, dihydromunduletone (DHM) [61, 114]. A calcium signaling-

based reporter screen for ADGRG3 identified beclomethasone dipropionate as a potential agonist [156]. Interestingly, both of these probes for similar ADGRG receptors share a four-ring steroid-like structure. The shared molecular skeletons of 3-α-DOG and beclomethasone suggests that ADGRG1 and ADGRG3 may have conserved binding pockets for these similar small molecules, and it probably lies within the 7TM, as 3-α-DOG activated an ADGRG1 ΔNTF variant [61]. A screen for small molecules that influenced ADGRG6 signaling in zebrafish recently identified apomorphine as a potential activator of ADGRG6 [157]. Outside of these examples, AGPCRs remain relatively untapped as targets for small molecule probe development. Discovery of high affinity agonists or antagonists could aid AGPCR-targeted therapeutic design and in stabilizing the receptors for much needed structural studies.

1.6 Conclusions and Overview of Thesis

AGPCRs are a widely expressed and diverse group of receptors with dramatic variations in the organization of their ECRs. Many mechanisms have been proposed for how ECRs mediate signaling by the 7TM. Given the evidence reviewed here, we propose that AGPCRs primarily engage in ligand- and shear force-dependent tethered-peptide-agonist or allosteric modes of activation. A fuller understanding of the modes of activation is desirable as two fundamental research questions linger: 1) There is little clarity to how endogenous ligands influence AGPCR activity; and 2) there exists no solved structure of a full-length or TA-activated AGPCR. Consequently, AGPCRs have few pharmacological tools and remain untapped as therapeutic targets. This thesis addresses these questions by detailing the first cryo-EM structures of active and inactive forms of two distantly related receptors, and by identifying novel, potent small molecule agonists and antagonists for a model AGPCR.

In Chapter 3, we discuss the high-resolution cryo-EM structures of the TA-activated forms of GPR56 (ADGRG1) and LPHN3 (ADGRL3). Our structures revealed a conserved mechanism whereby the tethered agonist, once decrypted from the GAIN domain, weaves under ECL2 to bind to the orthosteric site in a partial helix conformation. Using mutational analysis, we discovered that the TA forms critical interactions with TMs 1, 2, 6, 7, and ECL2. We also address current models of allosteric activation by highlighting low-resolution structures of the inactive, NTF-bound forms of these receptors. These structures revealed that the NTF is a flexible region distal to the CTF, and likely does not form lasting interactions with the extracellular face of the 7TM.

In Chapters 4 and 5, we discuss our efforts to expand the pharmacological toolbox for AGPCRs by conducting cell-based high throughput screens for agonists and antagonists of GPR56. Over 200,000 compounds were screened for their ability to activate a TA-compromised form of GPR56, and over 20,000 compounds were screened for their ability to inhibit constitutively active GPR56 7TM. After thorough reconfirmation and validation of hits, we identified hexahydroquinoline derivatives as potent, selective agonists for GPR56 that are predicted to bind to the orthosteric site. We also identified antagonists that robustly inhibited platelet aggregation in a seemingly GPR56-dependent manner. Our agonist screen is further discussed in Chapter 4, and our antagonist screen is further discussed in Chapter 5.

Chapter 2 Materials and Methods

2.1 Reagents and Antibodies

[^{35}S]- GTPγS was from PerkinElmer. GTPγS was from MilliporeSigma. Rhotekin-BD beads were from Cytoskeleton, Inc. Steady-Glo Luciferase kits were from Promega. Rabbit Anti-GPR56 C-terminus was purchased from EMD Milipore. Sheep Anti-GPR56 N-terminus was purchased from R&D Systems. Mouse Anti-Penta His was purchased from Qiagen. Mouse Anti-Flag (THETM DYDDDDK Tag Antibody-HRP) was purchased from GenScript. Donkey anti-sheep IgG Alexa-Fluor 647, Donkey anti-mouse 800CW, and Donkey anti-rabbit 800CW was purchased from LICOR. MonoQ 10/100, MonoS 10/100, HiTrap, Superdex 200, and HiPrep 26/60 columns were purchased from GE Healthcare. Fresh compound powders were obtained from MolPort, Inc. and reconstituted in anhydrous DMSO. Coelenterazine h for dual SRE-Luciferase assays was from NanoLight Technologies and reconstituted in 70% v/v ethanol. The synthetic peptidomimetics or activating peptides (AP) GPR56/GPR114 P19 (TYFAVLMQLSPALVPAELL-NH_2) and GPR56 P7 (TYFAVLM-NH_2) were synthesized and HPLC purified by GenScript, dissolved in anhydrous DMSO, and stored under argon.

2.2 Plasmids and Cloning

Human GPR56 (Accession number NM_201524) was used as a PCR template for full-length, 7TM, or ΔTA truncation variants and subcloned into pcDNA3.1+ or pFastBac1 [33]. GPR110 (DNAsu.org, HsCD00295179), GPR114 (DNAsu.org, HsCD00513127), LPHN3 (gift from Demet Arac), and GPR97 (DNAsu.org, HsCD00304871) were used as a PCR template for

7TM or truncation variants and cloned into pFastBac1 [33, 61, 114]. Human muscarinic acetylcholine receptor 1 (M1R) was purchased from cDNA.org (MAR0100000) and subcloned into pFastBac1. All point mutations were generated by QuickChange PCR using 33-bp primers (15 bases flanking each 3-base mutation). Renilla luciferase plasmid phRLuc-N1 was purchased from PerkinElmer, and firefly luciferase pGL4.33 (*luc2*/SRE/Hygro) was purchased from Promega.

2.3 Chemical Libraries

The use of all chemical libraries was purchased from the University of Michigan Center for Chemical Genomics. Chemical libraries were cherry-picked collections from larger libraries to select for available dry powders with low molecular weight (< 500 Da), favorable Lipinski drug-like properties [158], and flexibility for derivatization. The MB24K library is a set of ~23,500 compounds derived from the Maybridge™ library with an average molecular weight of 328 Da, LogP of 3.31, and over 99% rate of favorable Lipinski conditions. The ChemDiv library is a set of ~100,000 compounds derived from the public ChemDiv™ library with an average molecular weight of 364 Da, LogP of 2.73, and 100% rate of favorable Lipinski conditions. The DART90K library is a set of ~83,000 compounds cherry picked from a 264,000-compound library from Dart Neuroscience™ with an average molecular weight of 334 Da, LogP of 2.86, and 99.99% rate of favorable Lipinski conditions. All libraries are reconstituted in DMSO at stock concentrations of 10 mM.

2.4 Insect Cell Culture and Baculovirus Production

Spodoptera frugiperda 9 *(Sf*9) and *Trichoplusia ni* (*Tni*, High Five) cells were cultured in ESF921 medium (Expression Systems). Recombinant baculoviruses for G proteins and GPCRs

were prepared from pFastBac1 donor constructs using the Bac-to-Bac™ system as per the manufacturer's instructions. Briefly, pFastBac1 constructs were transposed into competent DH10Bac cells (Invitrogen), after which cells were plated onto triple antibiotic Luria-Broth (LB) agar plates containing 50 μg/mL kanamycin, 10 μg/mL tetracycline HCl, 7 μg/mL gentamicin, 40 μg/mL isopropyl β-d-1-thiogalactopyranoside (IPTG) and 75 μg/mL halogenated indolyl-β-galactoside (BluoGal) for blue/white colony screening. White colonies were restreaked and used to inoculate triple antibiotic LB liquid medium for bacmid DNA preparation. Bacmid DNA (3 μg) was transfected into 9 x 10^5 adherent *Sf*9 cells in 6-well format using Fugene HD™ transfection reagent (Promega). After five days, viral supernatants were harvested and amplified twice in *Sf*9 cells at an infection ratio of 1:100. For expression of receptor, high titer baculoviruses were used to infect 50-200 mL cultures of High-Five cells at a ratio of 1:100 for 48 h, after which cells were centrifuged at 2000 g and frozen for cell membrane preparation. For expression of G proteins, a dual-dual baculovirus system was used, whereby High-Five cells were infected with two viruses: one virus encoding both $His_8G\beta_1$ and $G\gamma_2$, and one virus encoding Gα and either Ric-8A (for $G\alpha_q$, $G\alpha_{13}$, and $G\alpha_{12}$) or Ric-8B (for $G\alpha_{s,short}$). $His_8G\beta_1/G\gamma_2$ virus was used to infect cells at a ratio of 1:100, and Gα/Ric-8 virus was used to infect cells at a ratio of 1:40.

2.5 Protein Purification

2.5.1 General Purification of G Protein Subunits

Purifications of G protein subunits $G\alpha_q$, $G\alpha_{12}$, and $G\alpha_{s,\ short}$ from Sf9 cells were done using a his-tagged $His_8G\beta_1\gamma_2$ association method as described [159-161]. Purification of untagged $G\beta_1\gamma_2$ from *E. coli* was done using a his-$G\alpha_{i1}$ association method as described [162].

2.5.2 Purification of $G\alpha_{13}$

$G\alpha_{13}$ was purified using a slight modification of the $His_8G\beta_1\gamma_2$ association method [159-161]. Large-scale membrane homogenates were prepared from pellets of *Tni* cells overexpressing $G\alpha$, Ric-8A, $His_8G\beta_1$ and $G\gamma_2$. Membrane homogenates were detergent extracted in 1% w/v sodium cholate with gentle stirring for 1 h at 4ºC. The cholate extract was centrifuged at 100,000 x g for 1 h, and the clarified supernatant was diluted 4-fold with 0.5% w/v decaethylene glycol mono-dodecyl ether (lubrol), filtered through a 0.4 μm filter, and loaded onto Ni^{+2}-NTA resin in a gravity driven column. The column was washed with a high salt buffer (20 mM Hepes pH 8.0, 300 mM NaCl, 1 mM $MgCl_2$, 10 mM imidazole, 10 mM βME, 10 μM GDP, 0.5% lubrol, and protease inhibitor cocktail [23 μg/mL phenylmethylsulfonyl fluoride, 21 μg/mL N-p-tosyl-L-lysinechloromethyl ketone, 21 μg/mL L-1-p-tosylamino-2-phenylethylchloroketone, 3.3 μg/mL leupeptin, and 3.3 μg/mL lima bean trypsin inhibitor]) and eluted with an aluminum fluoride (AMF) buffer (20 mM Hepes pH 8.0, 100 mM NaCl, 50 mM $MgCl_2$, 10 mM βME , 20 μM GDP, 10 mM NaF, 30 μM $AlCl_3$, 1% n-octyl-β-d-glucoside). The AMF eluate was resolved over a HiPrep 26/60 Sephacryl S-200 column to isolate monomeric $G\alpha$ and to buffer exchange the protein into storage buffer (20 mM Hepes pH 8.0, 100 mM NaCl, 0.5 mM EDTA, 2 mM $MgCl_2$, 1 mM DTT, 10 μM GDP, 11 mM CHAPS). The $G\alpha$ protein was collected and concentrated in an Amicon ultracentrifugal concentration device with 30,000 MWCO and cryopreserved at -80 ºC.

2.5.3 Purification of Inactive (NTF-bound) and Active (TA-bound) GPR56 and LPHN3

Construct design, expression, and purification of GPR56 and LPHN3 complexes for cryo-EM studies were conducted by a collaborating group as described [163].

2.6 AGPCR Membrane Homogenate Preparation

Insect cell pellets overexpressing adhesion GPCRs were thawed at 37 ºC and resuspended in 20 mL of lysis buffer (10 mM Hepes pH 7.4, 1 mM EGTA, and protease inhibitor cocktail). The cell suspension was lysed by nitrogen cavitation at 600 PSI. Cell lysates were centrifuged at 100,000 x g for 30 min. The supernatants were discarded, and membrane pellets were Dounce homogenized into 5 mL of ice-cold lysis buffer with or without 7M urea. The homogenates were recentrifuged at 100,000 g for 30 min and washed by Dounce homogenization into ice cold lysis buffer without urea. Membranes were recollected at 100,000 g and Dounce homogenized into 2 mL of lysis buffer containing 12% w/v sucrose and cryopreserved into small aliquots.

2.7 [^{35}S]-GTPγS Binding Assays

For all assays, adhesion GPCR membrane homogenates (5 µg non-treated homogenates / assay time point, or equivalent volume of urea-treated homogenates) were reconstituted with 200 nM purified Gα (Gα_{13}, Gα_{q}, or G$\alpha_{s,short}$) and 500 nM purified Gβ_1Gγ_2 in binding buffer (50 mM Hepes pH 7.4, 1 mM dithiothreitol (DTT), 1 mM EDTA, and 3 µg/mL purified BSA (NEB)). To initiate GTPγS binding, the reconstituted membrane homogenates were combined 1:1 with binding buffer containing 50 mM NaCl, 10 mM $MgCl_2$, 20 µM GDP, and 4 µM [^{35}S]-GTPγS (25-50,000 cpm / pmol). Endpoint assays were quenched with 20 mM Tris pH 7.7, 100 mM NaCl, 10 mM $MgCl_2$, 1 mM GTP, 0.08% w/v lubrol C12E10 and filtered through Whatman GF/C glass microfiber filters using a Brandel Harvester. The filters were washed, dried, and subjected to liquid scintillation counting. For compound activation and inhibition experiments, reconstituted membranes were pre-incubated with DMSO or compounds for 10 minutes at RT prior to the start of reactions with DMSO content of ≤ 1.0 % v/v.

2.8 Measurement of AGPCR Cell Surface Levels

Sf9 cultures were infected with 1/100 volume of amplified AGPCR viruses (GPR56 7TM WT, F454A, and W617A; LPHN3 7TM WT, F914A, and W1086A) for 36 h. Cells were washed with cold PBS and protease inhibitor cocktail prior to incubation with 2 mM Sulfo-NHS-LC-Biotin (ThermoFisher) in PBS for 15 min at RT. Cells were quenched and washed twice with TBS and lysed at 4 °C for 30 min in lysis buffer (25 mM Hepes pH 7.4, 150 mM NaCl, 2 mM $MgCl_2$, 1 mM EDTA, 1% w/v Triton X-100, 2% v/v glycerol, protease inhibitor cocktail). Lysates were clarified by centrifugation at 21,000g, incubated with a 50 μL bed volume of G25 Sephadex, and reclarification at 21,000g. The supernatant was tumbled at 4 °C for 1 h with a 40 μL bed volume of Streptavidin Sepharose HP (Cytiva). The resin was washed two times with lysis buffer and eluted with reducing SDS–PAGE sample buffer at 42 °C. AGPCRs were resolved by SDS–PAGE and immunoblotted with the pentaHis antibody (Qiagen).

2.9 Luciferase Reporter Assays

2.9.1 Large-Scale Transfection an Cryo-Preservation of Cells

HEK293T cells were seeded in Corning Hyper*Flasks* at 1.72 x 10^8 cells per flask in 550 mL of Dulbecco's modified Eagle's medium (DMEM) containing 10% v/v FBS 24 h prior to transfection. Cells were transfected with 200 μg of SRE-Luc plasmid and 400 μg of GPR56 (ΔTA or 7TM)-pcDNA3.1(+), or pcDNA3.1(+). Transfections were conducted using polyethylenamine (PEI) as described [33]. Plasmid DNAs were added to 15 mL of Optimem (Gibco), and mixed 1:1 with 15 mL of 100 μg/mL PEI in optimem. Transfection mixtures were incubated at 22 ºC for 15 min and added to 500 mL of fresh DMEM containing 10% v/v FBS. Medium in the Hyper*Flasks* was decanted and replaced with the transfection media. The flasks were incubated for 6 h at 37 ºC

with 5% CO_2. Medium was removed and cells were trypsinized using 0.05% w/v trypsin in Puck's G Salt Solution (PSG)-EDTA (137 mM NaCl, 5.4 mM KCl, 1.1 mM KH_2PO_4, 1.1 mM $NaHPO_4$, 1 mM EDTA, pH 7.0) for 5 min. Cells were diluted in medium, centrifuged at 500 g for 5 min, and suspended at 22 x 10^6 cells/mL in DMEM containing 10% v/v FBS and 10% v/v DMSO. The cell suspension (1 mL) was filled per Nunc cryopreservation vial cells and frozen at -80 ºC overnight in Mr. Frosty™ freezing containers prior to long-term storage under liquid N_2.

2.9.2 High Throughput Luciferase Assay

Cryopreserved cells were thawed at 37 ºC and diluted to 1.25 x 10^5 cells/mL in Fluorobrite™ medium (Gibco) supplemented with 0.1% v/v FBS, 20 mM HEPES pH 7.4, and 2 mM L-glutamine. Diluted cells were filtered through a 40 μm cell mesh and used to seed 8 x 384-well opaque white plates at 5,000 cells per well in 40 μL using a Thermo Scientific™ Multidrop™ combi reagent dispenser. Cells were incubated at 37 ºC in a 5% CO_2 atmosphere for 4 h. After incubation, 200 nL of 2 mM compounds in DMSO were added to each well using a Sciclone ALH 3000 V&P pintool to achieve a final compound concentration of 10 μM and 0.5% v/v DMSO. GPR56/114-AP 19-mer peptide in DMSO was diluted to 90 mM in Fluorobrite medium, and 11.5 μL was added to the final two columns of each 384-well plate using the combi reagent dispenser to achieve a final concentration of 20 μM. 18 h after compound and peptide dispensing, plates were centrifuged at 300 g for 3 min and the upper 20 mL of medium was aspirated using a Biotek EL 406 plate washer. Promega Steady-Glo (20 μL) was added to each well using the combi reagent dispenser, and the plates were placed on a plate shaker at 600 rpm for 5 min. After shaking, the plates were incubated for 10 min in the dark and luminescence was read using a PHERAstar FSX microplate reader. For evaluation of screen quality, the ratios between standard deviations

and means of positive and negative controls were used in a Z' score equation for each plate screened [164]:

$$Z' = 1 - \frac{(3\sigma_{c+} + 3\sigma_{c-})}{|\mu_{c+} - \mu_{c-}|}$$

Where σ represents the standard deviation and μ represents the mean of the positive (c+) or negative (c-) controls. A score of >0.5 was used as a threshold for an assay that was suitable for screening.

2.9.3 Reconfirmation of HTS Hits

A Sample Preparation Technologies (SPT) Labtech MosquitoTM instrument was programmed to dispense 200 nL of selected activator compounds in to 384-well white opaque plates. Cryopreserved HEK293T cells pre-transfected with the SRE-luciferase reporter and GPR56 ΔTA or pcDNA3.1 were thawed and seeded into the awaiting compound-seeded plates at 5,000 cells per well. The plates were processed as described above with Promega Steady-Glo to measure luciferase signals.

2.9.4 Directed Dual SRE-Luciferase Assay

Early passage HEK293T cells were used to seed 15 cm tissue culture plates at 15 x 10^6 cells per plate and were incubated at 37 ºC 5% CO_2 for 18 h. Each plate was transfected with 74 ng phRLuc-N1, 7.43 μg SRE-Luc plasmid, and 18.57 μg of either receptor plasmid (GPR56 ΔTA, GPR56 7TM, and GPR56 full-length) or empty pcDNA3.1(+) using the PEI method described above. After 6h the cells were lifted with 0.05% trypsin in PSG-EDTA, spun at 500 g for 5 min, and resuspended at 8 x 10^6 cells per mL in DMEM + 10% FBS + 10% v/v DMSO. Cells were aliquoted into cryopreservsation vials at 1 mL / vial and frozen at -80 ºC overnight in Mr. Frosty™ freezing containers prior to long-term storage under liquid N_2.

Prior to each assay, cells were thawed at 37 ºC, washed in warm DMEM + 10% v/v FBS, and seeded into 96-well plates at 80,000 cells per well in 100 µL of medium. After 16-18 hours, cells were serum starved for 4 h before being treated with 1 µL of compounds or peptides with a final DMSO content of < 1% v/v. After 8 h, the plates were spun at 300 g for 3 min and the top 50 µL from each well was withdrawn and replaced with 50 µl of Promega SteadyGlo reagent. Plates were shaken at 500 rpm for 5 min and luminescence was read at 1 second per well.

2.10 Preparation of Washed Platelets

Blood was drawn into vacutainers containing sodium citrate. Citrated blood was centrifuged at 200 g for 10 min to separate platelet-rich plasma (PRP) from RBCs. PRP was transferred to tubes containing 10% vol/vol acid citrate dextrose solution (ACD) and apyrase (0.02 U/mL) and centrifuged at 2,000 x g for 10 min. The platelet count was adjusted to 3 x 10^8 platelets/mL with Tyrode's buffer (137 mM NaCl, 2.7 mM KCl, 1 mM $MgCl_2$, 1.8 mM $CaCl_2$, 0.2 mM Na_2HPO_4, 12 mM $NaHCO_3$, 5.5 mM D-glucose) and the platelet suspension was allowed to sit at RT for 30 minutes prior to assays.

2.11 Platelet Aggregometry Assays

250 µL of washed platelets in Tyrode's buffer was pipetted into glass micro cuvettes containing stir bars and warmed to 37 ºC for 5 minutes within a Chrono-Log™ Model 700 Whole Blood/Optical Lumi-Aggregometer. 2.5 µL of compounds (DMSO, 5 mM GPR56-AP, or 5 mM PAR4-AP) was added to each cuvette, and aggregation was recorded over the course of 5 minutes. For inhibition experiments, 1.25 µL of Maybridge inhibitors were pre-incubated with platelets for 5 minutes prior to stimulation with 1.25 µL of either 10 mM GPR56-AP or 10 mM PAR4-AP.

Chapter 3 The Tethered-Peptide Agonist Activation Mechanism of Adhesion GPCRs

This chapter was adapted from the publication, Barros-Alvarez, X.*, Nwokonko, R.*, Vizurraga, A.*, Matzov, D.*, He, F., Papasergi-Scott, M., Robertston, M., Panova, O., Yardeni, E., Seven, A., Kwarcinski, F., Su, H., Peroto, M., Meyerowitz, J., Shalev-Benami, M., Tall, G., Skiniotis, G., *The tethered peptide activation mechanism of adhesion GPCRs.* Nature, 2022. **604**(7907): p. 757-762. [163]

*These authors contributed equally

3.1 Abstract

Adhesion G-protein-coupled receptors (AGPCRs) are a subset of class B receptors known for containing large, highly diverse extracellular regions that mediate *trans* interactions to regulate a variety of cellular processes. A conserved self-cleaving GPCR autoproteolysis-inducing (GAIN) splits the receptor into two fragments (the N-terminal fragment, and C-terminal fragment) that are held together by noncovalent interactions. Dissociation of the fragments results in exposure of a small stalk sequence on the N terminus of the C-terminal fragment that acts as a tethered agonist (TA) to bind to the GPCR component of the receptor and activate signaling. Despite an abundance of evidence for TA activation of AGPCRs, its mechanism of action remains poorly understood. In this study, we provide cryo-EM structures of two distantly related AGPCRs, GPR56 (aka ADGRG1) and LPHN3 (aka ADGRL3), in two activation states: an inactive, TA-encrypted state, and an active, TA-bound state with the N-terminal fragment removed. Low-resolution maps of the inactive structures indicate that the ECR is flexible and sequesters the TA far away from the

orthosteric site. High-resolution structures of the C-terminal fragments of GPR56 and LPHN3 reveal a conserved activation mechanism by which the decrypted TA bends down into the orthosteric site to adopt a partial helix conformation and interaction with TMs 1, 2, 6, 7, and extracellular loop 2. TA binding results in breaks in the middle of transmembrane helices 6 and 7 that enhance G protein coupling. Collectively, these structures highlight an activation mechanism that is likely conserved across all AGPCRs.

3.2 Introduction

Adhesion G protein coupled receptors (AGPCRs) are a 33-member subclass of class B receptors (family B2) that uniformly contain large, diverse extracellular regions (ECRs) and play critical roles in several cellular processes including cell migration, shape, polarity, differentiation, and immune response [21, 107, 165-167]. AGPCR regulation of these processes occurs through *trans* interactions between variable regions of their ECRs and soluble or anchored ligands. Every AGPCR ECR contains a highly conserved GPCR autoproteolysis incuding (GAIN) domain that constitutively cleaves the receptor into two components: the extracellular N-terminal fragment (NTF), and the C-terminal fragment (CTF), also known as the seven-transmembrane (7TM) or GPCR domain, that couples to G proteins. Autoproteolysis occurs early on the ER during protein maturation and the resulting fragments remain held together by non-covalent interactions within the GAIN domain as the receptors are trafficked to the cell surface ([30, 168]).

AGPCR cleavage occurs at the GPCR proteolysis site (GPS), located deep within the $GAIN_B$ subdomain on the loop between the final 12^{th} and 13^{th} β-strands [10]. Thus, the resulting NTF and CTF components are held together by a ~20-25 residue stalk tethered to the GPCR component of the receptor. The N-terminal seven residues of the CTF stalk, comprising GAIN β-strand 13 in the holoreceptor form, are extremely conserved across all AGPCRs and serve as a

hydrophobic *tethered-peptide-agonist*, or tethered agonist (TA), for the receptor following fragment dissociation. In the current model of AGPCR orthosteric activation, force-mediated dissociation of the NTF and CTF frees the cryptic tethered agonist from the GAIN domain, and unfavorable interactions with the aqueous environment force the TA to bend inward to interact with the orthosteric site of AGPCRs to activate the receptor and initiate G protein signaling. Fragment dissociation is hypothesized to occur via shear force in relation to a presented extracellular anchored ligand. Orthosteric agonism is supported by *in vitro* models of AGPCR dissociation, such as urea treatment or culture shaking, which result in dramatic increases of G protein signaling. Additionally, CTF-only truncation variants of AGPCRs demonstrate constitutively active signaling that is TA-dependent. [33, 50-53]. Tethered agonist activation is further supported by the use of synthetic TA peptidomimetics. Peptides mimicking the sequence of the TA robustly activate AGPCRs both *in vitro* and *in vivo* [33, 34, 56, 57, 59, 60]. However, despite an awareness that the TA engages the orthosteric site to initiate signaling, the exact mechanism for how the TA interacts with the CTF is largely unknown.

GPR56 and LPHN3 are two distantly related AGPCRs with distinct ECRs and physiologies. GPR56 is a widely expressed receptor of the G subfamily (also known as group VIII) known to regulate immune system functions, platelet activation and hemostasis, neuronal myelination and brain development, muscular function, and testicular development [110, 113, 149, 150, 169-173]. N-terminal to its GAIN domain, GPR56 possess a pentraxin/laminin/neurexin/sex-hormone-binding-globulin-like (PLL) domain that interacts with collagen III and transglutaminase-2 to initiate $G_{12/13}$ signaling [83, 110, 174, 175]. Dysregulation of GPR56 results in the pathogenesis of several types of cancer and the neurodegenerative disease bilateral frontoparietal polymicrogyria (BFFP), making it a notable oncogene and prospective biomarker

for cancer [68, 76, 112, 176-182]. LPHN3 is a member of the L subfamily (aka group I) and is abundant in the central nervous system, where it engages in transsynaptic signaling complexes with anchored ligands like teneurins or fibronectin-like-domain-containing leucin-rich transmembrane proteins (FLRTs) [89, 90, 120, 122]. Like GPR56, LPHN3 signals through $G_{12/13}$ family G proteins to regulate rho-dependent cytoskeletal changes involved in synaptogenesis and axonal growth [89, 120, 142]. In addition to the GAIN domain, LPHN3 ECR contains a lectin binding domain (LEC) and an olfactomedin-like domain (OLF) that stabilize transsynaptic complexes, as well as a hormone-binding (HormR) domain that resembles typical HormR regions on class B1 GPCRs [8, 89, 90]. Variations in LPHN3 has been linked to the development of attention deficit hyperactivity disorder (ADHD), making it as a potential therapeutic target [126, 183, 184].

Within the last decade structural knowledge of adhesion GPCRs has rapidly advanced, particularly with respect to their ECRs. Partial or full cryo-EM structures have been determined for the NTFs of GPR56, LPHN1, GPR126, BAI3, and GPR110 [10, 27, 80, 83]. Additionally, the structure of partially activated glucocorticoid-bound GPR97 7TM was recently solved in complex with G_o [185]. However, no structures have been revealed of an intact AGPCR 7TM domain with its tethered agonist bound to the orthosteric site, obscuring our understanding of tethered agonism. Here, we use protease activated receptor- (PAR-)AGPCR fusion proteins as a proof of concept to demonstrate the tethered agonist mechanism of activation *in vitro*. Following this, we reveal the first cryo-EM structures of both GPR56 and LPHN3 in their constitutively active, G protein-coupled 7TM form with the native peptide engaged. With the aid of biochemical functional data that directly measure G protein activation, we detail a mechanism whereby the tethered agonist, once freed from the GAIN domain, bends under ECL2 to adopt a partial helix conformation deep

within the orthosteric site. Following mutational analysis, we identified three critical residues on the tethered agonist that form hydrophobic interactions with $F^{2.64}$ and $W^{6.53}$ on the 7TM and $W^{45.51}$ on extracellular loop 2 (ECL2). These residues are highly conserved across all adhesion GPCRs, and thus these structures provide insight into a shared activation mechanism that will dramatically advance our understanding of AGPCR biology.

3.3 Results

3.3.1 Activation of Protease-Activated Receptor 1 (PAR1)-AGPCR Fusion Proteins

The tethered agonist mechanism of AGPCRs closely parallels that of the Protease Activated Receptors (PAR1-4). PARs are class A GPCRs that contain small N-terminal leader sequences that, in the activated state, bind to an orthosteric site on the 7TM that includes ECL2 [62-64]. In contrast to AGPCRs, PARs contain no GAIN domain, and their leader sequences are revealed following proteolysis *in trans* through proteases such as thrombin or trypsin. To assess GAIN dependence on AGPCR activation, we designed PAR1-AGPCR fusion proteins that more closely mimicked the thrombin-dependent PAR activation mechanism. We replaced the N-termini of GPR56 and the closely related GPR114, up to the GPCR proteolysis site (GPS), with a sequence that includes an HA signal peptide (HASP), a FLAG tag, and a 42-residue PAR1 sequence derived from the N-terminus of human PAR1, ending in a LDPR/S thrombin cleavage site (**Figure 3.1A**). Thrombin-mediated proteolysis occurs between the R and S residues, and results in a TA sequence of SFAVLM for both receptors.

GPR56 and GPR114 share identical TA sequences, but signal through different G proteins. GPR56 signals through $G_{12/13}$ family G proteins, which can be monitored in cell-based assays with an SRE-luciferase construct, while GPR114 signals through G_s, which can be measured with a CRE-luciferase construct [57]. We transfected PAR1-GPR56 and PAR1-GPR114 into HEK293T

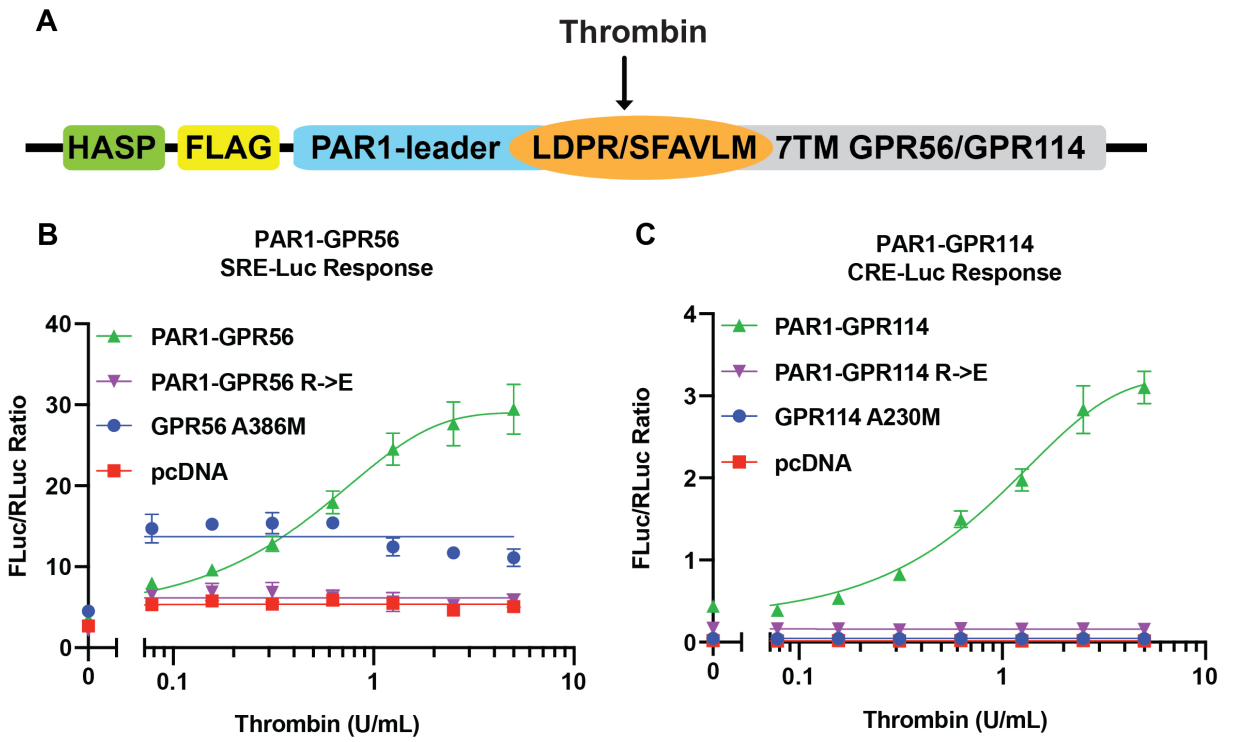

Figure 3.1 Activation of PAR1-AGPCR Fusion Proteins. A. Design of PAR1-AGPCR fusion constructs. The GAIN domains of both GPR56 and GPR114 were replaced with a PAR1 leader sequence that included an N-terminal HA signal peptide (HASP, green), FLAG tag (yellow), and a 42-residue leader derived from the N-terminus of human PAR1 (blue). The leader sequence ends in a thrombin recognition site where proteolysis occurs immediately N-terminal to the tethered agonist, resulting in a TA sequence of SFAVLM (orange). **B.** Activation of PAR1-GPR56 in the SRE-luciferase assay. PAR1-GPR56 and SRE-luciferase gene reporter was transfected into HEK293T cells, and luciferase activity was measured following addition of increasing amounts of thrombin. PAR1-GPR56 (green) is compared with a cleavage deficient R->E point mutant (purple), a low-activity truncation mutant lacking the PAR1 leader (blue), and no receptor at all (red). **C.** Activation of PAR1-GPR114 in the CRE-luciferase assay. PAR1-GPR114 and CRE-luciferase gene reporter was transfected into HEK293T cells, and luciferase activity was measured following addition of increasing amounts of thrombin. PAR1-GPR114 (green) is compared with a cleavage deficient R->E point mutant (purple), a low-activity truncation mutant lacking the PAR1 leader (blue), and no receptor at all (red). All data represent the mean ± SD of three independent experiments.

cells along with either SRE-luciferase or CRE-luciferase, respectively. Following transfection, cells were briefly treated with increasing amounts of human α-thrombin before harvesting for luciferase activity. We found that both fusion proteins demonstrated a robust concentration-dependent increase in signaling following addition of thrombin. Compared to vehicle control, addition of 5 U/mL thrombin resulted in an ~8-fold increase in signal for PAR1-GPR56 and ~7-fold increase in signal for PAR1-GPR114 (**Figure 3.1B-C**, green). We then mutated the arginine residue to a glutamate within the LDPR/S thrombin recognition site for both receptors to abrogate

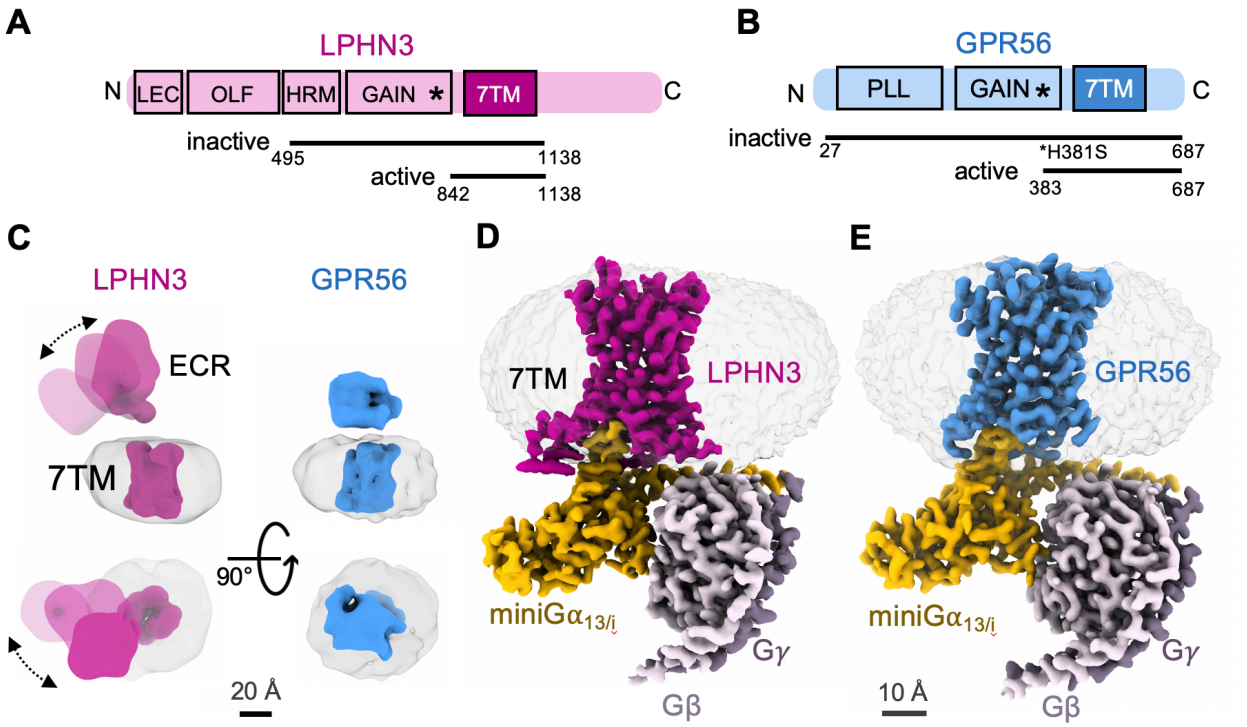

Figure 3.2 Cryo-EM reconstructions for GPR56 and LPHN3. A and **B**, Domain organization of full-length LPHN3 (**A**) or GPR56 (**B**). The GPCR proteolysis site (GPS) is indicated with an asterisk. The range of residues used for inactive and active structures are indicated below the colored full-length schemes. **C**, Low resolution maps for inactive states of LPHN3 (magenta) or GPR56 (blue). Side and top views are shown. For LPHN3, three distinct conformations are superimposed, illustrating the flexibility. Arrows indicate ECR mobility. **D** and **E**, High resolution cryo-EM maps for the activated 7TM forms of GPR56 and LPHN3 in complex with G_{13}.

thrombin cleavage. Both R->E point mutants were largely unaffected by addition of thrombin (**Figure 3.1B-C**, purple). PAR1-GPR56 R->E exhibited a modest ~2-fold increase in signaling, while PAR1-GPR114 R->E exhibited no increase at all. Given that PAR1-GPR56 R->E had basal activity identical to that of no receptor (**Figure 3.1B-C**, red), and that the thrombin response was independent of concentration, the observed increase in signaling is likely from activation of endogenous $G_{12/13}$-coupling PAR receptors. Supporting this, when we transfected GPR56 A386M, a three-residue truncation mutation of GPR56 7TM with no thrombin recognition site, we saw a similar concentration-independent increase in signaling following thrombin treatment. We did not observe this increase when we transfected GPR114 A230M, a truncation mutant similar to GPR56 A386M, in the CRE-luciferase assay.

3.3.2 Cryo-EM Structures of Inactive and TA-Activated GPR56 and LPHN3

We sought to evaluate the cryo-EM structures of two inactive, TA-encrypted AGPCRs to determine how the GAIN domain is positioned with relation to the 7TM domain in the holoreceptor form. Recombinant, cleaved LPHN3 was purified with a truncated ECR that contained the GAIN domain and HormR domain bound noncovalently to the 7TM via the TA (**Figure 3.2A**). Additionally, recombinant GPR56 was purified with a fully intact ECR that included the PLL and GAIN domains. We observed that the ECR of holoreceptor GPR56 spontaneously dissociated during purification, and thus used the cleavage deficient H381S point mutant (**Figure 3.2B**). Due to continuous flexibility of the ECRs, Both GPR56 and LPHN3 could only be resolved to low resolution 3D reconstructions (**Figure 3.2C**). ECR flexibility was more prominent in LPHN3, as its ECR exhibited a much larger range of motion with relation to the 7TM domain compared to GPR56. This is possibly due to a difference in lengths of the stalks between the GAIN and 7TM

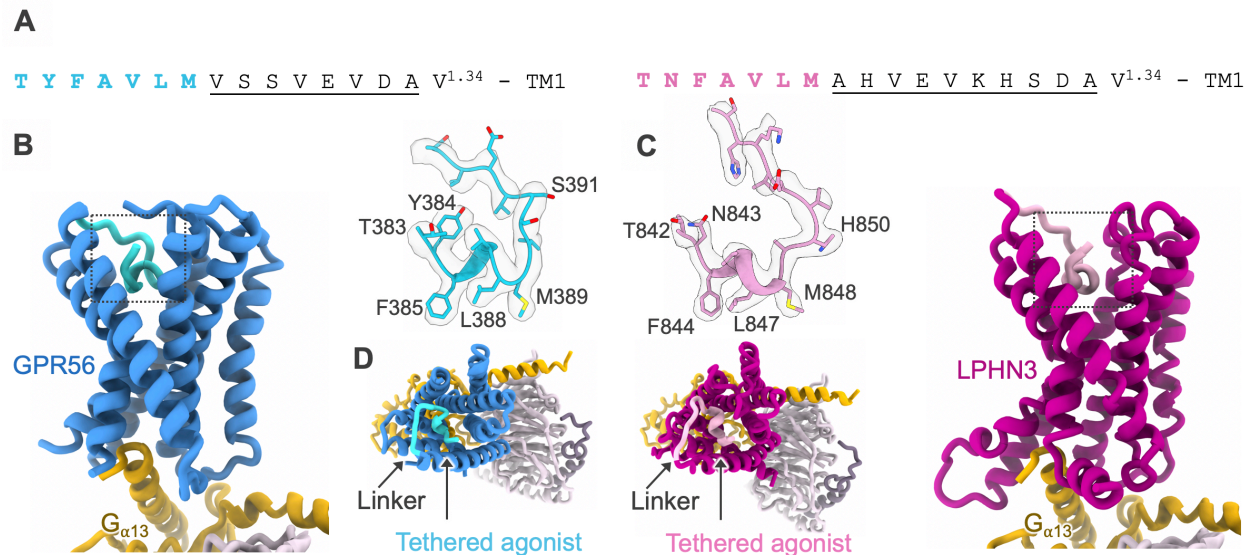

Figure 3.3 Structures of active GPR56 and LPHN3 complexes bound the tethered agonist (TA) peptide. A. Tethered agonist stalk sequences for GPR56 (left, cyan) or LPHN3 (right, pink). The core TA sequence is colored, while the stalk linkers are underlined in black and followed by the first residue of the 7TM, $V^{1.34}$. **B.** Model for the active TA-bound GPR56 7TM/miniG_{13} complex with a box surrounding the tethered agonist binding site (left). Cryo-EM densities and models for the TA peptide are shown with individual residues labeled (right). **C,** Model for the active TA-bound LPHN3 7TM/miniG_{13} complex with a box surrounding the tethered agonist binding site (right). Cryo-EM densities and models for the TA peptide are shown with individual residues labeled (left). **D.** Top-down views of GPR56 (left) or LPHN3 (right) 7TM/miniG_{13} complexes.

regions. LPHN3's stalk is two residues longer, resulting in an approximate 6 Å increase in length. Both low resolution structures collectively suggest that in the holoreceptor form, the GAIN domain does not align closely to the 7TM and instead juts out into extracellular space to serve as a flexible probe for ligands.

To determine the mechanism of TA engagement within the 7TM domain following NTF dissociation, we used constructs of GPR56 and LPHN3 that had their NTF removed up to the GPS, mimicking activated AGPCR CTFs. Both receptors were purified in stable complexes with thermostable miniG_{13} trimer, inspired by the design of mini$G_{\alpha 12}$ [186]. High resolution cryo-EM maps of GPR56-miniG_{13} and LPHN3-miniG_{13} were obtained, with local refinements yielding resolutions of 2.7 Å and 2.9 Å for GPR56 and LPHN3, respectively (**Figure 3.2D-E**).

3.3.3 Structure of the Decrypted Tethered Agonist Engaged in the Orthosteric Site

The N-termini of AGPCR CTFs comprise a 20-25 residue stalk that includes the highly conserved seven-residue core tethered agonist (**Figure 3.3A**). High resolution maps of GPR56 7TM-miniG_{13} and LPHN3 7TM-miniG_{13} allowed for the identification of well resolved densities of the N-terminal stalks embedded deep within the 7TM barrel, as predicted by previous models for tethered peptide agonism (**Figure 3.3B-C**) [15, 33, 34]. In this conformation, the core TA sequence is bent nearly 180º to engage the 7TM via interactions with TM1, TM2, TM6, TM7, and ECL2 (**Figure 3.3D**). Notably, the stalk adopts a semi-helical structure at its lowest point, across residues FAVLM in the TYFAVLM sequence. In both structures, the lowest interacting residues are P3, P6, and P7 on the peptide, which correspond with phenylalanine, leucine, and methionine. These residues are highly conserved across all AGPCRs, with 30 of 33 receptors possessing a TA containing at least two of these residues (**Figure 1.2**).

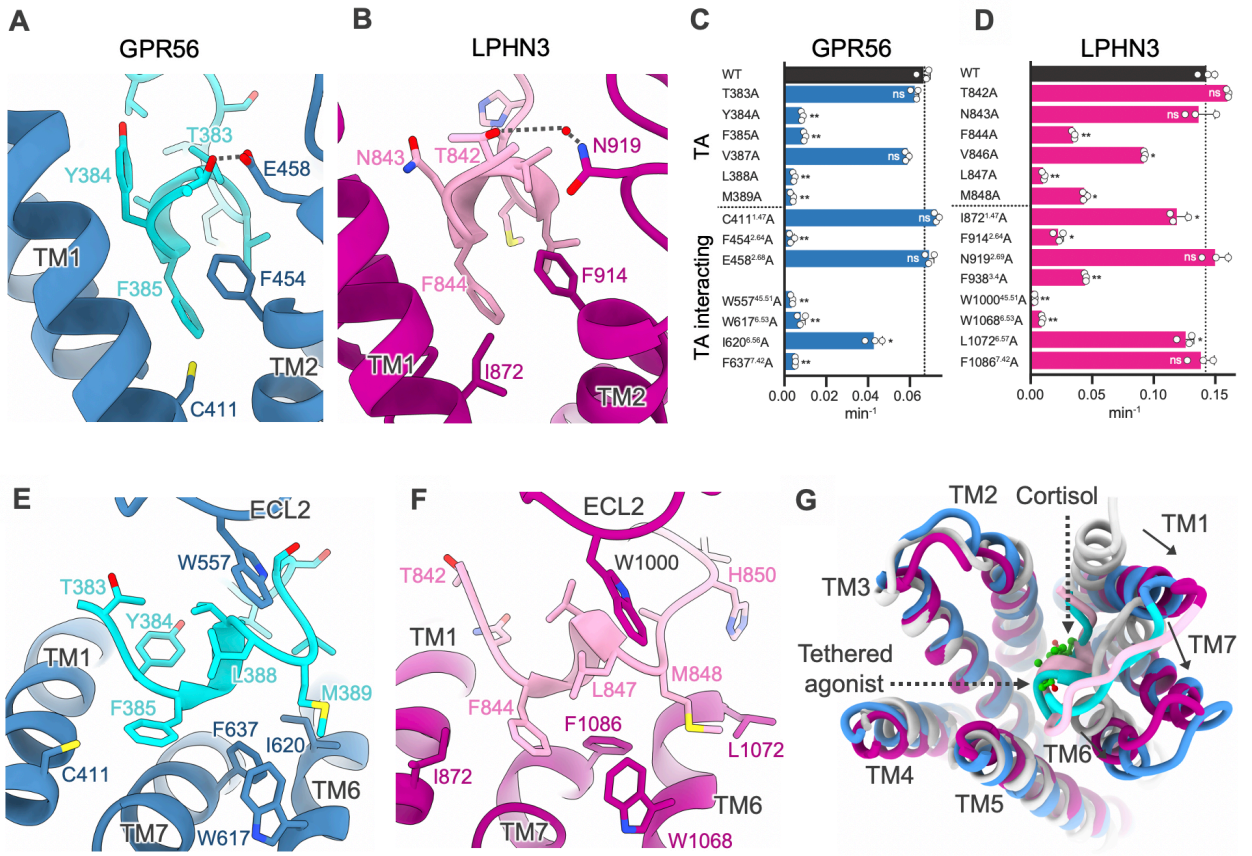

Figure 3.4 Validation of TA-7TM Interactions for GPR56 and LPHN3. A and **B**. Interactions between the TA of GPR56 (**A**) or LPHN3 (**B**) with TM1 and TM2. The TA is colored cyan for GPR56, and pink for LPHN3. **C** and **D.** GTPγS binding to recombinant G_{13} in the GPCR reconstitution assay using membrane homogenates enriched with select GPR56 (**C**) or LPHN3 (**D**) 7TM point mutants that disrupt TA binding. **E** and **F**. Interactions between the TA of GPR56 (**E**) or LPHN3 (**F**) with ECL2 and the hydrophobic core. **G**. Superposition of GPR56 7TM (blue), LPHN3 7TM (magenta), and cortisol-bound GPR97 (white, PDB: 7D77)) structures. Arrows indicate a shift in the relative positions of TM1, TM6, and TM7 with respect to GPR97. The TAs of both GPR56 and LPHN3 are shown to occupy the same region in the orthosteric site as cortisol (carbon atoms in green). Data represent the mean of three biologically independent reactions ± SD. NS, not significant; *P < 0.05, **P < 0.01.

We investigated the observed TA interactions with the 7TM using a GPCR reconstitution assay with membrane homogenates enriched for various alanine point mutants of both GPR56 and LPHN 7TM. One hydrophobic interaction we noticed across both receptors was between phenylalanine of the TA and C411$^{1.47}$ (GPR56) or I872$^{1.47}$ (LPHN3) on TM1 (Wootten numbering in superscript, adapted from the Ballesteros–Weinstein numbering for family A GPCRs [187, 188]) (**Figure 3.4A-B**). Mutating either residue on TM1 resulted in no decrease in G_{13} signaling for GPR56, and only a slight decrease for LPHN3 (**Figure 3.4C-D, Figure 3.8A-B**). However, mutating the phenylalanine on the TA for both GPR56 and LPHN3 resulted in a near complete

loss in signaling. This is consistent with previous observations that the third residue of the TA is highly conserved and essential for receptor activation [33]. In our models, this phenylalanine also forms hydrophobic interactions with F454$^{2.64}$ in GPR56 and F914$^{2.64}$ in LPHN3. These interactions are likely much more important for TA engagement, as mutating either residue resulted in a near complete loss in signaling (**Figure 3.8C-D**).

Another set of interactions we observed was between the TA and ECL2 of both structures. ECL2 is the largest extracellular loop and folds over the top of the orthosteric site to form a plug-like conformation against the TA. A conserved tryptophan in the loop (W557$^{45.51}$ in GPR56, or W1000$^{45.51}$ in LPHN3) dips down into a hydrophobic pocket to interact with the leucine of the TA (**Figure 3.4E-F**). Mutating either the leucine or the tryptophan resulted in abrogation of G_{13} signaling, demonstrating essentiality for tethered agonism. This is further supported by the recent structure of partially activated GPR97, as W421$^{45.51}$ in its ECL2 also dips down towards the orthosteric site near the bound glucocorticoid ligand [185]. Importantly, we noticed a conserved disulfide bond between C$^{3.29}$ on TM3 and C$^{45.50}$ on ECL2, immediately adjacent to W$^{45.51}$, that would confer a stable conformation. We propose that because of this, the tethered peptide of AGPCRs must act as a flexible ligand that weaves into a small opening on the extracellular face of the receptor that is capped by ECL2.

The seventh residue on the TA, a highly conserved methionine, has been previously shown to be essential for tethered agonism, and is further supported by our 7TM models [33]. M389 (GPR56) and M848 (LPHN3) extend deep into the orthosteric pocket to interact with TM6 residues I620$^{6.56}$ or L1072$^{6.56}$, respectively (**Figure 3.4E-F**). Mutation of the TM6 residues to alanine moderately decreased G_{13} signaling, whereas mutating the methionine on the TA eliminated signaling completely (**Figure 3.4C-D**). In both receptors, a much more critical interaction was

observed between the TA methionine and $W^{6.48}$ (W617 in GPR56, W1068 in LPHN3), a residue that also interacted with the glucocorticoid ligand in the partially activated GPR97 structure [185]. Mutating this residue to alanine completely abrogated G_{13} signaling, demonstrating its importance for TA engagement. We postulate that this tryptophan serves a function analogous to the "toggle switch" of class A GPCRs, which changes conformation following ligand binding in order to shift the positioning of TM6 and enable G protein engagement [189]. Taken together, these TA and TA-interacting point mutants reveal a conserved mechanism whereby the hydrophobic 3rd, 6th, and 7th residues of the tethered agonist (typically F, L, and M) interact predominantly with $F^{2.64}$, $W^{45.51}$, and $W^{6.53}$.

Notably, mutation of $W^{6.48}$ to alanine did not significantly decrease the abundances of either receptor in our membrane homogenate preparations (**Figure 3.5**). This observation extends to every other mutation we conducted in this study, save for two that likely destabilized 7TM intramolecular interactions: Q644A in GPR56 and E948A in LPHN3. However, receptor abundance in membrane homogenates is not a direct measurement of cell-surface levels. We additionally performed a cell-surface biotinylation-pulldown experiment of the two lowest activity mutants, $F^{2.64}$A and $W^{6.53}$A, in order to measure receptor expression on the exterior of the cell (**Figure 3.6**). In both receptors, neither mutant substantially lowered receptor abundance, demonstrating that targeted mutations of the 7TM do not dramatically affect receptor trafficking to the cell surface.

3.3.4 Conformation of the Activated AGPCR 7TM Domain

Despite being members of distantly related subfamilies, GPR56 and LPHN3 7TM domains are highly similar, with their tethered agonists aligning at identical locations within the orthosteric site. This site is also where cortisol is bound in the GPR97 structure (**Figure 3.4G, Figure 3.7E**).

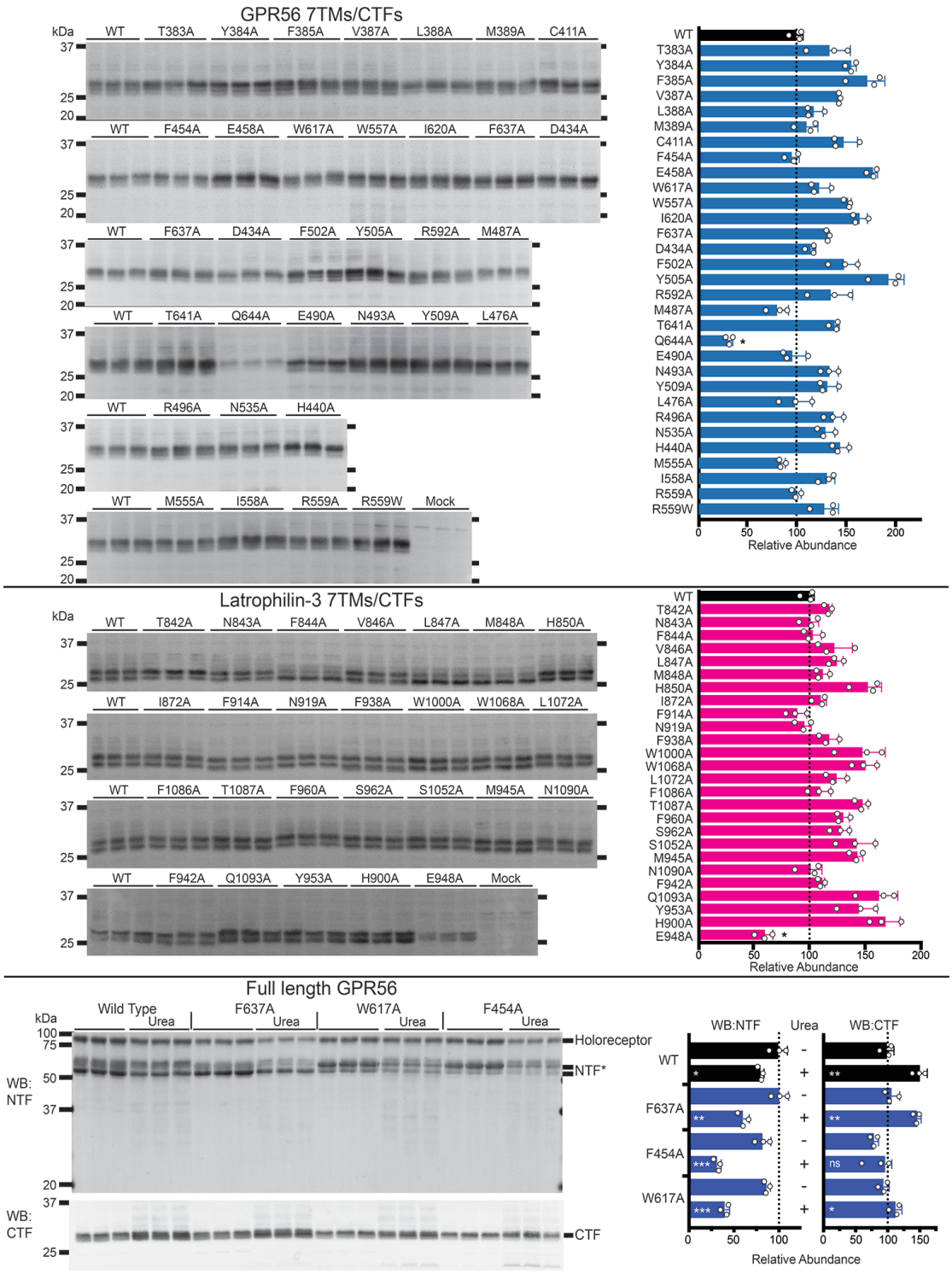

Figure 3.5 Mutant Receptor Abundance in Membrane Homogenates. **A** and **B**. Relative abundances of CTF-only truncated GPR56 (**A**) or LPHN3 (**B**) receptors in membrane homogenates determined by immunoblotting for anti-His tag. **C**. Relative abundances of holoreceptor GPR56 NTFs and CTFs before and after treatment of membrane homogenates with ice-cold 6M urea. CTF was immunoblotted for via a GPR56-specific CTF antibody, and NTF was immunoblotted for via a GPR56-specific NTF antibody. *Multiple glycosylated NTF bands. Data represent the mean band intensity of western blots performed in triplicate with error bars representing ± S.D. Unpaired, two-tailed student's t tests were used to determine significance between wild type and mutant receptors with reduced abundances. * = $p < 0.05$.

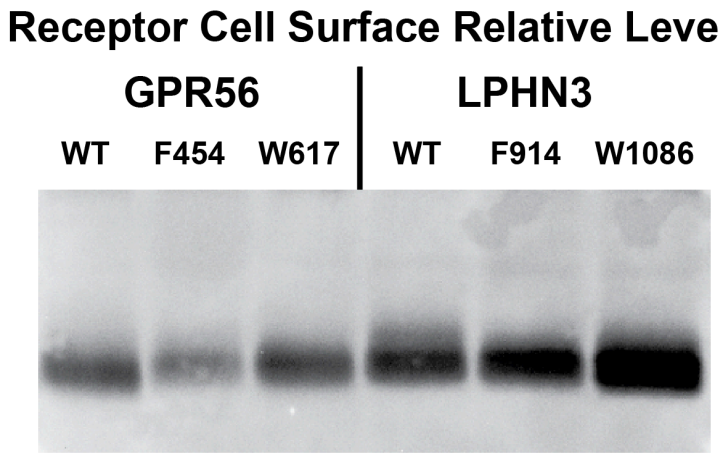

Figure 3.6 Cell-Surface Biotinylation-Pulldown of Low-Activity Mutants. Relative AGPCR cell surface levels for low-activity mutants with impaired TA binding and WT receptors were measured by intact cell biotinylation, followed by streptavidin pulldown and anti-His tag immunoblotting.

On the extracellular side, TM1 bends 180° inwards towards the 7TM barrel where it is stabilized by TA interactions in the orthosteric site. The TA and ECL2 wedge together to occupy a density above the orthosteric site in a plug-like conformation, accommodated by an outward shift of TM7. Paralleling the structure of activated family B1 receptors, TM6 and TM7 are kinked about the two pivot residues $G^{6.50}$ and $G^{7.50}$, respectively [190-192]. These kinks result in an opening of the intracellular side that allows for G protein engagement. Notably, TM6 is not kinked in the activated structure of glucocorticoid bound GPR97, and its TM7 shows only a modest opening on the cytoplasmic side. We anticipate that these differences are a consequence of cortisol acting as a partial agonist that stabilizes an intermediate state of GPR97, in contrast to the natural peptide that stabilized the fully active conformation.

Three residues adjacent to the kink in TM6, the toggle switch $W^{6.53}$ is stabilized in hydrophobic the core of the 7TM barrel by electrostatic interactions with $Q^{7.49}$ (**Figure 3.7C-D**). This residue is also stabilized through coordination with the P6 methionine on the TA, and $M487^{3.47}$ and $F637^{7.42}$ in GPR56 or $M945^{3.45}$ and $F1086^{7.42}$ in LPHN3. Towards the intracellular side of the receptor, the core is further stabilized by electrostatic interactions between $H440^{2.50}$ and

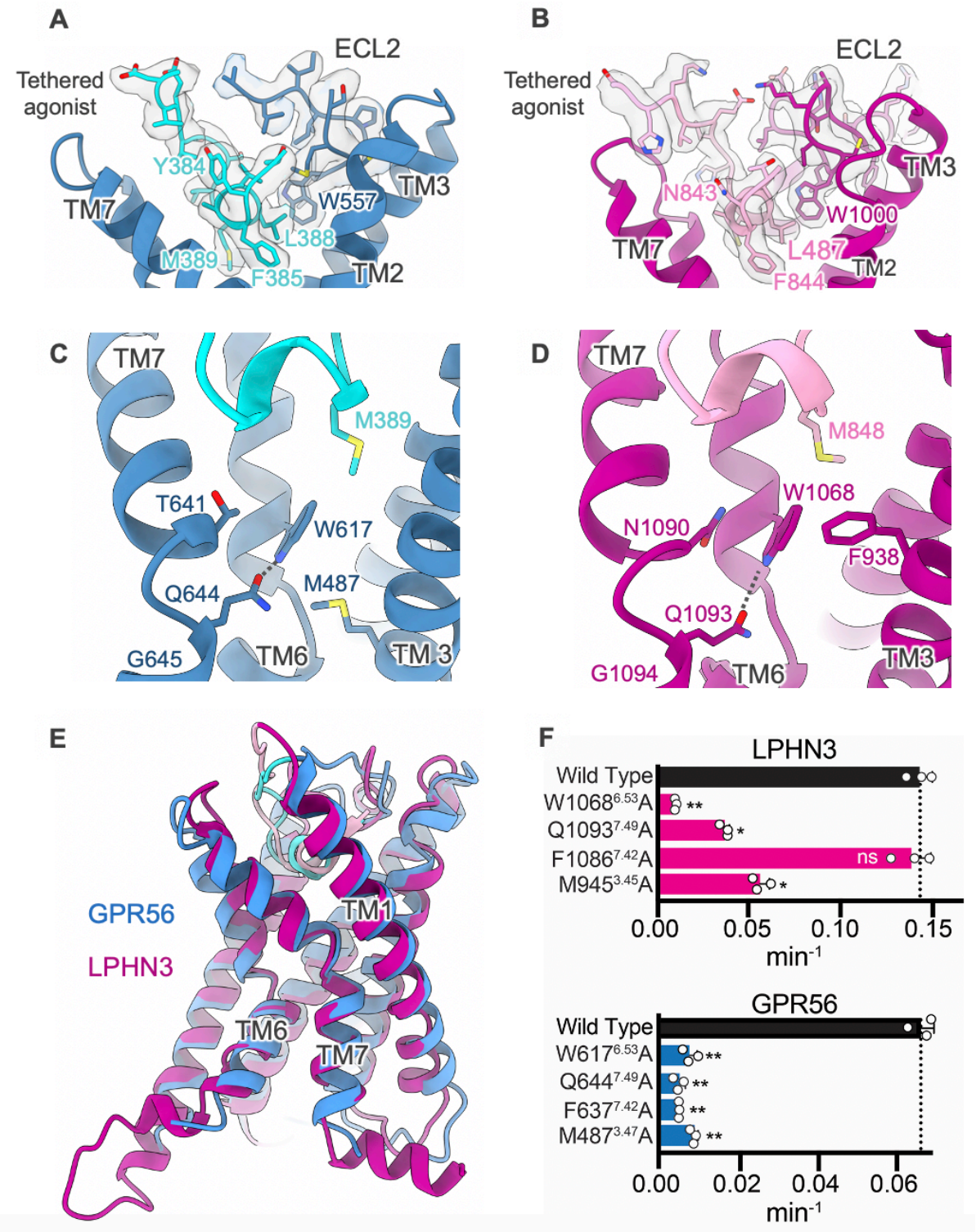

Figure 3.7 Additional Structural Elements Involved in the Active Conformation of TA-bound GPR56 and LPHN3 7TM Domain. **A** and **B**. Density corresponding to the TA peptide and ECL2 in GPR56 (**A**) and LPHN3 (**B**). **C** and **D**. Residues surrounding the toggle switch residue ($W^{6.53}$) in GPR56 (**C**) and LPHN3 (**D**). Dotted grey lines represent electrostatic interactions. **E**. Superposition of the 7TM domains of GPR56 and LPHN3. **F**. G_{13} GTPγS binding activity for mutants LPHN3 (magenta) and GPR56 (blue) that interact with $W^{6.53}$. Data represent mean of biologically independent reactions performed in triplicate with error bars representing +/- S.D. Repeat measures of one-way ANOVA was used to determine significance between mutants and WT. * = $p < 0.05$, ** = $p < 0.01$.

E490$^{3.5}$ in GPR56 or H900$^{2.50}$ and E948$^{3.6}$ in LPHN3. Disruption of most of these interactions destabilized the hydrophobic core and abrogated G_{13} signaling (**Figure 3.7F**, **Figure 3.8E-F**). It is possible that this decrease in signaling could be the result of a dysfunctional or misfolded receptor. To test this, we mutated key TA-binding residues (W617$^{6.53}$, F454$^{2.64}$, and F637$^{7.42}$) in full-length GPR56 with the GAIN domain intact and measured G_{13} signaling changes in response to urea treatment, which sheds the GAIN domain and frees the encrypted TA. Urea treatment caused an increase in initial signaling rates for all mutants, albeit to a much lower extent than in WT

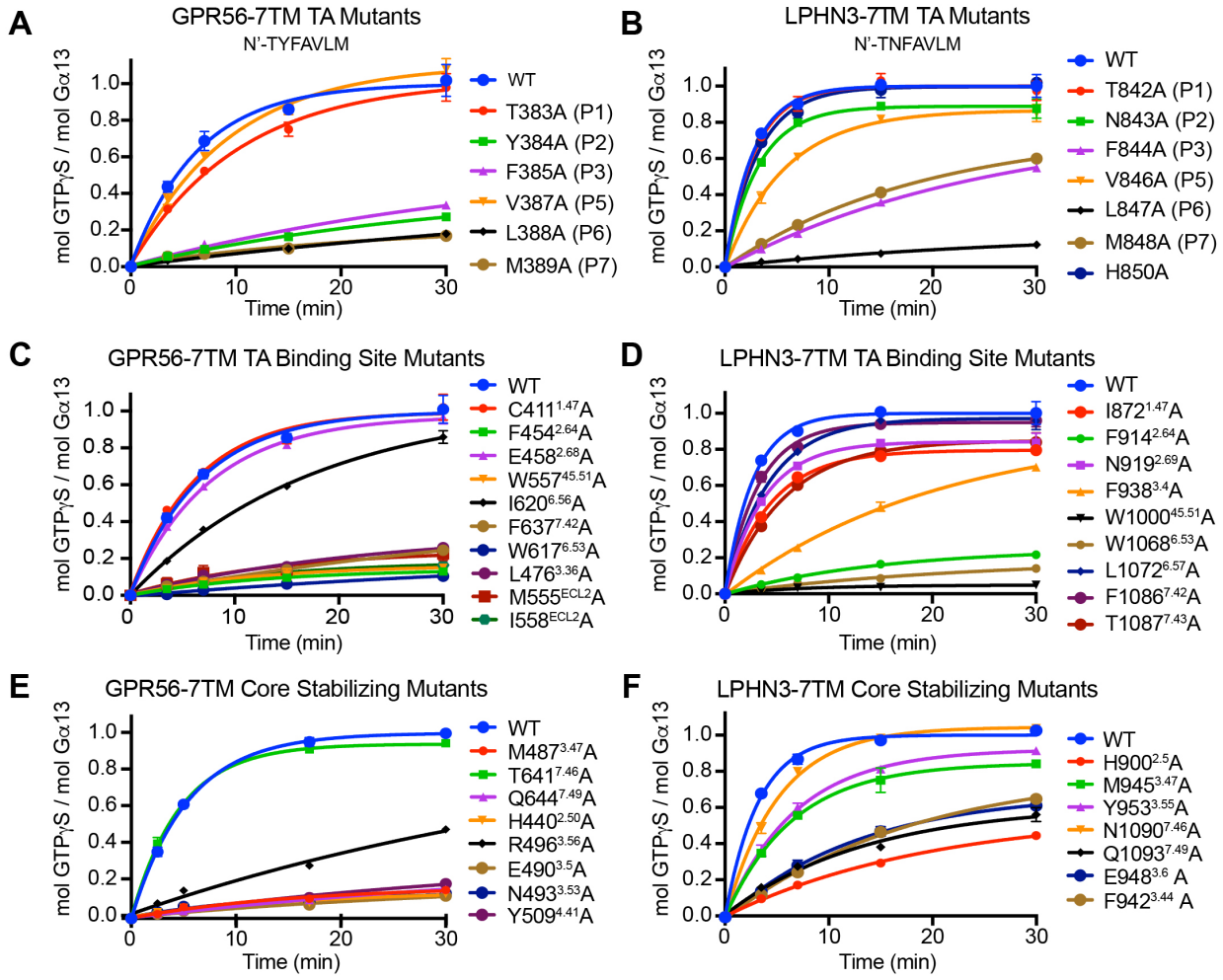

Figure 3.8 Kinetic Measurements of Receptor-Stimulated G_{13} [^{35}S]- GTPγS Binding. Activities of membrane homogenates overexpressing 7TM/CTF-only truncated receptors with point mutations at the TA residues (**A, B**), TA-interacting point mutants (**C, D**), or 7TM core-stabilizing point mutants (**E, F**) in the GPCR reconstitution assay. Note: GPR56 Q644A and LPHN3 E948A were found at low abundance, thus potentially explaining their reduced activities. Data represent the average of each kinetic reaction measured as technical triplicates with error bars representing ± S.D

membrane homogenates. This likely indicates that these mutant receptors are functional and still capable of GAIN cleavage and shedding, but improper TA engagement reduces their signaling capacities.

3.4 Discussion

The activation mechanisms of AGPCRs are poorly understood, especially with respect to their highly conserved tethered agonist ligands. Current literature suggests AGPCRs follow two fundamental modes of activation: allosteric modulation of the GAIN domain to "fine tune" signaling, and orthosteric TA engagement following dissociation of the ECR [15, 33, 45]. Allosteric activation occurs through NTF-targeted ligands that typically induce only modest signaling changes, and likely occurs for receptors that are not cleaved in their holoreceptor form. For instance, antibodies targeted toward the NTF of GPR56 have been used to stimulate modest

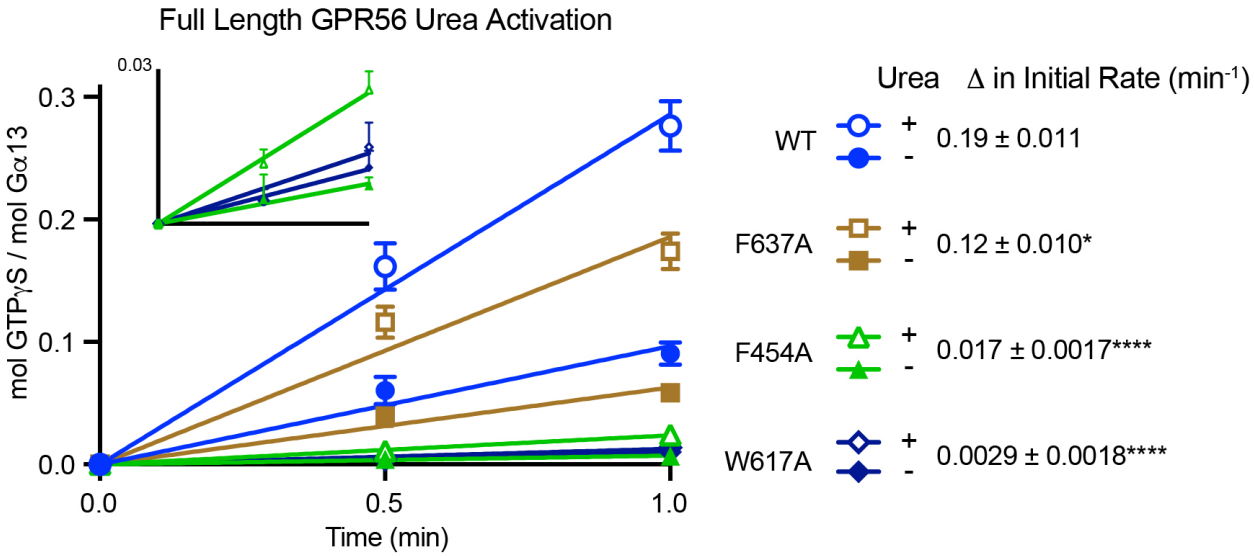

Figure 3.9 Kinetic Measurements of Full-Length GPR56 with TA-Binding Residue Mutations. Equivalent amounts of WT, W617$^{6.53}$A, F637$^{7.42}$A, and F454$^{2.64}$A full-length GPR56 holoreceptors were activated by ice-cold urea treatment to dissociate NTFs from CTFs prior to measurement of G_{13} initial GTPγS binding rates at 20 ºC. The urea-dependent changes in approximated initial linear rates demonstrate that wild type GPR56 was activated by urea significantly more than each mutant, indicating that the mutations impart reduced functional activity and that the mutant receptors are not completely dysfunctional or mis-folded. Data represent the average of each kinetic reaction measured as technical triplicates with error bars representing ± S.D. Unpaired, two-tailed student's t tests were used to determine significance between initial rates. * = $p < 0.05$, **** = $p < 0.0001$.

increases in $G_{12/13}$ signaling [58, 82, 83]. Evidence for orthosteric activation of AGPCR, or tethered agonism, has been observed much more frequently both *in vivo* and *in vitro*. Urea treatment of full-length receptor, or deletion of their ECRs, results in a dramatic increase in signaling, as seen for GPR56, GPR64, GPR126, GPR133, GPR110, and BAI1 [11, 33, 34, 50, 54]. Point mutations in the TA of several of these receptors abrogate G protein signaling, indicating a criticality of the TA. Several studies have also reported the detection of isolated AGPCR NTFs in many different tissue types, which is likely a consequence of an AGPCR activation event or spontaneous NTF shedding [15, 49]. Structures of the NTFs of LPHN1, BAI3, GPR56, and GPR126 show that the TA adopts a β-sheet conformation when encrypted within the GAIN domain. However, the conformation of the freed TA engaged in the orthosteric site, and its mechanism of activation, remained unknown until now.

AGPCR tethered agonism shares parallels with the PAR family of class A receptors, who possess an N-terminal leader sequence that is cleaved by proteases (typically trypsin or thrombin) to expose a tethered ligand that binds to its orthosteric site. The primary distinction between AGPCRs and PARs is that PARs lack a GAIN domain that catalyzes autoproteolysis. AGPCR tethered agonists also do not share sequence similarity with PAR peptides and are typically much more hydrophobic. This raises the question of whether AGPCR TAs can be encrypted in an analogous manner to PARs, and "freed" after exposure to exogenous proteases to activate the 7TM. To answer this, we created PAR1-AGPCR fusion proteins with an N-terminal, thrombin-responsive PAR1 leader sequence to encrypt the TA in place of the GAIN domain. Both of our receptors, PAR1-GPR56 and PAR1-GPR114, responded to thrombin exposure with a robust increase in G_{13} or G_s signaling, respectively. Furthermore, mutation of the thrombin recognition site on the PAR1 leader sequence completely abrogated this effect. These data provide a GAIN-

independent parallel to tethered agonist-mediated activation and suggest that AGPCR activity is exclusively dependent on its TA.

Here, we also report the cryo-EM structures of GPR56 and LPHN3 in two distinct activation states: the inactive NTF-bound holoreceptor form, and the activated 7TM form with the TA engaged. Our structures of the NTF-bound receptors were only low-resolution maps due to the inherent flexibility of the ECR, but clearly illustrated that the NTF does not closely interact with the 7TM domain and sequesters the TA far away from its binding site. Notably, the ECRs of GPR56 and LPHN3 displayed distinct levels of flexibility, likely due to differences in stalk length. LPHN3, the more flexible of the two receptors, has a stalk two residues longer than GPR56 that results in a 6 Å extension. It is not known if stalk lengths shorter than GPR56's stalk would correlate with a more rigid ECR, but the evidence of the inverse suggests it is possible. Many receptors, such Group II AGPCRs (EMR1-4 and CD97), are predicted to have stalk lengths up to three or four residues less than in GPR56 [15]. In these instances, it is plausible that the ECR is within close enough proximity to interact with the 7TM domain in a more stable holoreceptor structure. More is left to be discovered on the structure of AGPCRs in their holoreceptor form. High resolution maps of stabilized, full-length receptors will allow further characterization of the interactions between the GAIN and 7TM domains, or lack thereof.

Our high-resolution structures of TA-activated GPR56 7TM and LPHN3 7TM reveal a unifying mechanism of TA engagement that critically depends on the flexibility of the peptide. Once exposed to extracellular space, the tethered agonist loses the β-strand conformation it normally contains when inside the GAIN domain, bends 180°, and threads into the narrow opening beneath the rigid ECL2 to engage the orthosteric site (**Figure 3.10**). There, the TA adopts a partial

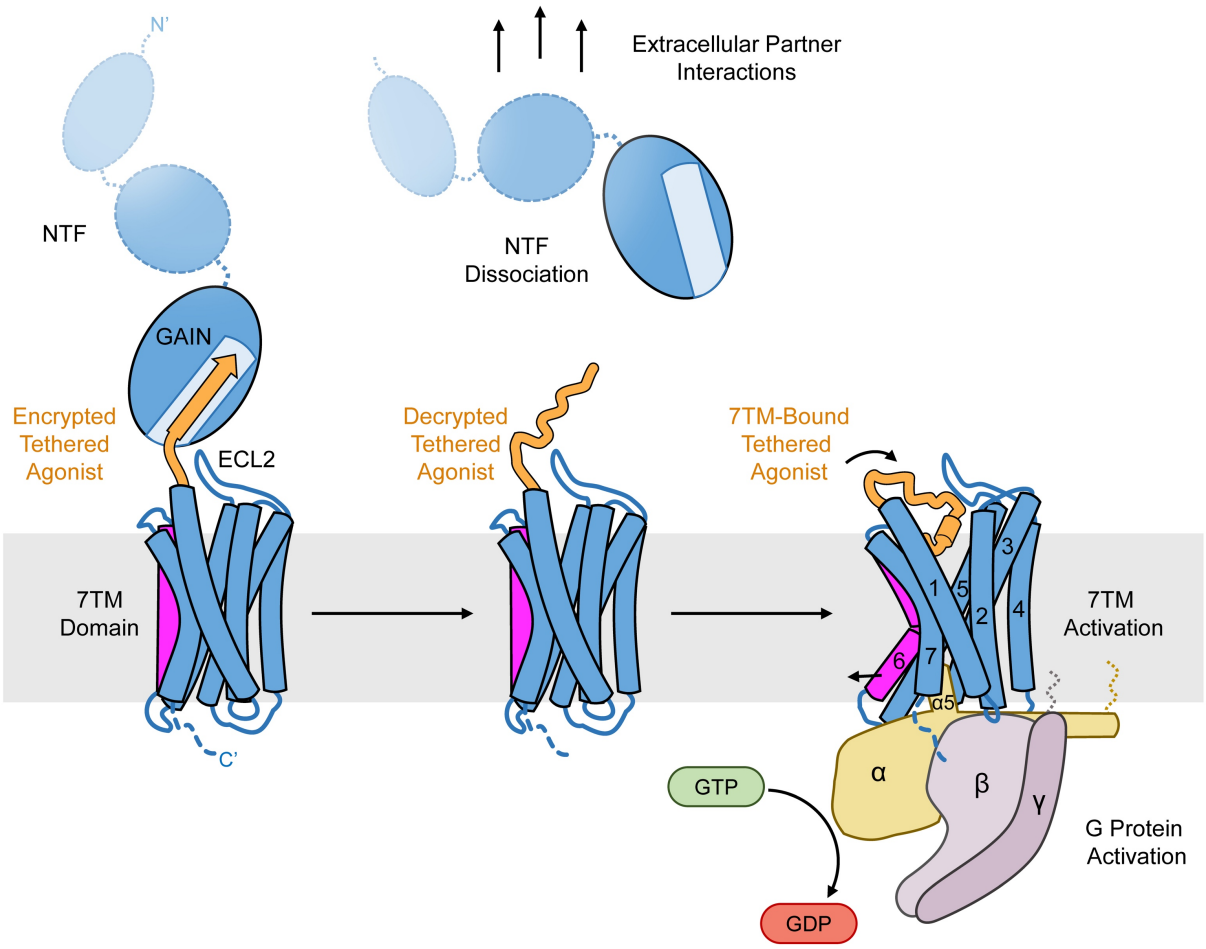

Figure 3.10 Model for Tethered Agonist Activation of Adhesion GPCRs. In the inactive state, the AGPCRs exist as two-fragment receptors held together by noncovalent interactions between the encrypted tethered agonist and the GAIN domain (left). Interactions between the NTF and extracellular binding partners allows for the dissociation of the NTF, decrypting the hydrophobic tethered agonist and exposing it to extracellular space (middle). Once freed, the tethered agonist bends 180º, weaves underneath ECL2, and adopts a partial helix conformation within the orthosteric site. Engagement of the peptide results in a breaking of TM6 that opens the intracellular side of the receptor to increase G protein signaling (right).

helix conformation and stabilizes the active state of the 7TM via hydrophobic interactions between its P3, P6, and P7 residues (typically phenylalanine, leucine, and methionine), and TM1, TM2, TM6, TM7, and ECL2. Following activation, TMs 6 and 7 break into a kinked conformation near the "toggle switch" residue $W^{6.53}$, causing an opening on the intracellular face of the receptor to allow for G protein coupling. The breaking of TM6 and TM7 is seen with other activated class B1 receptors such as GLP1R or GCCR, but was not observed in the recent structure of glucocorticoid-bound GPR97, likely indicating that cortisol and beclomethasone act as a partial agonists for

GPR97 that stabilize an intermediate state [185, 190, 191]. Collectively, the observed interactions between the TA and the 7TM suggest that the conformational flexibility of the TA allows for proper decryption following NTF dissociation to bind deep within the orthosteric site.

Despite being distantly related, the activated structures of GPR56 and LPHN3 show a high degree of similarity, suggesting that the TA-7TM interactions detailed in this study are a universal mechanism of AGPCR activation. Future structural work on additional AGPCRs will likely reveal intricate differences between receptors with distinct tethered agonist sequences.

Chapter 4 Hexahydroquinoline Derivatives are Selective Agonists for the Adhesion G Protein-Coupled Receptor ADGRG1/GPR56

This chapter was adapted from the publication, Vizurraga, A., Robertson, M., Yu, M., Skiniotis, G., Tall1, G., *Hexahydroquinoline Derivatives are Selective Agonists for the Adhesion G Protein-Coupled Receptor ADGRG1/GPR56,* Molecular Pharmacology, 2023, *Manuscript in revision*

4.1 Abstract

GPR56 is a widely expressed member of the adhesion GPCR (AGPCR) family that has pleotropic roles in brain development, platelet function, cancer, and more. Nearly all AGPCRs possess extracellular regions that bind protein ligands and conceal a cryptic tethered peptide agonist. AGPCR reception of force is thought to release the tethered agonist permitting its binding to the AGPCR orthosteric site for consequent activation of G protein signaling. This multi-step mechanism of AGPCR activation is difficult to target, emphasizing the need for tool compounds and potential therapeutics that modulate AGPCRs directly. We expanded our cell-based pilot screen for GPR56 small molecule activators to screen >200,000 compounds and identified two promising agonists: 2-(furan-2-yl)-1-[(4-phenylphenyl)carbonyl]pyrrolidine, or compound 4, and propan-2-yl-4-(2-bromophenyl)-2,7,7-trimethyl-5-oxo-1,4,5,6,7,8-hexahydroquinoline-3-carboxylate, or compound 36. Both compounds activated GPR56 receptors engineered to have impaired tethered agonists, and/or be cleavage deficient. Compound 4 activated a subset of Group VIII AGPCRs while compound 36 had exclusive specificity for GPR56 among the GPCRs tested. Compound 36 SAR analysis identified an analog with the isopropyl R group replaced with a

cyclopentyl ring and the electrophilic bromine replaced with a CF_3 group. Analog 36.40 had a 40% increased potency over compound 36 and was 20-fold more potent than synthetic peptidomimetics designed from the GPR56 tethered agonist. The new GPR56 tool compounds discovered in this screen may be used to further advance understanding of GPR56 function and aid development of AGPCR-targeted therapeutics.

4.2 Introduction

Adhesion GPCRs (AGPCRs) or Family B2 GPCRs consist of 33 members that have variable extracellular regions with adhesive modules that bind a variety of affixed protein ligands. They are important mediators of diverse processes including tissue and organ development, blood cell function, and synaptic regulation [6, 89, 115, 120, 142, 170, 193, 194]. Common to AGPCRs is the highly conserved extracellular GPCR autoproteolysis-inducing (GAIN) domain [195]. The GAIN domain is a constitutive protease that self-cleaves AGPCRs at a small, conserved loop that links the penultimate and last β-strands of the GAIN domain. The two resulting fragments termed the extracellular N-terminal fragment (NTF) and the C-terminal fragment (CTF) or 7TM domain remain noncovalently bound via the dense network of hydrogen bonds within the GAIN domain. The stalk that emanates from the first transmembrane span of the 7TM lies encrypted within the GAIN domain in the cleaved, holoreceptor form. Dissociation of the two AGPCR fragments exposes this peptide and its N-terminus adopts a new conformation that permits it to bind the orthosteric site of the 7TM domain to act as a tethered peptide agonist (TA) and activate signaling [33, 196]. The first cryogenic-electron microscopy structures of several TA-activated AGPCRs were solved, affirming this unified mechanism of TA-mediated activation; upon decryption, the TA stalk threads into the orthosteric site beneath ECL2 as a partial α-helical hook-like structure

and interacts with the 7TM domain primarily through the P3, P6, and P7 hydrophobic residues of the TA (typically Phe, Leu, and Met, respectively) [163, 197-199].

GPR56/ADGRG1 is an AGPCR that is widely expressed in tissues including glial cells, muscle, testis, and platelets [110, 113, 149, 169, 170, 173, 200]. GPR56 possesses a Pentraxin/Laminin/neurexin/sex-hormone-binding-globulin-Like (PLL) domain N-terminal to its GAIN domain that binds collagen and transglutaminase-2 (TG2) [83, 110, 174, 175]. It couples to $G_{12/13}$ to mediate proliferation of oligodendrocyte precursor cells (OPCs) via RhoA signaling, which supports nerve myelination [110, 150, 172]. In platelets, GPR56 interacts with vessel wall-injury exposed collagen via its PLL domain to fulfill shear force-dependent platelet shape change via Rho signaling prior to platelet activation [170]. GPR56 is also an oncogene in several types of cancer, including colorectal cancer, gliomas, and melanomas [112, 176-181]. In these cancers, GPR56 upregulation may provide Rho signaling to drive cancer progression and metastasis, marking it as a potential biomarker or therapeutic target for cancer. Dysregulation of GPR56 also results in the pathogenesis of the recessive human neurodegenerative disease bilateral frontoparietal polymicrogyria (BFPP), the patients of which suffer from severe intellectual deficiencies, epilepsy, and ataxia [68, 76]. Despite a wide variety of roles in biological functions and disease, no drugs have been designed to target GPR56, or any other adhesion GPCR. Small molecule probes targeting AGPCRs could fill this role or may also serve as useful molecular tools to study AGPCRs *in vivo*.

We previously sought to find small molecule agonists and antagonists for AGPCRs using GPR56 as a model. We identified the steroid-like partial agonist 3-α-acetoxydihydrodeoxygedunin (3-α-DOG) and the isoflavonoid antagonist dihydromunduletone (DHM) from pilot cell-based high throughput screens. These compounds served as vital probes for identifying the role of GPR56

in platelet shape change [170]. Here, we expanded upon these previous screens and conducted a large-scale high throughput screening effort to identify more potent and efficacious activators of GPR56 from three libraries comprising ~200,000 compounds. We developed techniques for large scale handling and culturing of HEK293T cells to overcome technical challenges that ensured integrity of the screening assay across all 200,000 compounds. From our primary screen we identified 1,327 initial hits, which was narrowed to 155 candidates following counter screening. Seventy-four of the 155 candidates demonstrated promising concentration-dependent responses. Further vetting and testing in an orthogonal biochemical GPCR reconstitution assay identified 16 final candidate compounds that had equivalent or improved efficacies and potencies over the positive control GPR56-Activating Peptide (GPR56-AP), a peptidomimietic of the tethered agonist.

One compound, propan-2-yl-4-(2-bromophenyl)-2,7,7-trimethyl-5-oxo-1,4,5,6,7,8-hexahydroquinoline-3-carboxylate, or compound 36, showed substantial activity in the cell-based luciferase assay and GPCR reconstitution assay with potency several fold higher than GPR56-AP and the previously identified partial agonist 3-α-DOG. Compound 36 and one other compound, 2-(furan-2-yl)-1-[(4-phenylphenyl)carbonyl]pyrrolidine, or compound 4, also activated a cleavage-deficient holoreceptor mutant of GPR56. Compounds 36 and 4 selectively activated the G subfamily of AGPCRs. Compound 36 was exclusive for GPR56/ADGRG1, while compound 4 activated both GPR56 and GPR97/ADGRG3. Following structure activity relationship analysis of compound 36 using commercially available analogs, we identified an analog of compound 36 that had ~40% increased potency over the base compound. Compound 36 and the improved analog were docked in the GPR56 orthosteric site by *in silico* analysis, which predicted that the *R* enantiomer interacted more productively than the *L* enantiomer with features of the binding pocket

that are critical for TA engagement. The compounds discovered in our study may be used to advance knowledge of GPR56 function and potentially be tailored to become first generation AGPCR-targeted therapeutics.

4.3 Results

4.3.1 Cell-Based High Throughput Screening for GPR56 activators

GPR56/ADGRG1 activates $G_{12/13}$ and the human homolog modestly activates G_i [33, 50, 82, 170, 172]. Rho signaling through G12/13 can be monitored in HEK293T cells via a firefly luciferase reporter driven by the serum response element (SRE) promoter (**Figure 4.1A**). We utilized this previously to conduct pilot screens of a small chemical library and identified a corticoid-like partial agonist and isoflavonoid antagonist for GPR56 [61, 114]. Engineered GPR56 receptors lacking the NTF were used to selectively screen for molecules that target the 7TM. GPR56 7TM with an intact TA exhibited maximal SRE-Luc activity that was several fold higher than the GPR56 holoreceptor and was used to screen for inhibitory compounds [114], while a GPR56 7TM construct encoding a four-residue truncation of its TA (GPR56 ΔTA) exhibited low activity and was used to screen for agonists (**Figure 4.1B-D**). A synthetic peptide modeled from GPR114 that mimics the identical TA sequences of GPR56 and GPR114 was used as a positive control for the activator screen assay (GPR56/114-AP, Figure 1C) [57, 61]. This 19-mer peptide agonist (20 μM) provided strong activation of GPR56 ΔTA (Z' = 0.65, **Figure 4.1D**). As a positive control for the GPR56 7TM inhibitory screen, the actin polymerization inhibitor Latrunculin B (1 μM) provided complete inhibition (Z' = 0.51, **Figure 4.1D**). A receptor-minus counter screen assay was developed to vet GPR56 activating compounds obtained in the primary screen. Cells were transfected with the luciferase reporter only and treated with FBS or GPR56/114-AP (**Figure**

4.1E). These SRE reporter-only cells were activated by FBS (Z' = 0.57), but not by the GPR56/114-AP.

We expanded our previous pilot activator screen of 2,000 compounds to conduct a large screen of over 200,000 compounds (**Figure 4.2**) [61]. It was not logistically possible to freshly transfect a sufficient amount of HEK293T cells to screen all compounds at once given our

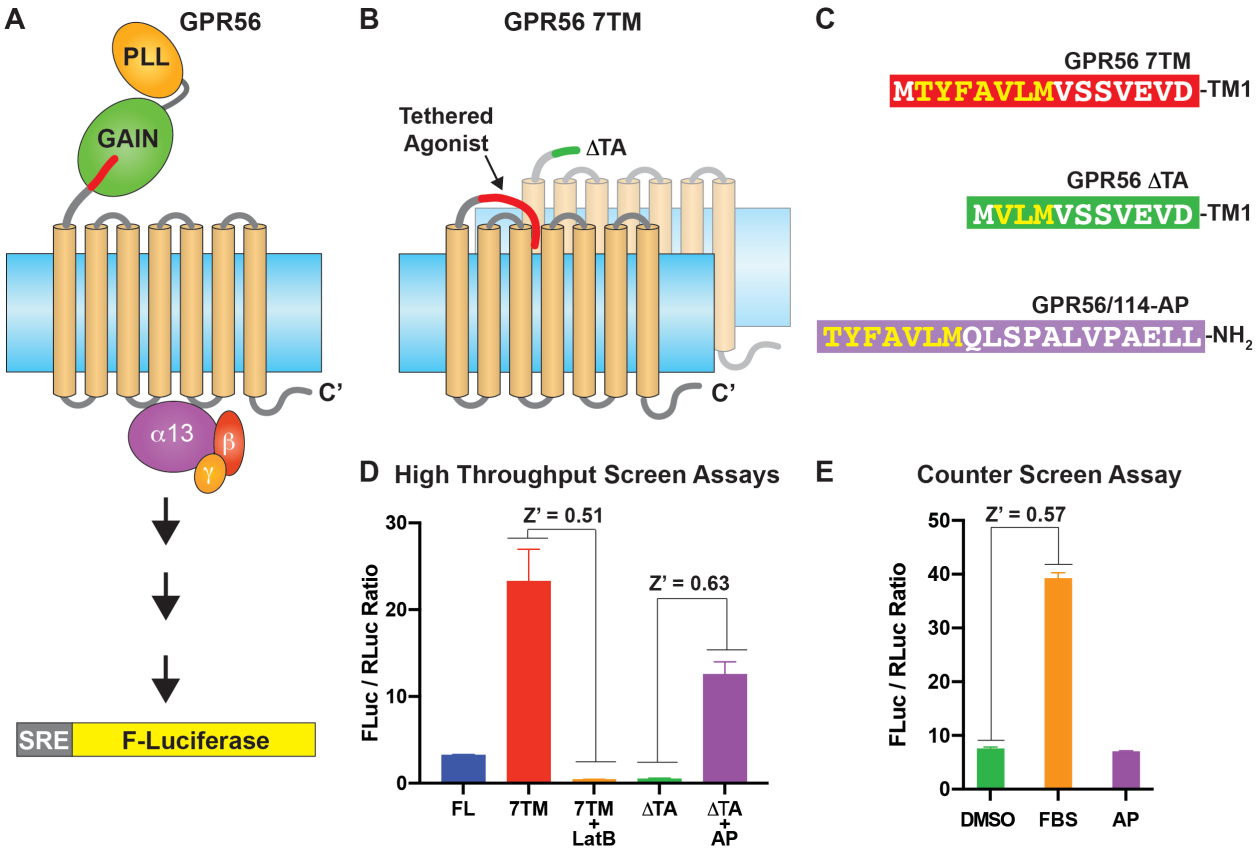

Figure 4.1 GPR56 Small Molecule Modulator Screens. GPR56 is a two-fragment adhesion GPCR with a cryptic tethered agonist (red) embedded within the GAIN domain. GPR56 activates G13 and Rho signaling which was measured using the SRE- firefly luciferase reporter. **B.** GPR56 constructs lacking the NTF used for screening. Constitutively active GPR56 7TM has an intact tethered agonist (TA, red) and GPR56 ΔTA (green) has a compromised tethered agonist resulting from a four-residue truncation. **C.** TA (yellow text) and stalk sequences (white text) of the GPR56 7TM constructs used for high throughput screening aligned with a synthetic peptidomimetic agonist that activates GPR56 or GPR114 (GPR56/114-AP, purple) and was used to calibrate the screening assays. **D.** Calibration of HEK293T cell-based high throughput SRE-luciferase screening assays. The GPR56 7TM assay exhibits high activity that was blunted with Latrunculin B (LatB) and used to screen for inhibitors. The GPR56 ΔTA assay exhibits low activity that could be surmounted with GPR56/114-AP and was used to screen for activators. **E.** Calibration of the HEK293T cell target-minus high throughput counter assay, which uses cells that only express the SRE-luciferase reporter. FBS, but not GPR56/114-AP, activated the SRE-luciferase reporter in the absence of GPR56. Z' scores are of assay quality, with 0.5 being the threshold suitable for high throughput screening. Error bars are the mean ± SD of three biological replicates.

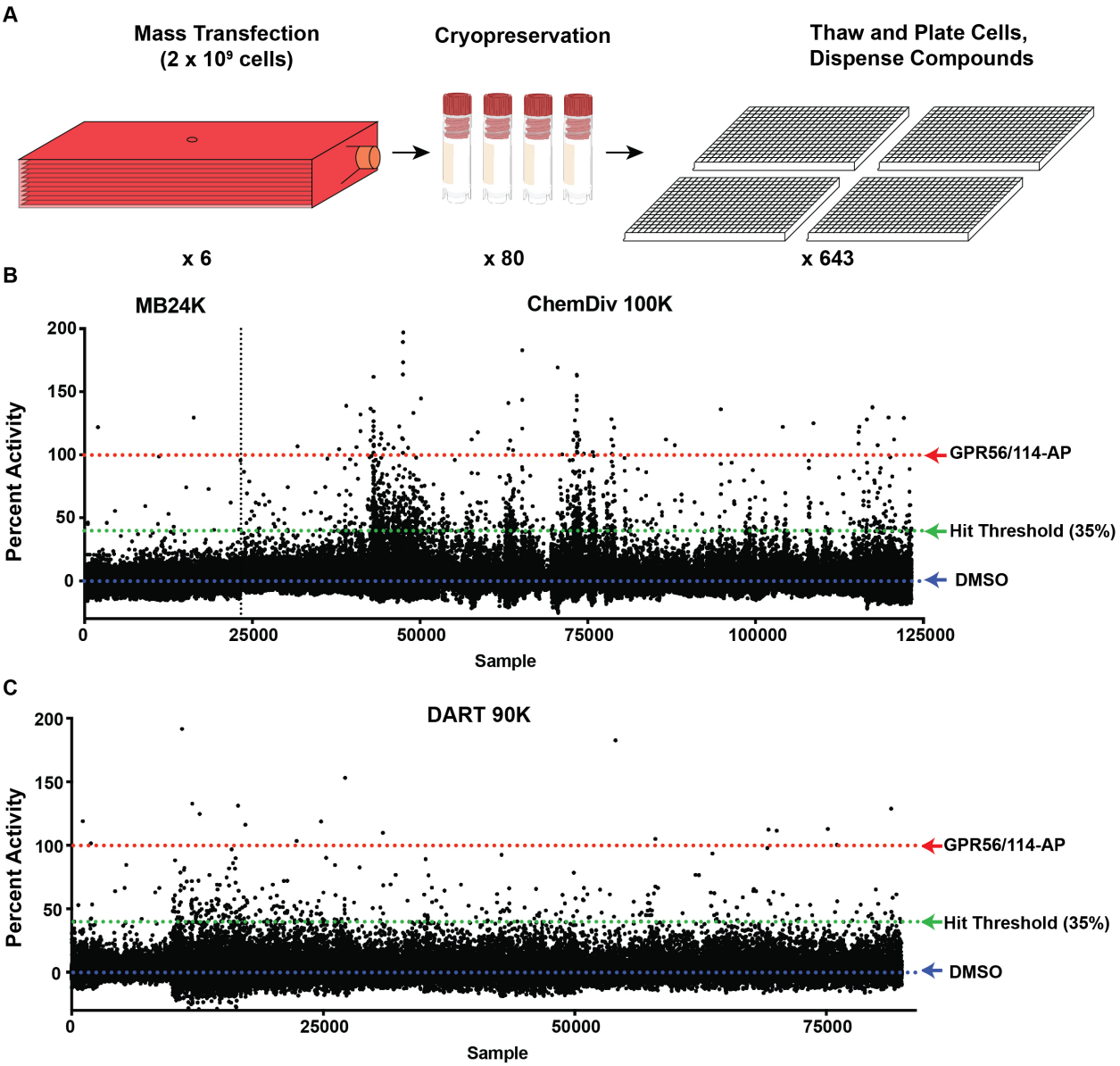

Figure 4.2 Primary Screen for GPR56 Small Molecule Activators. **A.** Workflow of high throughput screening procedure. HEK293T cells were transfected *en masse* with GPR56 ΔTA and the SRE-Luciferase reporter 24h prior to being harvested, pooled and cryopreserved in assay-ready aliquots. Thawed cells were disbursed into 384-well plates and small molecules were pin-tooled into the wells at 10 μM for 18 h prior to measurement of SRE-luciferase activity. **B** and **C.** Primary results of GPR56 activator screens using the MayBridge and ChemDiv or DART90K small molecule libraries. ~123,000 compounds were screened from the MayBridge (left) and ChemDiv (right) libraries, and 82,000 compounds were screened from the DART90K library. Each dot represents the luciferase activity of a single compound, with luminescence normalized to 20 μM GPR56/114-AP (positive control, red). DMSO (vehicle) was the negative control and established as 0% activity (blue). Compounds that elicited activity ≥35% of GPR56/114-AP activity were considered primary hits (green).

equipment, so we developed a cell transfection/cryopreservation regime that ensured plate-to-plate reproducibility over an extended time. Corning HYPER*Flasks*™ were used to culture 2 x 10^9 HEK293T cells for transfection *en masse* with the SRE-luciferase gene reporter and GPR56 ΔTA

receptor. After transfection, cells were pooled and cryopreserved in assay-ready aliquots that were thawed and seeded in increments of eight 384-well plates for stimulation with robotically dispensed compounds (**Figure 4.2A**). Small molecules were screened from three commercial libraries: a Maybridge 24K library (MB24K), a Chemical Diversity 100K library (ChemDiv100K), and a DART 90K library (DART90K). For the screens, luminescence signals were normalized to DMSO as the negative control and 20 μM GPR56/114-AP as positive control. A threshold of 35% activity was used to classify hits. We established this threshold as it closely matches the HTS standard of three standard deviations above the negative control on plates with few hits, while not excessively excluding compounds from plates with many hits. From the screen we identified 1,327 primary hits as candidate GPR56 activators, 801 of which were from the MB24K and ChemDiv libraries and 526 were from the DART90K library (**Figure 4.2B-C**). The overall hit rate of the screen was 0.64%.

A limited confirmatory check and counter-screen were conducted to eliminate false positives or pathway activators downstream of GPR56 in the serum response. Compounds were robotically cherry picked via an STP Mosquito^{TM} instrument and consolidated into 384-well plates in triplicate. HEK293T cells pre-transfected with GPR56 ΔTA and the SRE-Luc reporter or reporter alone were cultured atop the compounds before measurement of luciferase activities. We found that 796 of the 1,327 initial hits (516 from the ChemDiv library + 280 from the DART library) stimulated activity >35% of the positive control, thereby reconfirming the original activities (**Figure 4.3A-B**). Counter screening found that 891 of the 1,327 initial hits (533 from the ChemDiv library + 358 from the DART library) elicited >35% of the serum response and were thus eliminated as off target or pathway activators (**Figure 4.3C-D**). A lower hit rate was obtained using the Maybridge library screen with only 8 candidate hits, of which two were eliminated as

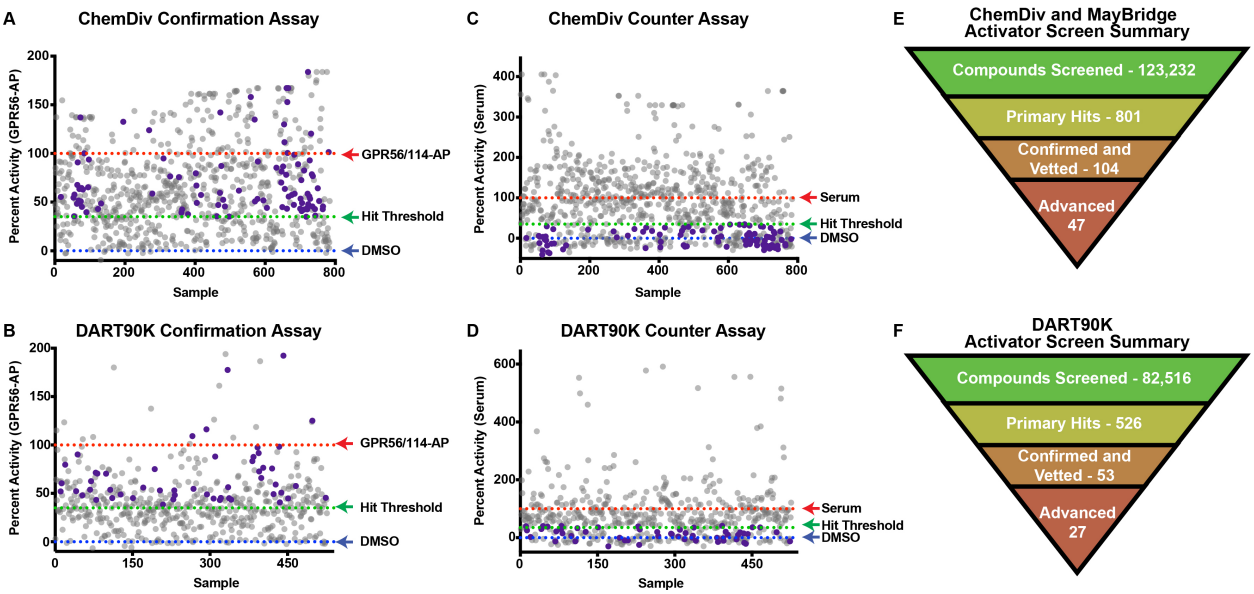

Figure 4.3 Confirmation of GPR56 Activator Hits. Confirmation and counter assays of primary hits from the (**A, C**) ChemDiv or (**B, D**) DART libraries. Compounds (10 µM, 200 nL) were pre-spotted in triplicate 384-well plates, overlaid with pre-transfected assay- or counter assay-cells and incubated for 18 h prior to measurement of SRE-luciferase activity. Luminescence was normalized to that of positive controls GPR56-AP (20 µM) or FBS (10%), respectively. DMSO was the negative control and established as 0% activity (blue). Compounds that elicited activity at ≥35% the GPR56-AP activity threshold (green line) and ≤35% the serum activity threshold (green line) are highlighted as purple dots and represent confirmed hits. Error bars representing standard deviation have been omitted for ease of reading. **E. and F.** Denotes the numbers of compounds honed at each stage of confirmation. Hits that were advanced are the subset of confirmed and vetted hits that were readily available for commercial purchase as fresh powders.

pathway activators (**Figure 4.4**). In total, 155 hits across all three libraries (96 from ChemDiv, 6 from Maybridge, and 53 from DART) survived confirmation and counter screening, giving a final hit rate of 0.076% for the entire screen. To further hone the list of GPR56 agonist candidates, we tested compounds in concentration response assays between 2.8 and 100 µM to acquire initial measurements of efficacy and potency. 73 of the 155 candidate activators were eliminated after demonstrating peak efficacies or potencies substantially below that of GPR56/114-AP (**Figure 4.5**). Eight additional compounds were eliminated for eliciting concentration responses with poor hill slopes, that we attributed to compound cytotoxicity, instability, and/or insolubility. From this analysis 74 compounds with favorable concentration response profiles were purchased as fresh powders for follow-up validation testing (**Figure 4.3E-F**). Sixty-three of these compounds were structurally distinct, but eleven were grouped into four clusters as analogs.

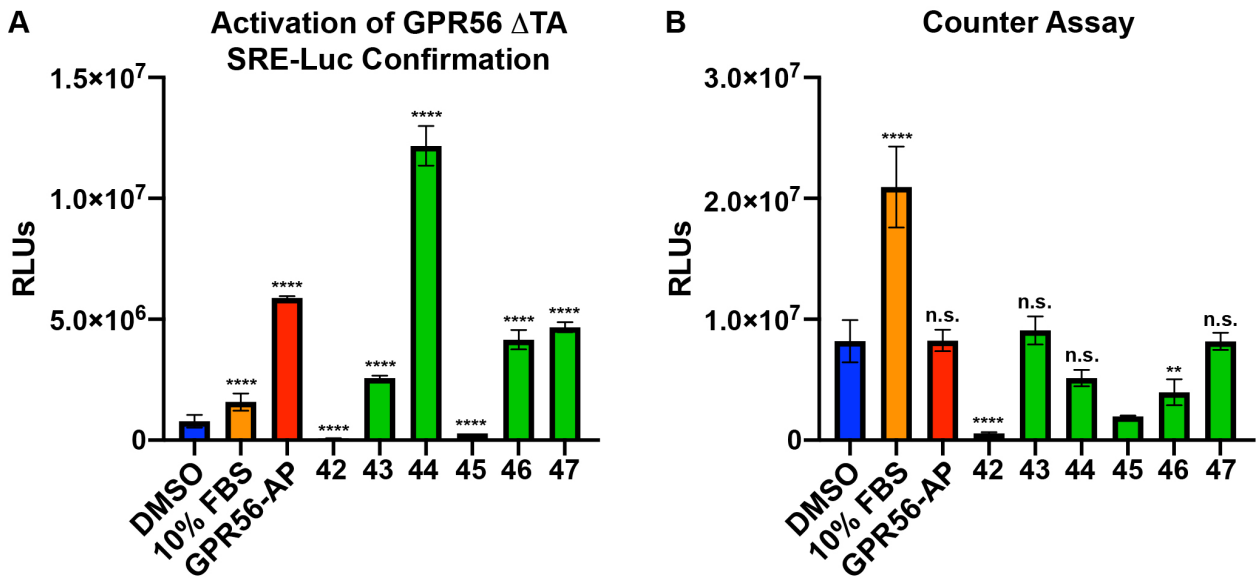

Figure 4.4 Validation of GPR56 Activators from the Maybridge Library. A. HEK293T cells pre-transfected with GPR56 ΔTA and SRE-Luciferase were treated with 5 μM compound, 5 μM GPR56-AP, FBS, or DMSO prior to measurement of SRE luciferase activity. **B.** HEK293T cells pre-transfected with SRE-Luciferase only were treated with the same as in A prior to measurement of SRE luciferase activity. Data are the mean ± SD of three independent reactions. Statistical significance was determined by repeated measures of one-way analysis of variables. **P*<0.05, ***P*<0.01, ****P*<0.001, *****P*<0.0001

4.3.2 Orthogonal Assay Validation of GPR56 Activators

The activities of GPR56 agonists were evaluated using an orthogonal biochemical GPCR reconstitution assay that directly measures GPR56-stimulated G protein activation. Agonists were pre-incubated with membrane homogenates prepared from cells overproducing GPR56 ΔTA and reconstituted with purified heterotrimeric G proteins ($G\alpha_{13}$ and $G\beta_1G\gamma_2$). Kinetic reactions were initiated and the accumulation of $G\alpha_{13}$-bound [^{35}S]-GTPγS was measured. Sixteen of the 74 compounds exhibited efficacy ≥ 75% of GPR56-AP (**Figure 4.6A-C**). Four of these compounds, Compounds 32, 33, 36, and 41, comprise a cluster of structurally related analogs that each had efficacy exceeding GPR56-AP (**Figure 4.6D**). The remaining 58 compounds had reduced efficacies or apparent solubility issues. Notably, none of the compounds discovered in the screen

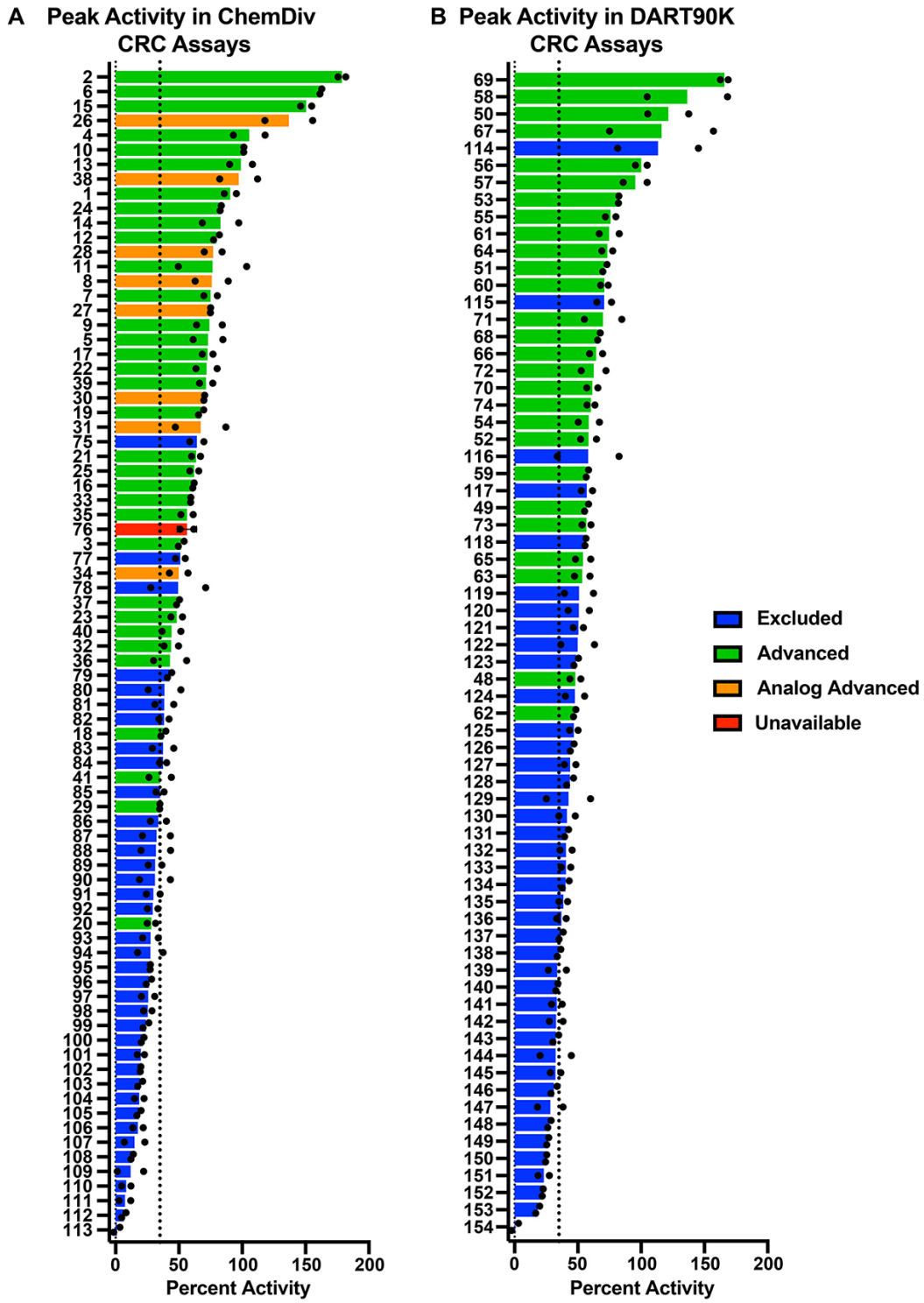

Figure 4.5 Summary of Robotically Pipetted Concentration Response Curves. GPR56 activators from **(A)** the ChemDiv or **(B)** DART libraries were robotically pipetted into 384-well format in a dilution series ranging from 2.8 μM to 100 μM before HEK293T cells pre-transfected with GPR56 ΔTA and SRE-Luciferase were overlaid into the wells. Data represent the mean of two data replicates from the highest activity achieved from each concentration response curve (CRC) and were normalized as a percentage of 20 μM of GPR56-AP (100%). The dashed lines are the 35% activity threshold used for considering valid GPR56 hits. Advanced compounds were purchased as fresh powders for follow-up validation.

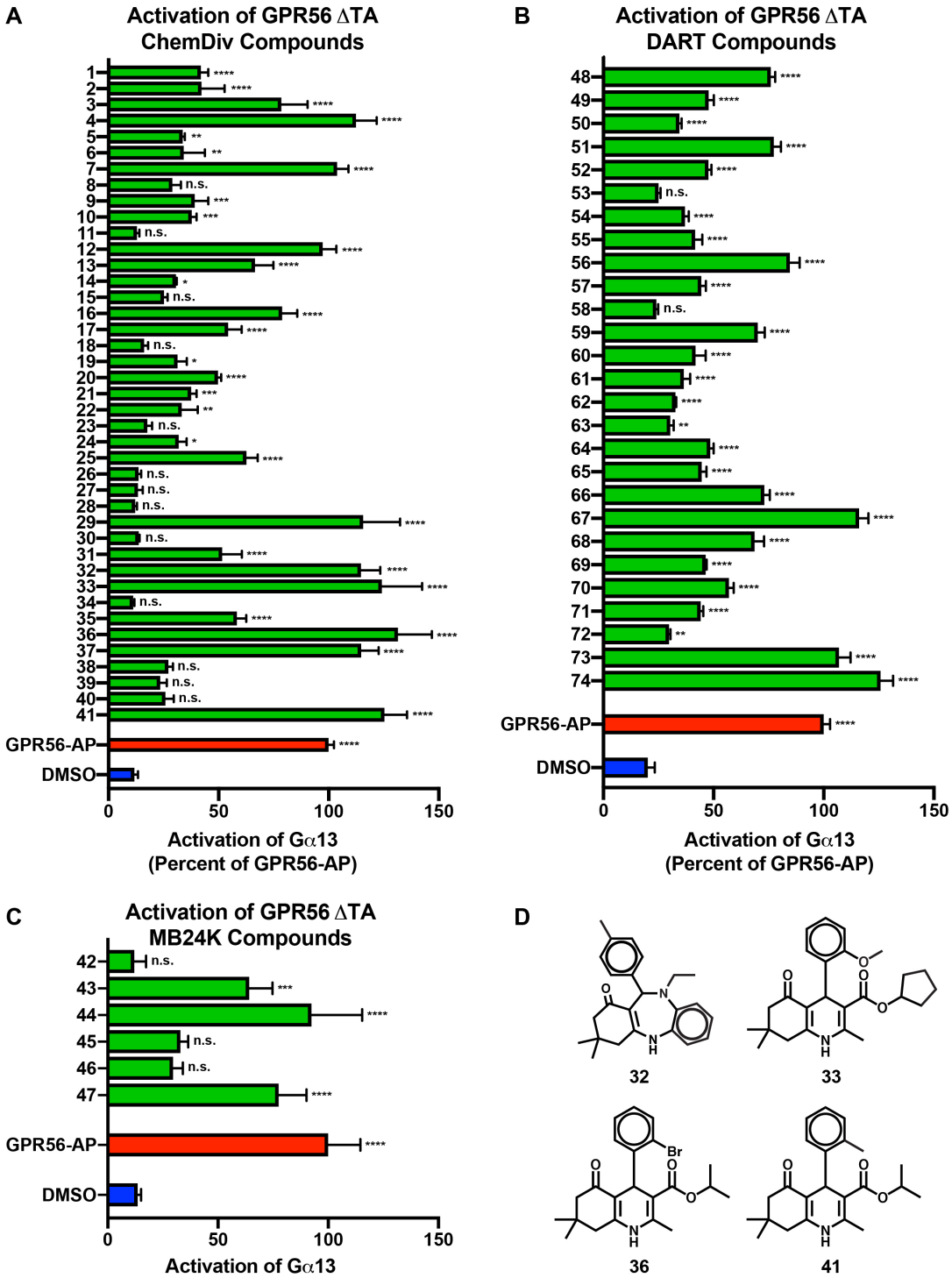

Figure 4.6 Validation of Purchased GPR56 Activators by GPR56 Reconstitution Assay. A-C. All purchased compounds (80 μM ea.) from the (**A**) ChemDiv and (**B**) Maybridge and (**C**) DART libraries were tested in the GPR56 DTA / G protein 13 reconstitution assay. GPR56 DTA membrane homogenates were reconstituted with purified G_{13} heterotrimer prior to measurement of receptor-stimulated G13 GTPγS binding. **D**. Chemical structures of the four analogs that were independently identified as hits for GPR56. Data were normalized as a percentage of 80 mM GPR56-AP peptide (red) and are the mean ± SD of three independent reactions. Statistical significance between compounds and DMSO was determined by repeated measures of one-way analysis of variance. *P<0.05, **P<0.01, ***P<0.001, ****P<0.0001

were analogs of the previously identified GPR56 partial agonist 3-α-DOG, as steroid-like compounds were not present in the screened libraries [61].

We compared the efficacies of the top 12 compounds plus two compounds from the structural cluster, compounds 36 and 32, to the activity of constitutively active GPR56 7TM that contains an intact TA (**Figure 4.7A-C**). Compound 36 was the only one of the 14 compounds capable of activating GPR56 ΔTA with efficacy equivalent to GPR56 7TM. Compound 36, or propan-2-yl-4-(2-bromophenyl)-2,7,7-trimethyl-5-oxo-1,4,5,6,7,8-hexahydroquinoline-3-carboxylate, is a hexahydroquinoline (HHQ) derivative that contains a central 1,4-dihydropyridine ring (1,4-DHP). Another interesting compound identified was 2-(furan-2-yl)-1-[(4-phenylphenyl)carbonyl]pyrrolidine, or compound 4. Compound 4 has a simple structure consisting of two benzene rings connected to a 2-(furan-2-yl)pyrrolidine group by a carbonyl group. We compare compound 36 and compound 4 in a concentration response format for activation of GPR56 ΔTA (**Figure 4.7D**). Compound 36 had an EC_{50} of 2.95 ± 0.41 μM and an efficacy matching that of GPR56 7TM. This is over 10-fold more potent than GPR56-AP (EC_{50} = 35 μM [33]), and was ~40% more potent than the previously identified partial agonist 3-α-DOG (EC_{50} = 4.8 μM [61]). By contrast, Compound 4 has a maximum efficacy ~50% of GPR56 7TM. The potency of Compound 4 was too low to accurately determine an EC_{50}.

4.3.3 Compound Activation of the GPR56 Holoreceptor

Following validation of the 14 activators in the GPR56 ΔTA / G13 reconstitution assay, we evaluated whether the compounds could activate the GPR56 holoreceptor. Measuring small molecule agonist stimulation of the GPR56 holoreceptor is not straightforward because GPR56 is efficiently self-cleaved and incidental dissociation or shedding of its NTF results in substantial

TA-dependent background G13 signaling that confounds measurement of compound agonist activities [33, 61, 163]. We used three full-length GPR56 mutants that have impaired autoproteolytic activity and/or an impaired TA to minimize TA-dependent background signaling.

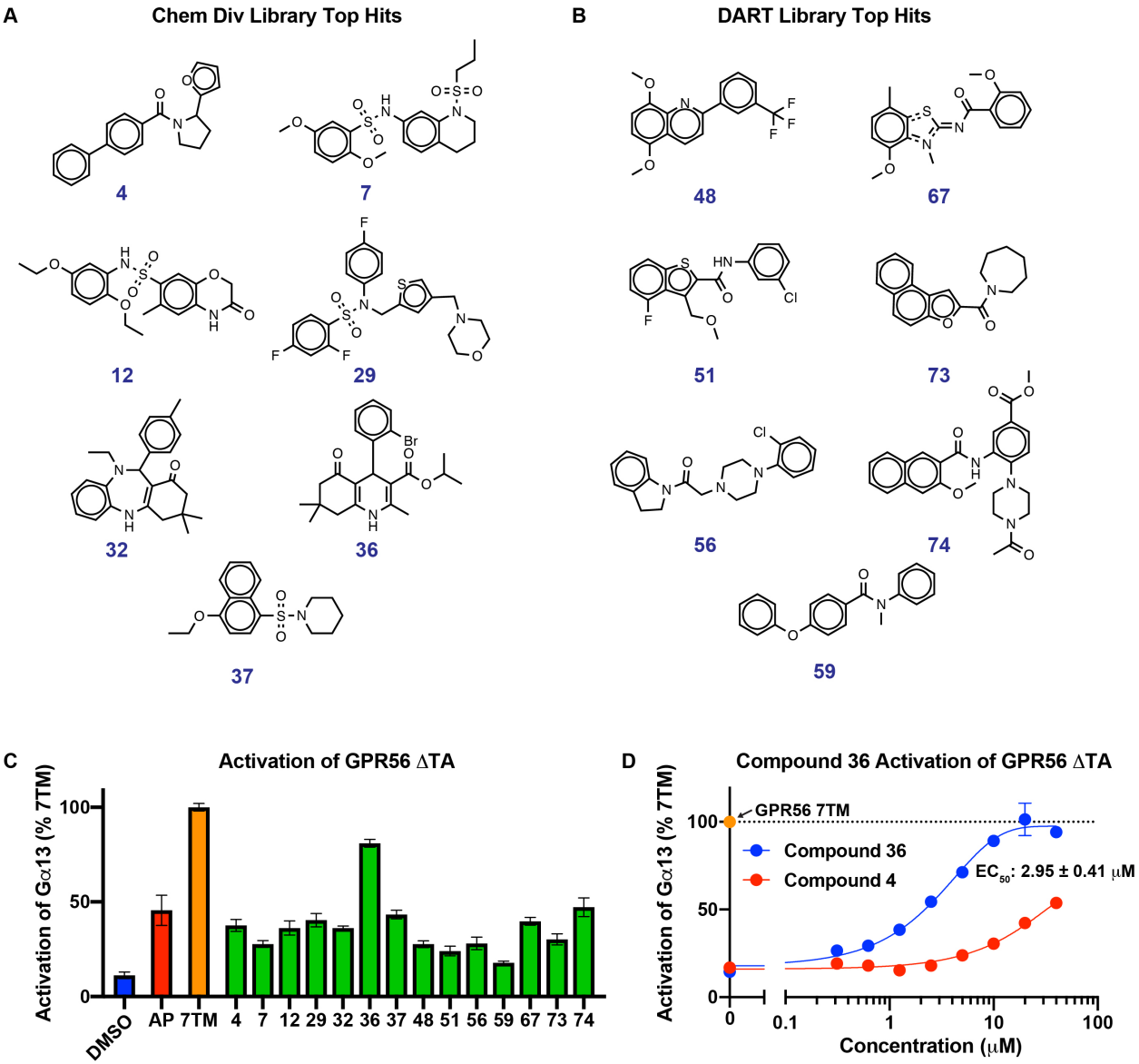

Figure 4.7 Orthogonal Assay Testing of the top GPR56 Small Molecule Activators. Structures of the top 14 unique activators that were confirmed from the **A.** ChemDiv or **B.** DART libraries. Two compounds, compound 32 and 36, are representative analogs of a structural cluster found in primary screening. **C.** Compounds (20 μM ea.) or GPR56-AP (80 μM) were tested in the GPR56 ΔTA / G protein reconstitution GTPγS binding assay. Data were normalized as a percentage of GPR56 7TM activity (Orange). **D.** Concentration responses of compounds 36 and 4 for activation of GPR56 ΔTA. Data were normalized to the activity of constitutively active GPR56 7TM and are the mean ± SD of three independent reactions. Statistical significance between compounds and DMSO was determined by repeated measures of one-way analysis of variance. *P<0.05, **P<0.01, ***P<0.001, ****P<0.0001

GPR56 H381S is a point mutant of the GPCR proteolysis site (GPS) that abrogates autoproteolysis; GPR56 F385A/M389A contains two point mutations within the TA that are vital for its ability to engage the 7TM orthosteric site; and GPR56 L388A/M389A contains a different set of TA point mutations that are more distal to the cleavage site and retain full autoproteolytic activity (**Figure 4.8A-B**) [141, 163, 197-199].

GPR56 holoreceptor membrane homogenates were treated with urea to dissociate the NTFs from membrane intercalated CTFs/7TMs. Both GPR56 H381S and F385/M389A mutants were predominantly un-cleaved, whereas urea treatment markedly reduced the amount of NTF in the membrane fraction of wild type GPR56 and GPR56 L388A/M389A (**Figure 4.8B**). However, only the wild type GPR56 holoreceptor exhibited appreciable urea-dependent (*i.e.,* TA-dependent) activation (**Figure 4.8C**). GPR56 H381S, GPR56 F385A/M389A, and GPR56 L388A/M389A had low basal signaling that were not enhanced by urea treatment. For the GPR56 L388A/M389A double mutant, this demonstrates that TA-impairment fully blocks the ability of this efficiently cleaved receptor to activate G proteins [141].

The GPR56 H381S mutant was used to assess whether the 14 GPR56 agonists could activate the holoreceptor. GPR56 H381S membrane homogenates were pre-incubated with each compound (20 μM) prior to measurement of G13 GTPγS binding. Compounds 4, 29, 32, 36, 37, 59, and 73 stimulated GPR56 H381S significantly above basal signaling, with compounds 4 and 36 being the most effective agonists that exceeded greater than four-fold signaling above basal activity (**Figure 4.8D**). GPR56-AP was incapable of activating the GPR56 H381S holoreceptor, as reported, with speculation that the NTF hinders its access to the orthosteric site [61]. Compounds 4 and 36 were tested in GPR56 H381S concentration response assays. Both compounds substantially increased receptor-mediated G protein activation (**Figure 4.8E**).

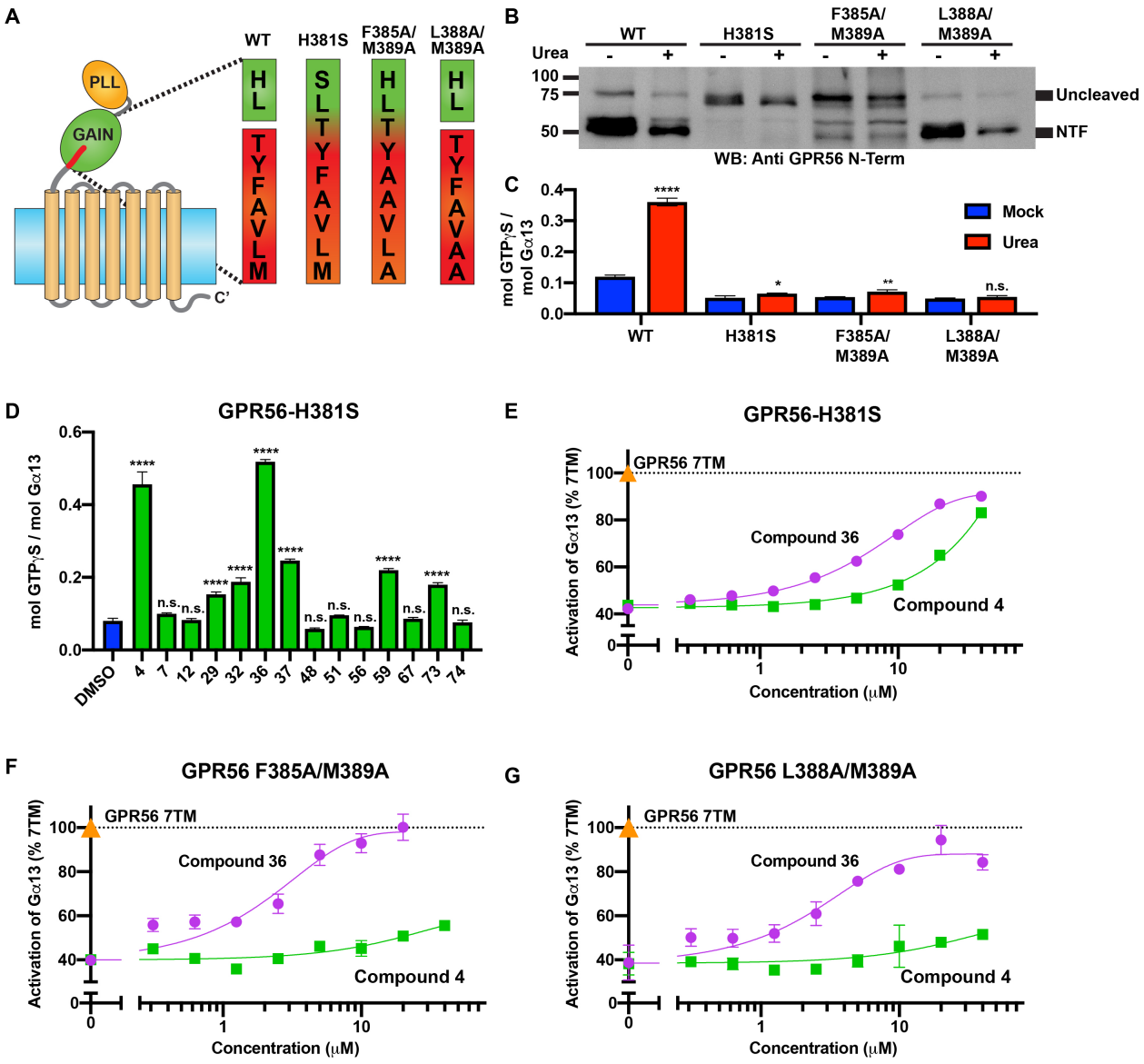

Figure 4.8 Compounds 36 and 4 Activate Cleavage-Defective and TA-Impaired GPR56 Holoreceptors. A. Schematic of holoreceptor GPR56 constructs, with the sequence of the TA and cleavage site highlighted. **B.** Wild type and mutant GPR56 holoreceptor membrane homogenates were treated with or without urea to dissociate non-covalently bound NTFs and immunoblotted with an antibody directed at the GPR56 NTF. **C.** The GPR56 membrane homogenates prepared in (B) were subjected to G13 GTPγS binding assay to evaluate the urea dependence (*i.e.,* NTF dissociation / TA engagement) of receptor activation. **D.** Top compounds (20 μM ea.) activation of the urea-treated GPR56 H381S holoreceptor. **E.** Concentration responses of compounds 4 and 36 for GPR56 H381S activation of G13 in comparison to constitutively active GPR56 7TM. **F.** Concentration responses of compounds 4 and 36 for GPR56 F385/M389A activation of G13 in comparison to the constitutively active GPR56 7TM. **G.** Concentration responses of compounds 4 and 36 for GPR56 L388A/M389A activation of G13 in comparison to the constitutively active GPR56 7TM. Data points are the mean ± SD of three independent reactions. In (C), Statistical significance between mock and urea was determined by unpaired student's t tests. In (D), statistical significance was determined by repeated measures of one-way analysis of variance. Some error bars are smaller than the graphed symbols. *P<0.05, **P<0.01, ***P<0.001, ****P<0.0001.

Compound 36 had an EC_{50} of 6.69 ± 0.56 μM, while the right shifted curve of compound 4 did not reach maximal efficacy and could not provide an accurate estimation of EC_{50}. Interestingly, compound 36 provided near full activation of the GPR56 F385A/M389A and GPR56 L388A/M389A receptors, but compound 4 had negligible activation (**Figure 4.8F-G**). We do not have a full explanation for this but speculate that both double mutants possess some population of freed CTF receptor that may have the defunct TA embedded within the orthosteric site. It is possible compound 4 is not potent enough to compete with the mutated tethered agonist and activate the receptor, whereas compound 36 is sufficient. GPR56 H381S is strongly cleavage deficient with no or little population of receptor engaged by its TA, which may account for its ability to be activated by compound 4.

4.3.4 GPCR selectivity of Compounds 4 and 36

Compounds 4 and 36 were tested for the abilities to modulate a small panel of adhesion GPCRs and two Class A GPCRs. ADGRG5/GPR114, ADGRG3/GPR97 and ADGRG1/GPR56 are from the same adhesion GPCR subfamily. GPR114 and GPR56 have identical tethered agonists and can be activated by 3-α-DOG and the same TA-peptidomimetics [33, 57, 61]. ADGRL3/Latrophilin-3 and ADGRF1/GPR110 are representatives of two distinct adhesion GPCR subfamilies. Compounds 4 and 36 (20 μM) were tested for their abilities to activate TA-impaired 7TM versions of each adhesion GPCR and compared to the activity of intact TA 7TM receptors. Compound activities towards the β2 adrenergic receptor (β2AR) and the M1 muscarinic receptor (M1R) were compared to the activities stimulated by the agonists isoproterenol and carbachol, respectively. This profile of GPCRs also allowed us to probe potential off-target effects for representative members of all four G protein families (*i.e.,* Gi, Gq, Gs, G13). Compound 36 had exclusive specificity for GPR56, whereas compound 4 activated GPR56 and GPR97, but none of

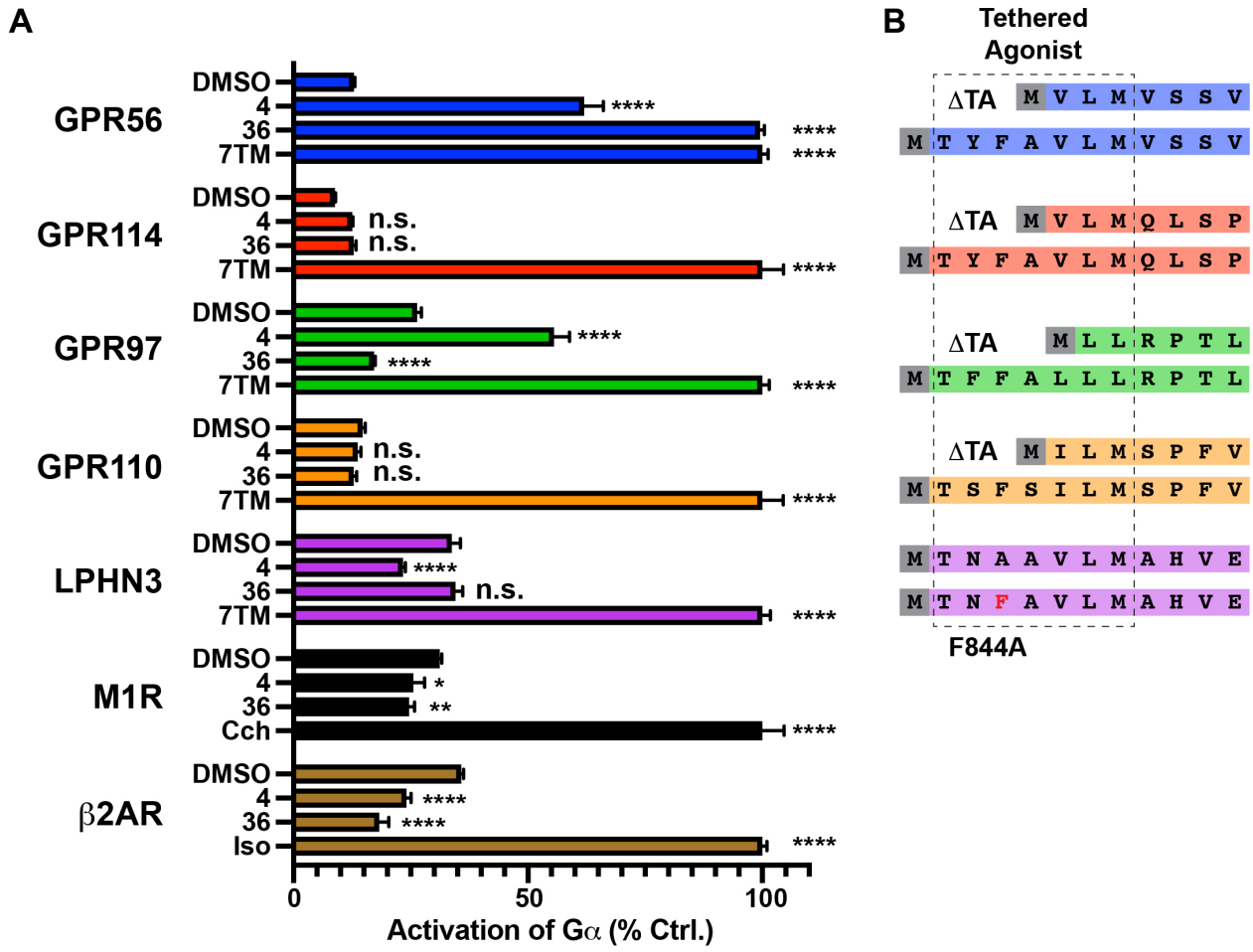

Figure 4.9 Selectivity of Compounds 4 and 36. **A**. Activity of Compounds 4 and 36 with various adhesion and two Class A GPCRs. Compound 4 and 36 (20 μM ea.) were pre-incubated with GPCR membrane homogenates that were reconstituted with purified heterotrimeric G proteins prior to measurement of GTPγS binding. Adhesion GPCRs were constructs lacking the NTF and with intact (7TM) or impaired tethered agonists (deletions or the LPHN3 F844A mutation). Muscaranic acetylcholine receptor 1 (M1R) and the β2 adrenergic receptor (β2AR) were stimulated with 50 μM carbachol (Cch) or 10 μM isoproterenol (Iso) as indicated. **B**. Sequences of the intact and compromised tethered agonists for each AGPCR. Data points are the mean ± SD of three independent reactions. Statistical significance compounds activity was determined by repeated measures of two-way analysis of variance. *P<0.05, **P<0.01, ***P<0.001, ****P<0.0001.

the other GPCRs (**Figure 4.9**). Compound 36 exhibited modest inhibition of GPR97 and β2AR, while compound 4 weakly inhibited LPHN3 and the β2AR.

4.3.5 Structure-Activity-Relationship of Compound 36 Analogs

Commercially available analogs of compound 36 were investigated to identify critical functional groups and to identify derivatives with improved potency and efficacy. A first set of 22

analogs were obtained that had functional group deletions or functional groups with altered positions. **Figure 4.10** shows the structures of all compound 36 analogs that were evaluated for the ability to activate GPR56 ΔTA via GPCR reconstitution assay (**Figure 4.11**). All functional groups were essential for full compound 36 activity, but two regions of the structure seemed suitable for optimization: the bromine and isopropyl groups (**Figure 4.11A**). Analog 36.4, which lacks a bromine on the bromobenzene group and contains a *tert*-butyl group instead of an isopropyl group, activated GPR56 at an efficacy approximately 60% that of the original compound. Analog 36.18 is identical to compound 36 but has a truncation of the isopropyl to a methyl group, which resulted in almost complete abrogation of GPR56 activity. These results suggested that both an electrophilic *ortho* group on the benzene ring and a hydrophobic group adjacent to the ester are necessary for full activity and might be positions to place alternative functional groups to optimize compound potency. This may explain how compound 32, which contains large differences in the positioning of its rings, was still capable of activating GPR56 to the level of GPR56-AP (**Figure 4.6**). Compound 32 has an additional benzene ring that may fill a hydrophobic pocket normally occupied by the hydrophobic isopropyl group of compound 36, giving it some capacity to activate GPR56. Additionally, we noticed the positioning of the bromine on compound 36 could not be altered without abrogating activity, as analog 36.15 has a shift of the bromine to the *meta* position and could only activate GPR56 with ~35% efficacy. Given the importance of the electrophilic bromine group and the aliphatic isopropyl group, we designated them as the X and R functional groups, respectively.

A second set of analogs that consisted of modifications to the X and R functional groups were tested. Most of these analogs retained some ability to activate GPR56, but with variable efficacies (**Figure 4.11B**). We again observed some malleability of the X group, as replacing the

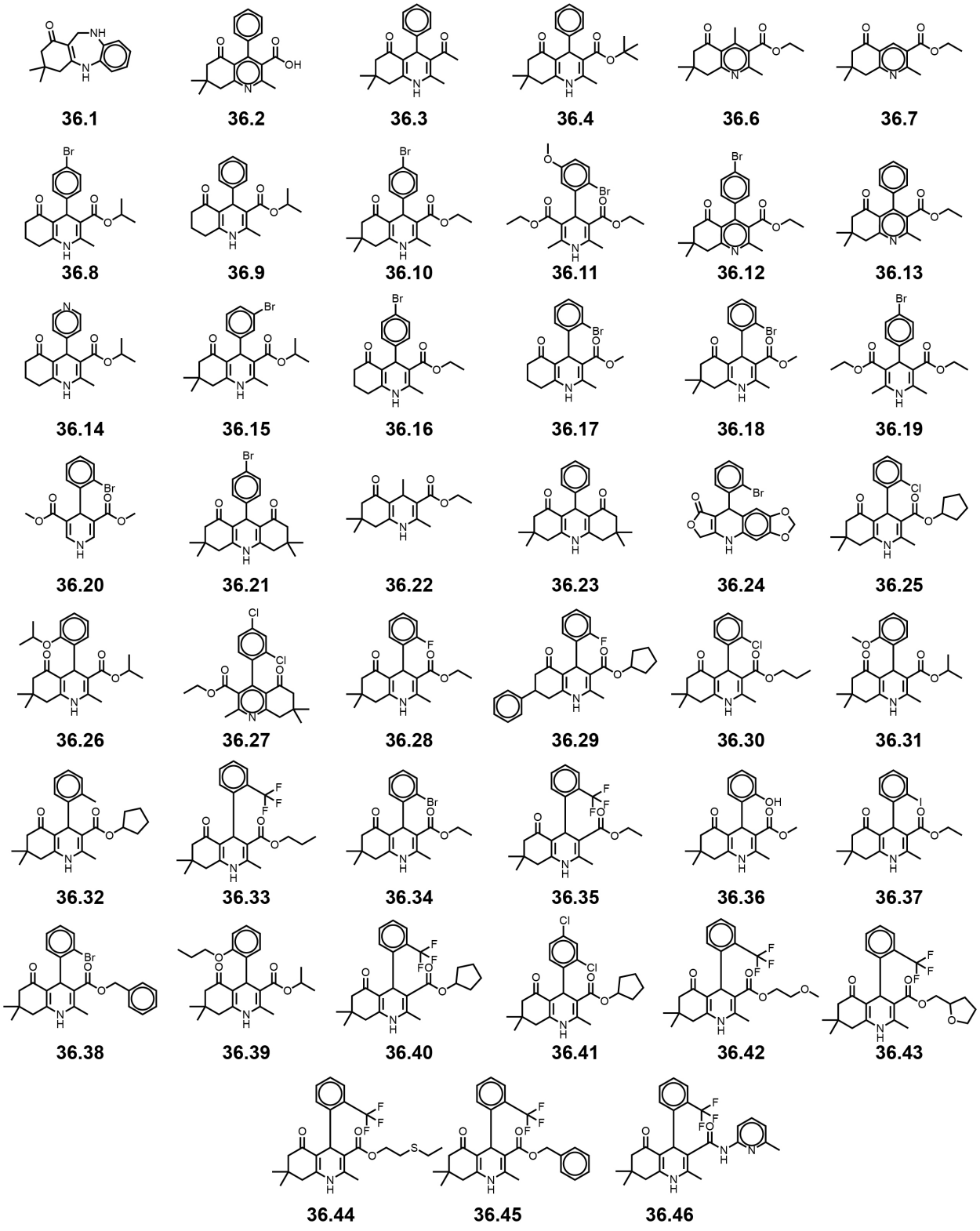

Figure 4.10 Structures of All Compound 36 Analogs Measured in the SAR. Compounds 36.01 through 36.23 constitute the first round of SAR, comprising mostly functional group deletions. Compounds 36.24 to 36.46 constitute the second round of SAR and comprise mostly functional group substitutions.

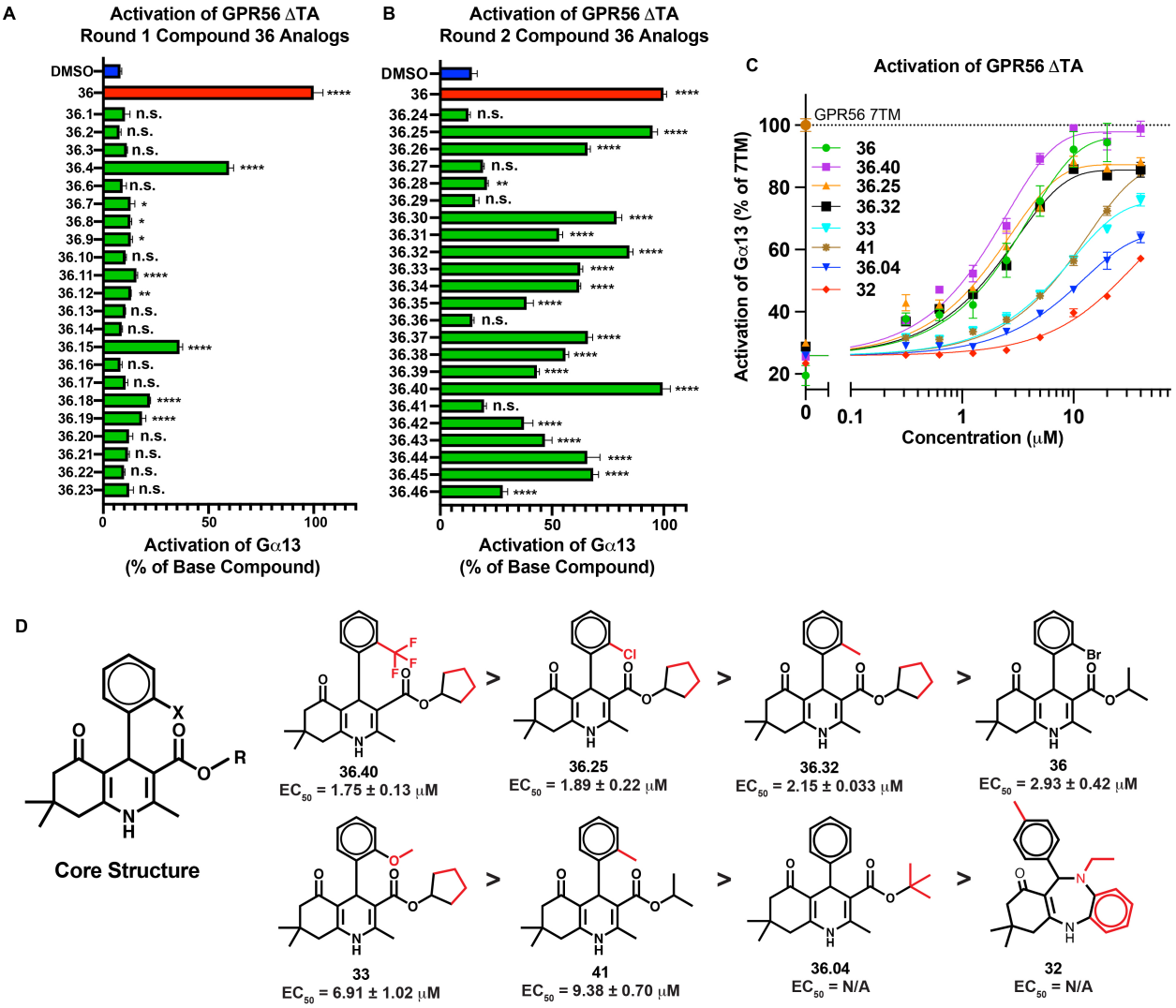

Figure 4.11 Structure Activity Relationships of Compound 36 analogs. A and B. Analogs of compound 36 (20 μM each) were incubated with GPR56 ΔTA prior to measurement of reconstituted G13 activation by GTPγS binding. Round 1 analogs were predominantly fragments of compound 36 with functional groups deleted, while round 2 analogs predominantly had functional group substitutions and additions (Supplemental Figure S5 shows the full detail of analog structures). **C.** Concentration response assays of top compound 36 analogs measured by GPR56 ΔTA / G13 reconstitution GTPγS binding assay. Analogs 32, 33 and 41 were found as independent hits in the initial screen for GPR56 activators. **D.** Structures of the best analogs of compound 36. The core pharmacophore is shown alongside a list ranking of each analog by potency. Functional groups in red represent significant changes from compound 36. All datapoints are the mean ± SD of three independent reactions. Statistical significance was determined by repeated measures of one-way analysis of variance. **P*<0.05, ***P*<0.01, ****P*<0.001, *****P*<0.0001

bromine with various functional groups caused reductions in efficacy, but not complete loss of activity. These substitutions included chlorine (36.30), iodine (36.37), CH_3 (36.32), CH_3O (36.31), and CF_3 (36.33, 36.35, 36.40, and 36.42 through 36.46). The degree of hydrophobicity of the R group was also observed to impact activity. Analogs 36.28, 36.35, and 36.36 had truncated R groups and exhibited reduced activity. A one-carbon extension of the ethyl group of analog 36.28 to the propyl group of analog 36.30 strongly accentuated activity to ~80% efficacy. These data suggest that larger and bulkier R groups correlate with higher activity. This was supported by analogs 36.25 and 36.40, which have large cyclopentane rings and activate GPR56 to near full efficacy. Compounds 36.32 and 36.41 also contain this cyclopentane ring, but alterations of its benzene ring reduced efficacy. A lack of an electrophilic group in analog 36.32 slightly reduced efficacy, while addition of a *para* chlorine atom completely abrogated activity. In sum, compounds with large aliphatic R groups and/or additional functional groups substituted for the X group activated GPR56 most effectively.

The most efficacious compound 36 analogs from both rounds of SAR were tested in concentration response assays (**Figure 4.11C**). Included were the three compound 36 analogs identified in the primary screens, compounds 32, 33, and 41. Compound 33 has a CH_3O X group and a cyclopentane ring as its R group, and compound 41 has a CH_3 X group with an unchanged R group. Compound 32 is much more different in structure, with a central 7-membered ring replacing the 1,4-DHP ring of compound 36, and an additional benzene ring adjacent to it. All three compounds activated GPR56 ΔTA with efficacies greater than GPR56-AP peptide (**Figure 4.6**). In concentration response assays, three analogs were found to have modestly increased potencies over compound 36 (EC_{50} 2.95 ± 0.41 μM). Analogs 36.40, 36.25, and 36.32 activated GPR56 ΔTA with EC_{50s} of 1.75 ± 0.13 μM, 1.89 ± 0.22 μM, and 2.15 ± 0.033 μM, respectively.

All three analogs contained the aforementioned cyclopentyl group in place of the isopropyl R group but had different X groups in place of the bromine (**Figure 4.11D**). Analog 36.40 had a CF_3 group, analog 36.25 had a chlorine group, and analog 36.32 had a CH_3 group in the X position. Of these analogs, compound 36.40 had efficacy equivalent to compound 36 that approached GPR56 7TM full agonism. Overall, the combination of the cyclopentyl R group and trifluoromethyl X group of 36.40 contributed to its ~40% increased potency over compound 36. Future efforts of compound 36.40 derivatization may be taken to enhance its activity towards GPR56.

4.3.6 In silico docking of compound 36 and 36.40 in the GPR56 orthosteric site.

Compound 36 and its higher potency analog 36.40 have a chiral center in which the bromo- or trifluoromethyl-benzene ring may rotate. The syntheses of these compounds are most likely racemic mixtures. To model the binding sites of the compound 36 pharmacophore, we conducted *in silico* docking of the *R* and *L* enantiomers to active-state GPR56 7TM (PDB: 7SF8) [163] that had its TA deleted (*i.e*. residues T383 through V395). Both compound 36 enantiomers docked within the orthosteric site at a region normally occupied by the intact TA and was proximal to several residues that are critical for TA interactions, notably $F^{2.64}$, $W^{45.51}$, $W^{6.53}$, and $F^{7.42}$ (**Figure 4.12A-B**) [163]. The bromobenzene ring of both enantiomers was locked in a fixed position proximal to $W^{45.51}$ of ECL2 and the poses of the other rings were nearly mirror images along a vertical axis about the central pyridine ring. The isopropyl group of the *L* enantiomer of compound 36 was facing TM5, close to $N^{5.39}$, whereas the *R* enantiomer was docked such that the isopropyl group occupied a larger hydrophobic pocket next to $F^{2.64}$. In both poses the pyridine ring was positioned deep within the orthosteric site in a hydrophobic region proximal to both $W^{6.53}$ and $F^{7.42}$. When analog 36.40 was docked, the CF_3 group of the *R* enantiomer appeared to fit readily into the pocket adjacent to ECL2 and the cyclopentyl group occupied the additional available hydrophobic

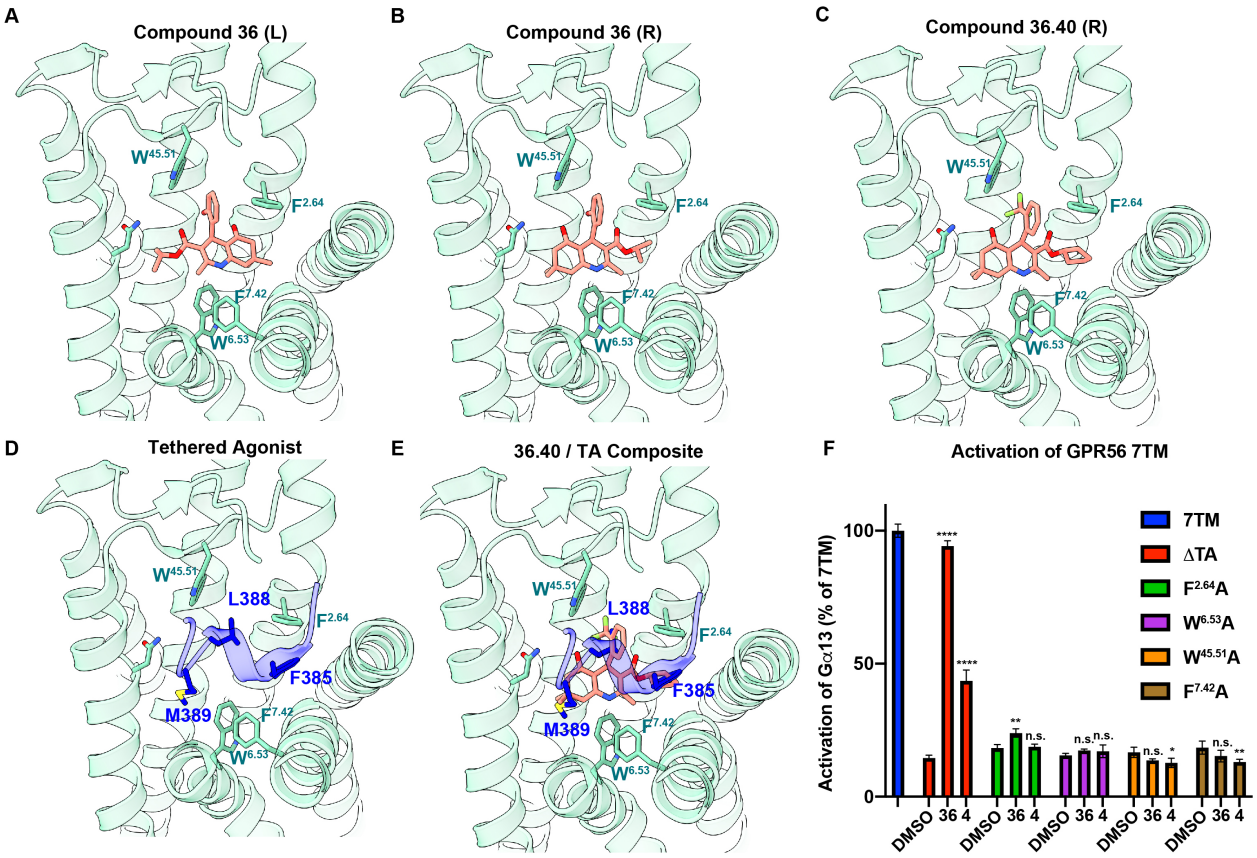

Figure 4.12 *In silico* docking prediction of compound 36 and 36.40 enantiomers. A and B. Compound 36 (red) docked within the orthosteric site of GPR56 7TM (teal, PDB: 7SF8) with its tethered agonist removed. The *L* (A) or *R* (B) enantiomers docked in a similar position within the orthosteric site. Prominent residues that interact with the GPR56 TA are denoted (dark green). **C**. Compound 36.40 (*R* enantiomer) was docked into the same pocket in the same manner as compound 36. **D.** The structure of the tethered agonist (blue) engaged within the orthosteric pocket. The three residues vital for TA engagement are highlighted. **E**. The structure of the tethered agonist overlaid with docked compound 36.40. **F.** Activation of GPR56 7TM with various point mutations that abrogate TA binding in the GPCR reconstitution assay. Either DMSO or 20 μM of compound 36 or compound 4 was pre-incubated with membrane homogenates prior to the start of assay. Data points are the mean ± SD of three independent reactions. statistical significance was determined by repeated measures of two-way analysis of variance. **P*<0.05, ***P*<0.01, ****P*<0.001, *****P*<0.0001

space proximal to $F^{2.64}$ (**Figure 4.12C**). In active-state GPR56 7TM, these pockets are occupied by residues L388 and F385 of the TA, respectively (**Figure 4.12D**). When the compound 36.40 *R* enantiomer pose was overlaid with the TA, the cyclopentyl ring overlapped almost entirely with the aromatic ring of TA residue F385 (**Figure 4.12E**). These models indicate that the *R* enantiomer of the compound 36 pharmacophore may be the active compound, thereby explaining why substituting the isopropyl group of compound 36 with larger hydrophobic groups improved its activity. Overall, these models predict that compound 36 *R* enantiomer analogs interact with the

critical residues that also interact with the tethered agonist. To assess the importance of these TA-interacting residues for compound 36 activation, we tested compound 36 or compound 4 with GPR56 7TM point mutants $F^{2.64}A$, $W^{45.51}A$, $W^{6.53}A$, or $F^{7.42}A$ for G protein activation. All four mutations resulted in near complete abrogation of activity compared to the constitutively active 7TM (**Figure 4.12F**). Compounds 36 and 4 were unable to rescue the activities of the four point mutants, but stimulated GPR56 ΔTA.

4.4 Discussion

Knowledge of adhesion GPCR function and therapeutic potential is emerging rapidly. The recent solution of active-state structures of seven adhesion GPCRs including GPR56 [163, 197-199] affirmed a common mechanism whereby the tethered agonist adopts a partial α-helical hook-like conformation that binds its orthosteric site within the 7TM core beneath ECL2. The P3, P6, and P7 residues of the TA are typically phenylalanine, leucine, and methionine, respectively and form critical hydrophobic interactions with residues of the TM spans and ECL2. Despite this new understanding, most AGPCRs are orphans with few molecular tools to study them. Synthetic peptides that mimic the tethered agonists have some utility but often suffer from poor solubility, low potency, and receptor inaccessibility [33, 57, 59, 60, 196, 201]. This calls for a need for small molecule AGPCR agonists and antagonists with improved characteristics. Here, we expanded on our previous small molecule pilot screens to identify a potent full agonist that has apparent exclusive specificity for GPR56. The compound has improved characteristics and may serve as a future lead in the development of a first-in-class AGPCR therapeutic.

The activator screen for GPR56 agonists comprised over 200,000 compounds and was 100-fold larger than our previous pilot screen that revealed 3-α-DOG as a partial agonist for GPR56 [61]. After secondary vetting and counter assay testing in cell-based assays, 74 hits were identified

which was then narrowed to 16 hits following orthogonal assay testing. Within these final hits, compounds 32, 33, 36, and 41, are close structural analogs. The remaining 12 hits are structurally distinct but shared common moieties, including a sulfonamide linker (compounds 7, 12, 29, and 37), a carboxamide linker (compounds 67, 51, 73, 56, and 74), or a terminal 2,5, dimethoxybenzene ring (compounds 7, 12, and 48). These common structural features may indicate similar binding modalities for GPR56. Additionally, the sulfonamide compounds may serve as therapeutically viable leads, given that sulfonamide analogs are noteworthy for their ability to improve therapeutic properties of drugs [202].

The two most promising compounds identified were propan-2-yl-4-(2-bromophenyl)-2,7,7-trimethyl-5-oxo-1,4,5,6,7,8-hexahydroquinoline-3-carboxylate, or compound 36, and 2-(furan-2-yl)-1-[(4-phenylphenyl)carbonyl]pyrrolidine, or compound 4. Compound 36 was the most efficacious of its structural cluster and is a 1,4-DHP derivative of hexahydroquinoline. 1,4-DHP compounds, including those that are HHQ derivatives, were identified as L-type calcium channel blockers and marketed as drugs (*e.g.* nifedipine) to treat hypertension [203-206]. It is possible that compound 36 and its analogs could have off target hypotensive effects, as previous SAR work showed that closely-related HHQ derivatives inhibited $Ca_v1.1$ channel activation [207]. However, compounds with larger hydrophobic R groups were less efficacious at inhibiting $Ca_v1.1$. The inverse is true for GPR56 activation; compounds with larger R groups were most effective. Consequently, we expect that the 36.40 derivative with its bulky cyclopentyl R group would have limited activity for L-type calcium channels. We also predict that L-type calcium channel blockers would be poor GPR56 agonists. Many 1,4-DHP-based calcium channel blockers possess functional groups at the 3rd and 4th carbons of the aryl group. We observed in our SAR analysis that electron withdrawing groups at these positions render the compounds incapable of activating

GPR56. Included in our SAR analysis were compounds with symmetric 1,4-DHP rings that closely match structures of calcium channel blockers: compounds 36.11, 36.19, 36.20, 36.21, and 36.23. Each of these compounds had little effect on GPR56.

Compounds 36 and 36.40 are full agonists that stimulated GPR56 ΔTA to the maximal efficacy of GPR56 7TM that has an intact, endogenous tethered agonist. Compound 36 did not synergize with GPR56-AP, as GPR56 ΔTA co-activation by peptide and compound 36 showed no enhanced potency or efficacy (**Figure 4.13**). In fact, GPR56-AP diminished the maximal efficacy imparted by compound 36, suggesting that the TA peptidomimetic is a partial agonist that may

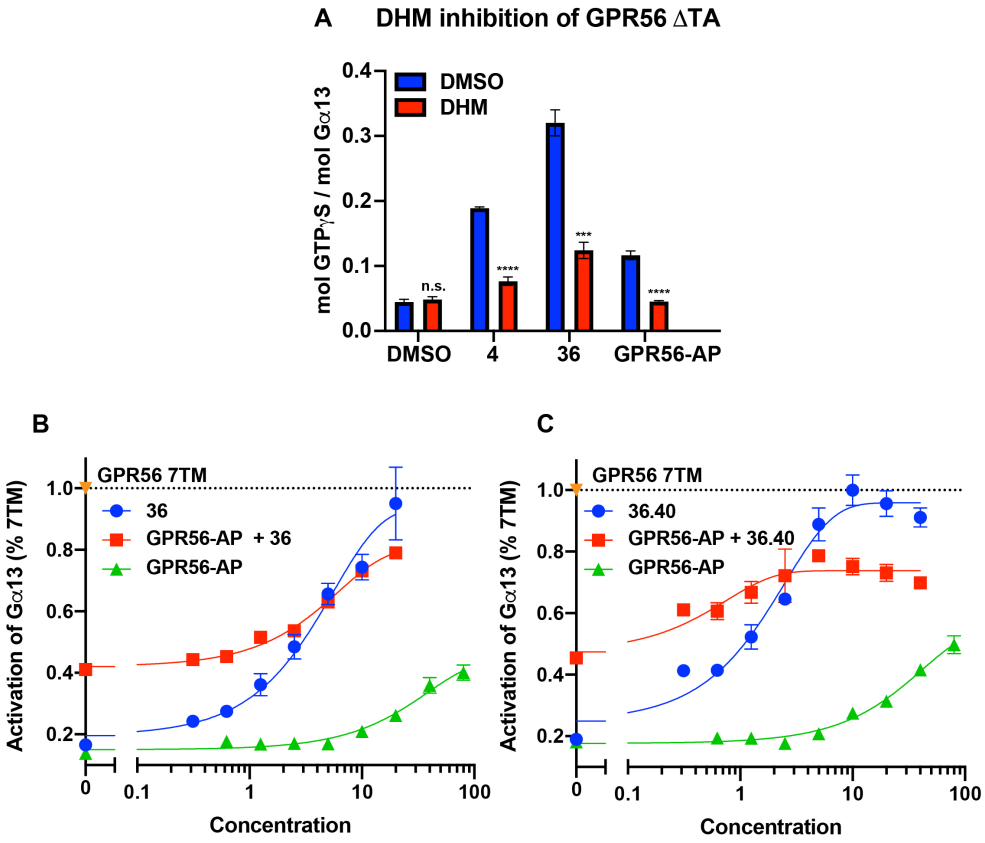

Figure 4.13 Compound 4 and 36 Activation of GPR56 is Inhibited by Dihydromunduletone (DHM) and does not Synergize with GPR56-AP. **A.** GPR56 ΔTA membrane homogenates were reconstituted with purified G13 heterotrimer and pre-incubated with 50 μM DHM or DMSO before being stimulated with GPR56 activators (20 μM), prior to measurement of receptor-stimulated G13 GTPγS binding. **B.** GPR56 ΔTA membrane homogenates were reconstituted with purified G13 heterotrimer and DMSO or 80 μM GPR56-AP before being stimulated with the indicated concentrations of Compound 36. Receptor-stimulated G13 GTPγS binding was measured. Data are the mean ± SD of three independent reactions. Statistical significance between compounds and DMSO was determined by repeated measures unpaired students t tests. *P<0.05, **P<0.01, ***P<0.001, ****P<0.0001

compete with compound 36. Compound 4 was less potent than compound 36, and only activated GPR56 ΔTA to ~50% maximal efficacy of GPR56 7TM. Compounds 4 and 36 were the only hits that activated the cleavage deficient GPR56 holoreceptor. GPR56-AP and the partial agonist 3-α-DOG are incapable of activating the GPR56 holoreceptor *in vitro* [33, 61]. It is possible that these agonists do not activate GPR56 due to NTF-mediated occlusion of the 7TM orthosteric site. However, low-resolution structural models of AGPCR holoreceptors demonstrated NTF flexibility in relation to the 7TM. A full understanding of the basis of agonist entry to AGPCR orthosteric sites awaits further investigation [163].

Interestingly compound 36, but not compound 4 activated GPR56 F385A/M389A and GPR56 L388A/M389A double TA mutant holoreceptors, the former being partially cleavage deficient, and the latter cleaved efficiently. We do not fully understand the basis of why compound 4 activated the severely cleavage-defective H381S holoreceptor, but not the compromised tethered agonist holoreceptors. We speculate this may be due to a combination of factors including differential access to the orthosteric site and the prospect that the TA impaired mutants may experience some spontaneous NTF shedding followed by mutant tethered agonist non-productive engagement of the orthosteric site, but in a manner that blocks compound 4 binding.

An *in silico* approach predicted that compounds 36 and 36.40 dock in the GPR56 orthosteric site through a binding mechanism that has parallels to tethered agonist binding. The positioning of the 2-bromophenyl or 2-trifluormethylphenyl groups of the compounds near $W^{45.51}$ may explain why addition of functional groups to the 3rd or 4th carbons of the aryl group dramatically decrease compound activity in our SAR analysis. Electron withdrawing groups like bromine or chlorine in these positions would be positioned in proximity to $W^{45.51}$ and interact unfavorably. The *R* and *L* enantiomers of compounds 36 and 36.40 docked as mirror images within

the orthosteric site. Our analysis suggests that the *R* enantiomer is the active species, as the cyclopentyl R group of compound 36.40 closely overlaps with the position of TA residue F385 and may likewise engage TM2 residue $F^{2.64}$. This provides a plausible explanation of why substituting the isopropyl R group of compound 36 with larger hydrophobic groups increased activity. Bulkier hydrophobic groups at this position may allow the compound to interact more favorably with $F^{2.64}$. Notably, we included in our SAR analysis an analog that contained a benzene ring as its R group (analog 36.45) which could potentially form favorable pi-pi interactions with $F^{2.64}$. This compound exhibited only ~70% efficacy compared to the base compound. The reduction in efficacy may be explained by the presence of a one-carbon extension prior to the benzene compared to analog 36.40. With these models in mind, we plan to conduct future derivatization of compound 36.40 by targeting its hydrophobic R group. We anticipate variations of a benzene ring will increase activity towards both GPR56 ΔTA and the holoreceptor. Substitutions of the electron withdrawing X group are unlikely to provide enhanced activity, as steric hinderance within the pocket beneath ECL2 is a concern.

Interestingly, compound 36 was selective for GPR56 and did not activate other AGPCRs, even within the same G subfamily. This includes GPR114, which contains an identical TA to GPR56 and consequently a similar orthosteric binding site [198]. However similar, GPR114 has slightly altered positions for $F^{2.64}$, $F^{7.42}$, $W^{45.52}$ and $W^{6.53}$ within its orthosteric site, enough so that it may not bind productively to compound 36 [163, 198]. In sum, compound 36 and its analog 36.40 are the most potent activators identified thus far for GPR56. Their selectivity towards GPR56 and capacity to activate the holoreceptor make them viable candidates as lead compounds for further development and to serve as improved tool compounds to probe GPR56 activity.

Chapter 5 Cell-Based High Throughput Screens Reveal Platelet-Responsive Antagonists of GPR56

5.1 Abstract

Adhesion GPCRs (AGPCRs) uniformly share a perplexing topology and activation mechanism that confounds our ability to study them both *in vitro* and *in vivo*. They possess large, variable extracellular domains ranging from hundreds to thousands of residues in length that are autoproteolytically cleaved by a conserved GPCR autoproteolysis-inducing (GAIN) domain N-terminal to the start of the 7-transmembrane domain (7TM) region of the receptor. GAIN domain-mediated cleavage splits the receptors into two fragments that remain held together noncovalently, the extracellular N-terminal fragment (NTF) and membrane intercalated C-terminal fragment (CTF). Dissociation of the NTF and CTF exposes a small stalk region on the CTF termed the tethered agonist (TA) that binds to the orthosteric site to activate the receptor. This two-step activation mechanism was recently validated by the first cryo-EM structures of activated AGPCRs with their tethered agonists bound within in the orthosteric site. However, many of these receptors remain as orphans with few molecular tools to bypass this activation mechanism and study them *in vivo*. Consequently, there currently exists no drugs that target AGPCRs, despite their high therapeutic potential. Here, we seek to ameliorate this by expanding a previous inhibitor screen of the model AGPCR GPR56 to identify novel, potent AGPCR antagonists. From a screen of over 20,000 compounds, we identified a collection of 15 structures that potently inhibited GPR56 in our cell-based assays. We purchased eight of these inhibitors for early-stage characterization, and

found that two of them, MBI19 and MBI48, attenuated platelet aggregation in a GPR56-dependent manner. Additional work is underway to further characterize these compounds, but the inhibitors identified thus far show high potential as vital tool compounds and may serve as leads for first-in-class AGPCR drugs.

5.2 Introduction

Adhesion G Protein Coupled Receptors (AGPCRs) are class B1 receptors that notably possess large extracellular regions that mediate self-cleavage to split the receptor into two fragments that remain noncovalently attached. A highly conserved GPCR autoproteolysis-inducing (GAIN) domain N-terminal to the start of transmembrane helix 1 (TM1) mediates the self-cleavage event, which occurs as the protein folds on the ER membrane before it is trafficked to the cell surface [30, 168]. Dissociation of the extracellular N-terminal fragment (NTF) exposes a small stalk sequence on the N-terminus of the C-terminal fragment (CTF, or 7TM domain) that acts as a tethered agonist (TA) for the GPCR. Recent cryo-EM structures of AGPCRs in their activated state have revealed that following NTF dissociation, the TA bends 180º inward and weaves underneath extracellular loop 2 (ECL2) to adopt a partial helix conformation within the orthosteric site [163, 197-199]. There, the P3, P6, and P7 residues of the TA (typically phenylalanine, leucine, and methionine) form hydrophobic interactions with residues located on TMs 1, 2, 6, 7 and ECL2. Binding of the TA also causes a break in TM6 and TM7 that opens the intracellular side of the 7TM barrel, allowing for G protein engagement.

Despite a newfound knowledge of how AGPCRs are fully activated, there is still much that is not known about how the receptors function. Low-resolution cryo-EM structures of AGPCR holoreceptors have shown that the NTF is a flexible region that is tethered to the CTF, rather than closely ordered against it, but leaves the question of how allosteric binding of extracellular ligands

influences receptor activity [163]. Additionally, it is not well known how different AGPCRs are activated in endogenous tissue systems. There are 33 receptors in the AGPCR subclass, each with a diverse arrangement of N-terminal "adhesive" domains that bind to a variety of different anchored or soluble ligands. Current literature suggests that these ligands can interact with the NTF to result in either allosteric or orthosteric (*i.e.,* tethered agonist) activation, but it is not well understood exactly how either occurs *in vivo*. This issue is further confounded by the lack of available tool compounds to probe receptor activity. Such compounds could be small molecule agonists or antagonists that bypass the two-step activation process of AGPCRs to bind their orthosteric site in an TA-independent manner. Currently, this can be achieved with moderate success using small peptides that mimic the sequence of the tethered agonist [33, 34, 56, 57, 59, 60]. However, these peptidomimetics are very hydrophobic and have low potencies due to the properties of the peptide they're derived from, and thus have poor therapeutic potential. By contrast, small molecule compounds can be optimized to have a much higher potency and solubility, making them much more promising as leads for AGPCR-targeted therapeutics. Indeed, AGPCRs are one of the last frontiers for GPCR medicine, as there currently are no FDA approved drugs that target them.

In search of novel high-potency tool compounds, we have conducted high throughput screens for the model AGPCR GPR56. GPR56 couples to $G_{12/13}$ family G proteins and has well established roles in neuronal development, muscular function, testicular development, and platelet activation [110, 113, 149, 169, 170, 173, 200]. Additionally, GPR56 has been repeatedly identified as an oncogene, making it a promising chemotherapeutic target [112, 176-181]. N-terminal its GAIN domain, GPR56 possesses a pentraxin/laminin/neurexin/sex-hormone-binding-globulin-like (PLL) domain that binds to collagen and transglutaminase-2 [83, 110, 174, 175]. We

established a cell-based luciferase screen that reports on $G_{12/13}$ signaling to search for small molecule agonists and antagonists for GPR56 constructs with a deleted NTF and an intact TA (GPR56 7TM) or a truncated TA (GPR56 A386M, or ΔTA). In a ~2,000 compound pilot screen, we identified the steroid partial agonist 3-α-acetoxydeoxygedunin (3-α-DOG) and the isoflavonoid antagonist dihydromundunetone (DHM) [61, 114]. These compounds aided us in the discovery of platelet activation as a novel function for GPR56, but their low efficacy (3-α-DOG) or cytotoxic off-target effects (DHM) prevent them from being effective drug leads.

Here, we've expanded our previous cell-based inhibitor screen ten-fold to identify additional potent antagonists from a library of ~23,000 compounds. Given the high hit rate of preliminary screens against GPR56 7TM, we employed a simultaneous counter screen that vetted all compounds against cells transfected with a constitutively active mutant of $G_{\alpha 13}$, $G_{\alpha 13}$ Q226L (or $G_{\alpha 13}$-QL). Primary and counter screens revealed 145 initial hits, which was reduced to 50 total compounds following a secondary reconfirmation assay. These inhibitors were assayed in robotically pipetted concentration response curves, which eliminated 35 compounds for low efficacy or poor hill slopes that were likely a result of cytotoxicity. The remaining 15 compounds were purchased in two batches for follow-up validation. Within the first batch of eight compounds, two exhibited notable activity in both the cell-based SRE-Luc gene reporter assay, and the biochemical GPCR reconstitution assay: MBI19 and MBI48. Notably, both compounds inhibited the aggregation response of platelets that had been stimulated with GPR56-activating peptide (GPR56-AP) with low micromolar potency. MBI19 and MBI48 could not inhibit platelets stimulated by PAR4-activating peptide (PAR4-AP), suggesting that the inhibitors attenuated platelet activity in a GPR56-dependent manner. The second batch of GPR56 inhibitors are currently being tested, and early-stage SAR has commenced on MBI19 and MBI48. Knowledge

of AGPCRs and their ligands is rapidly emerging. Biological studies in the last two decades have deorphanized a nearly half of the 33-membered family, and recent structural work of the receptor in the activated form has detailed a conserved activation mechanism for orthosteric activation. The inhibitors detailed in this study have the potential to advance AGPCR research even further by providing novel tool compounds that have a high potential to serve as leads for first-in-class AGPCR-targeted therapeutics.

5.3 Results

5.3.1 Primary Screening for Inhibitors of GPR56

To screen for inhibitors of GPR56, we used an approach similar to our large-scale agonist screen as outlined in Chapter 4 of this thesis (**Figure 4.1**). Human GPR56 primarily signals through $G_{12/13}$ family G proteins and its activity can be monitored via a serum response element (SRE-) Luciferase gene reporter. We transfected HEK293T cells with SRE-Luciferase and a GPR56 construct that shifted the initiator methionine up to before the first threonine of the tethered agonist (T383) to remove the NTF (GPR56 7TM). To normalize luminescence counts, cells were also transfected with a small amount of Renilla luciferase construct that lacked an SRE promoter. GPR56 7TM exhibited constitutively active signaling with a luminescence signal that was several folds higher than that of holoreceptor GPR56 (**Figure 4.1D**). As a positive control for inhibition, we added 1 μM of the actin polymerization inhibitor Latrunculin B (LatB). LatB completely eliminated G13 signaling and was set as the positive control for the high throughput inhibitor screen (Z' = 0.51). As with our agonist screen, we employed a counter screen assay to eliminate compounds that interfered with the signaling pathway. Our counter screen replaced GPR56 7TM transfection with $G_{\alpha13}$ Q226L ($G_{\alpha13}$-QL), a constitutively active point mutant of $G_{\alpha13}$. Compounds

that inhibited signaling in both GPR56- and $G_{\alpha 13}$-QL-transfected cells were deemed pathway inhibitors and eliminated from the study, while compounds that only inhibited GPR56 progressed onto further validation [114].

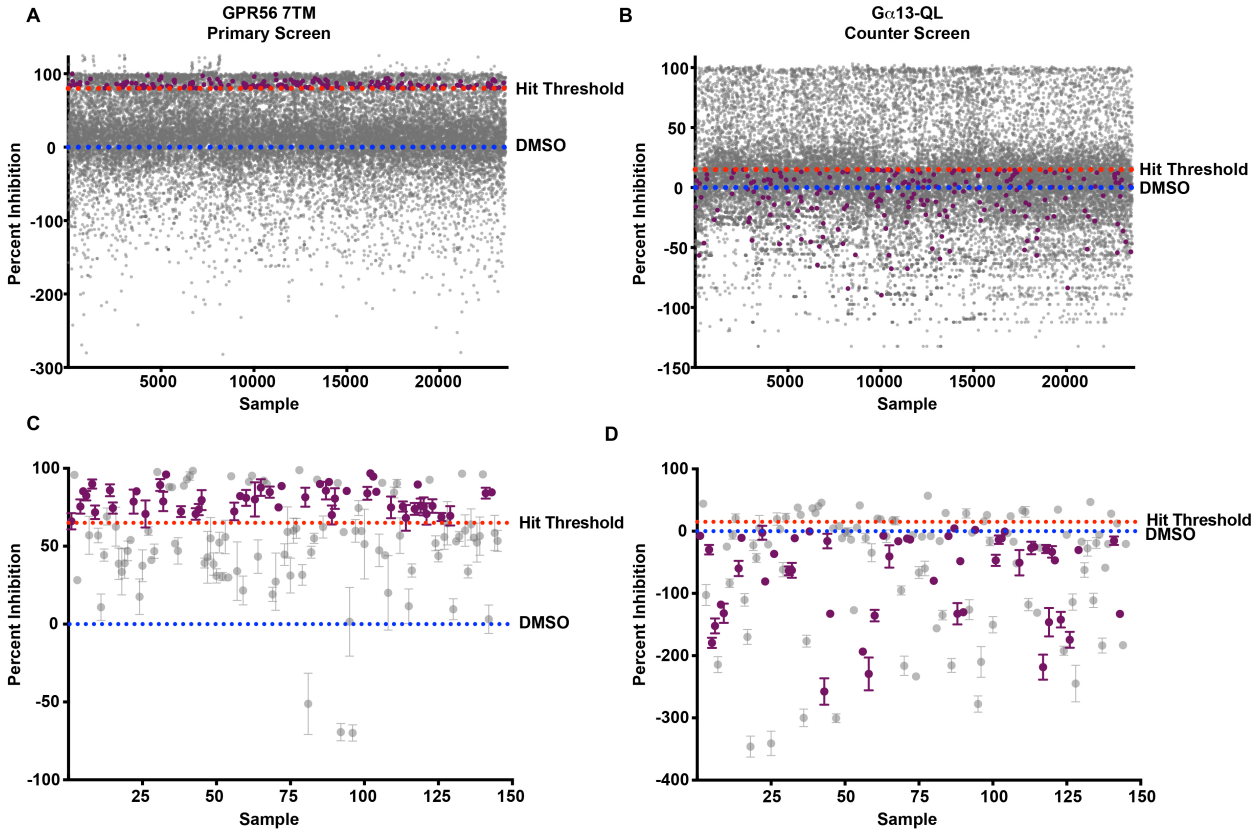

Figure 5.1 GPR56 Inhibitor Primary Screen Results. A and **B.** 23,552 compounds from the MayBridge chemical library were screened for inhibitory activity against 293T cells transfected with SRE-Luciferase reporter and GPR56 7TM (**A,** primary screen) or $G_{\alpha 13}$-QL (**B,** counter screen). Activity was normalized to 1 μM of the actin polymerization inhibitor Latrunculin B. 85% activity was used as a threshold for hits in the primary screen, and 15% activity was used as an elimination threshold for the counter screen. Highlighted in purple are the 145 hits that inhibited above 85% in the primary screen and did not inhibit above 15% in the counter assay. **C** and **D**. Reconfirmation assays for the primary screen (**C**) or counter screen (**D**). The 145 hits identified in the primary screen were robotically pipetted into 384-well plates in triplicate before being overlaid with cells transfected with GPR56 7TM (**C**) or $G_{\alpha 13}$-QL (**D**). Purple dots represent the 50 compounds that reconfirmed their activity by having above 65% inhibition in the primary assay and below 15% inhibition in the counter assay.

Using cryopreserved aliquots of HEK293T cells pre-transfected with GPR56 7TM and SRE-luciferase, we screened the Maybridge library of 23,552 compounds using 1% DMSO as a negative control and 1 μM LatB as a positive control. Luminescence counts was normalized such that 1 μM LatB represented 100% inhibition, and a hit threshold of 85% inhibition was used to

identify hits. We chose this threshold as our previous pilot screen revealed that the primary hit rate for screening GPR56 7TM was too high to use the standard threshold of three standard deviations above the negative control (approximately 35% inhibition) [114]. We identified 2,892 hits in the primary screen, yielding an initial hit rate of 12.3% (average Z' = 0.53) (**Figure 5.1A**). To further narrow these hits and eliminate false positives, we re-ran entire Maybridge library in our counter assay using cells pre-transfected with $G_{\alpha 13}$-QL and SRE-Luciferase. Compounds that elicited activity above 15% inhibition in the counter assay were eliminated from further validation. 8,524 compounds in the counter assay exhibited activities higher than 15% and thus were eliminated (**Figure 5.1B**, average Z' = 0.71). 2,747 of the eliminated compounds also inhibited in the GPR56 screen, leaving final list of 145 candidate inhibitors and an adjusted hit rate of 0.61% (**Figure 5.1A-B**, purple dots).

5.3.2 Confirmation of GPR56 Inhibitors

Given that the primary screen was conducted in n=1 to increase assay throughput, we conducted a reconfirmation assay of the candidate inhibitors of GPR56 to further eliminate any false positives. All 145 compounds identified in the primary screen were robotically pipetted in triplicate and spotted into 384-well plates before being overlaid with 293T cells transfected with SRE-Luciferase reporter and either GPR56 7TM or $G_{\alpha 13}$-QL. For reconfirmation, we used a less severe hit threshold of 65% inhibition and retained the elimination threshold of 15% inhibition for the counter assay. 71 compounds failed to reconfirm their activity, and 24 of the remaining 74 compounds also inhibited in the counter assay, leaving 50 validated inhibitors of GPR56: MBI1 through MBI50 (**Figure 5.1B)**. Notably, we observed that a substantial number of compounds exhibited "negative" inhibition in the counter assay. These compounds caused an *increase* in

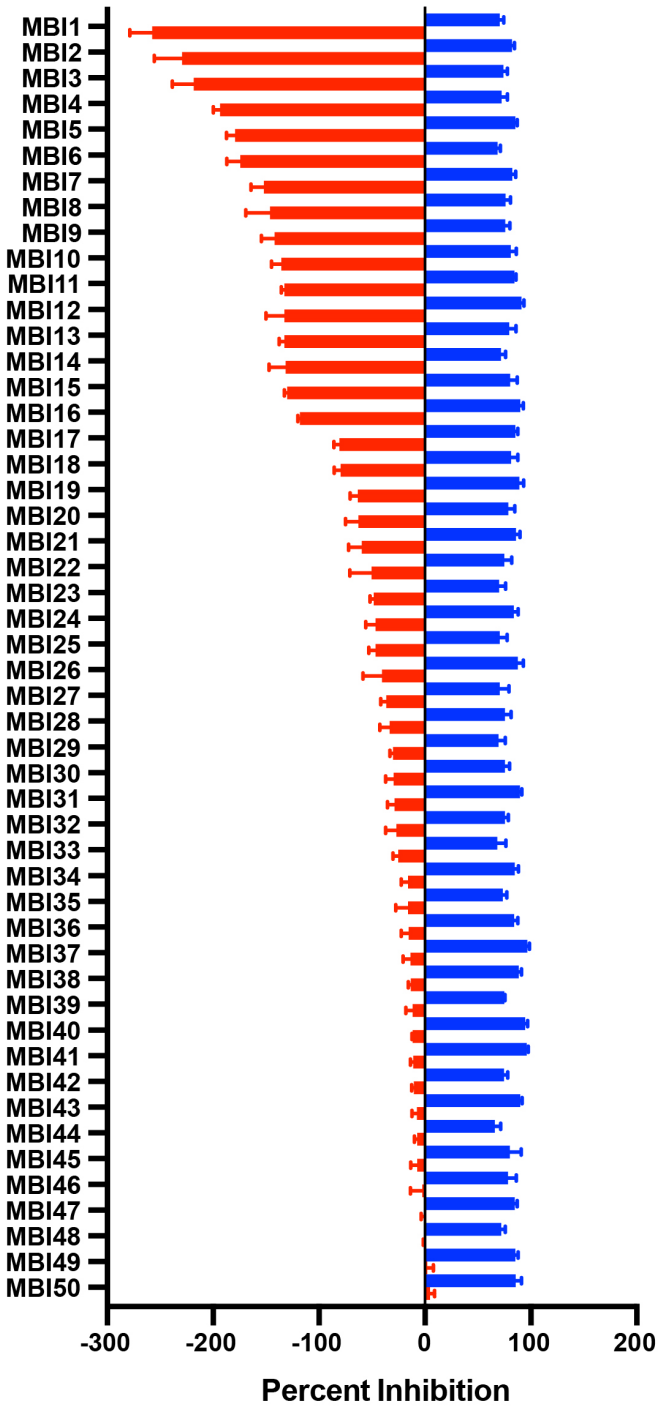

Figure 5.2 Activities of GPR56 Inhibitors in the Primary and Counter Assay. Shown are the reconfirmed activities of the top 50 inhibitors in either the primary screen (blue) or the counter screen (red). Data represent the mean ± SD of three technical repeats and are normalized to 1 μM Latrunculin B. Negative inhibition represents an increase in luminescence signal compared to the negative control.

luminescence signal when added to cells transfected with $G_{\alpha 13}$-QL, as high as two to three-fold over the DMSO control (**Figure 5.2**). While this observation is likely a result of signaling interference downstream of $G_{\alpha 13}$, we opted to continue validation of these compounds to see if this interference would hold in our other assays.

To acquire early estimates of potency and efficacy, and to further narrow the list of GPR56 inhibitors, compounds were robotically pipetted into concentration response curves (CRCs) that ranged from 375 nM to 48 μM. These assays revealed that 23 of 50 compounds poorly inhibited GPR56 at concentrations below 6 μM and then spiked in activity above 12 μM (**Figure 5.3**). This is likely an observation of cytotoxicity and consequently these compounds were eliminated from further characterization. Twelve additional compounds were eliminated for exhibiting "negative" inhibition at concentrations below 10 μM, leaving 15 inhibitors with approximate IC_{50}s of below 10 μM. Eight compounds were purchased in powder form for follow-up characterization (MBI50, MBI19, MBI48, MBI43, MBI49, MBI37, MBI33, MBI31). The remaining seven compounds are planned to be tested in the near future.

5.3.3 Reconstitution and Validation of Purchased Inhibitors

To reconfirm the activities of our eight purchased GPR56 inhibitors, we reconstituted fresh powders into DMSO and tested them in additional concentration response curves with 293T cells freshly transfected with SRE-Luciferase, Renilla luciferase, and either GPR56 7TM or $G_{\alpha 13}$-QL. Cells were seeded into 96-well format before being subjected to compounds at concentrations ranging from 781 nM to 50 μM. All eight compounds robustly decreased luminescence signal in cells transfected with GPR56 7TM (**Figure 5.4A**). 6.25 μM of each compound was sufficient to

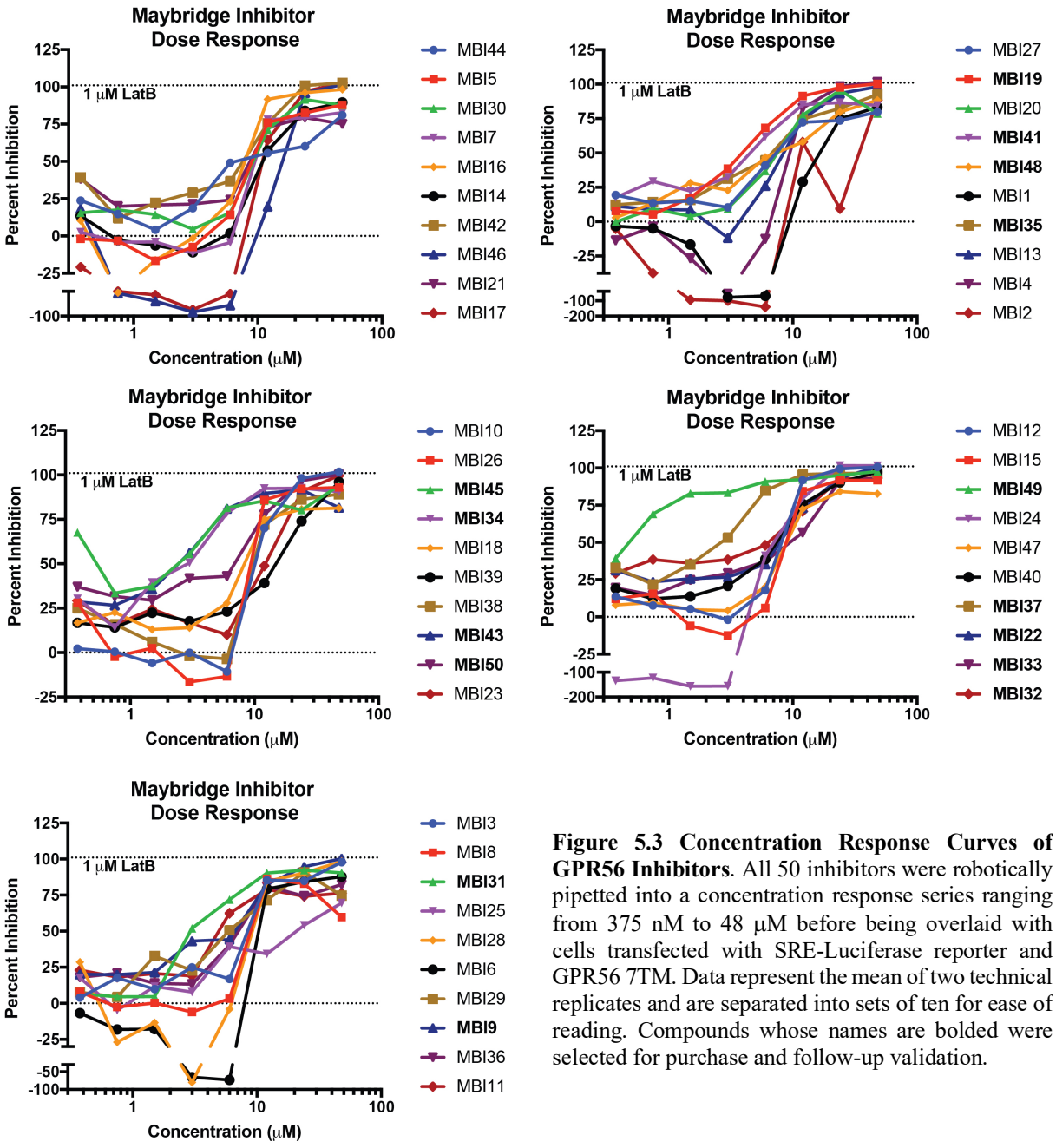

Figure 5.3 Concentration Response Curves of GPR56 Inhibitors. All 50 inhibitors were robotically pipetted into a concentration response series ranging from 375 nM to 48 μM before being overlaid with cells transfected with SRE-Luciferase reporter and GPR56 7TM. Data represent the mean of two technical replicates and are separated into sets of ten for ease of reading. Compounds whose names are bolded were selected for purchase and follow-up validation.

inhibit GPR56 to at least 50% the level of the DMSO control, with the most efficacious compounds being MBI50, MBI48, MBI49, and MBI33. MBI49 appeared the most potent of the compounds, as it could inhibit GPR56 to 25% activity with less than 1 μM. When added to cells transfected with $G_{\alpha 13}$-QL, half of the compounds (MBI50, MBI19, MBI49, and MBI33) slightly reduced signaling at higher concentrations but had limited effects at concentrations lower than 6

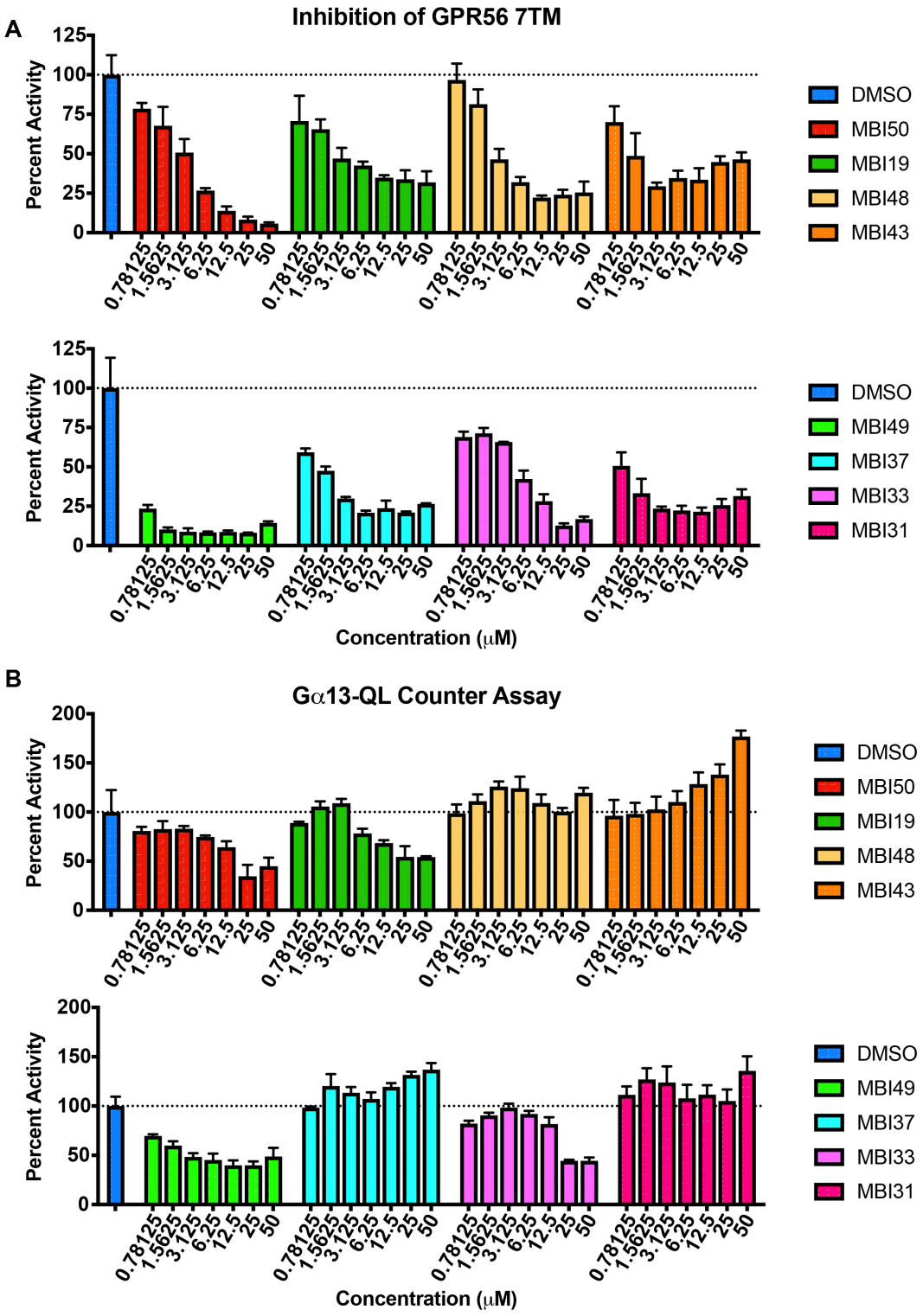

Figure 5.4 Reconstitution of Purchased GPR56 Inhibitors. **A.** Activity of GPR56 inhibitors in the primary SRE-Luc assay. Eight inhibitors purchased in powder were reconstituted in DMSO before being titrated into 293T cells freshly transfected with luciferase reporter and GPR56 7TM. Data are normalized to the negative control. **B.** Activity of GPR56 inhibitors in the counter assay. Purchased inhibitors were instead added to 293T cells freshly transfected with luciferase reporter and $G_{\alpha 13}$-QL. Data represent the mean ± SD of three biological triplicates.

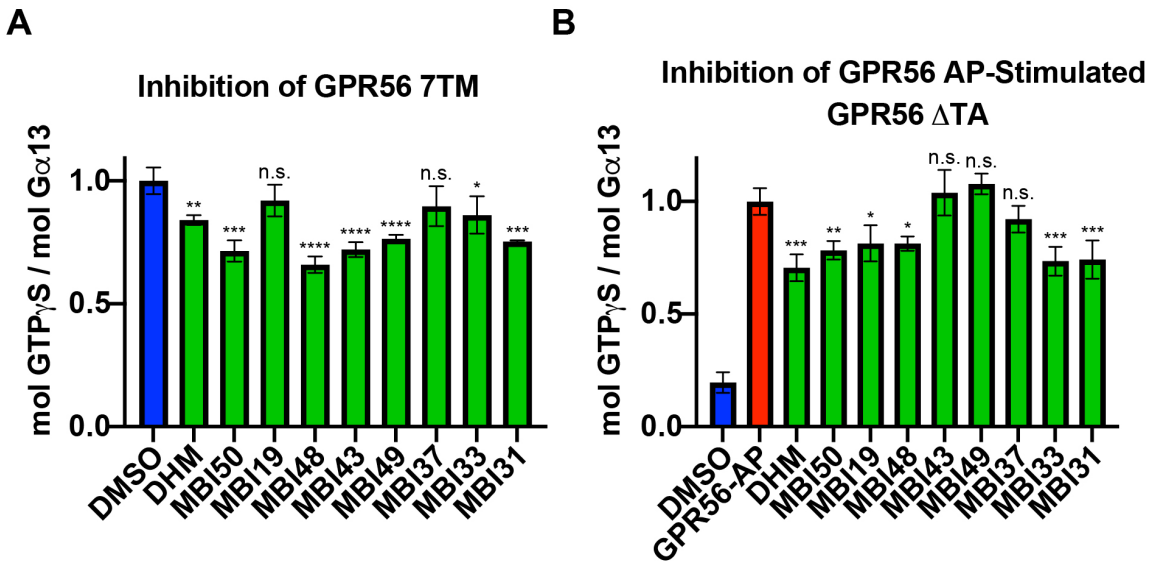

Figure 5.5 GPR56 Inhibitors Modestly Reduce Signaling in the GPCR Reconstitution Assay. **A**. Inhibition of constitutively active GPR56 7TM. 20 μM inhibitors were pre-incubated with membrane homogenates overexpressing GPR56 7TM before reconstitution with recombinant G13 trimer and reactions were initiated with radiolabeled GTPγS. **B.** Inhibition of GPR56-AP stimulation of GPR56 ΔTA. 20 μM inhibitors were pre-incubated with membrane homogenates overexpressing GPR56 ΔTA before reconstitution with recombinant G13 trimer and stimulation by 80 μM GPR56-AP and reactions were initiated with radiolabeled GTPγS. All reactions were quenched at 15 minutes and normalized to either DMSO (**A**) or GPR56-AP alone (**B**). Data represent the mean ± SD of three independent reactions. Statistical significance between compounds and DMSO (**A**) or compounds and GPR56-AP alone (**B**) was determined by repeated measures of one-way analysis of variance. **P*<0.05, ***P*<0.01, ****P*<0.001, *****P*<0.0001

μM (**Figure 5.4B)**. These data suggest that these four compounds may potently inhibit GPR56 but have off-target effects or cytotoxicity at higher concentrations.

5.3.4 GPR56 Inhibitors Exhibit Modest Activity in the GPCR Reconstitution Assay

We next vetted our eight compounds in an orthogonal biochemical GPCR reconstitution assay that directly measures activation of G proteins to evaluate their ability to inhibit GPR56 in a cell-free environment. Insect cell membrane homogenates overexpressing either constitutively active GPR56 7TM or low activity GPR56 ΔTA were reconstituted with recombinant G13 trimer and preincubated with 20 μM of small molecule inhibitors prior to the addition of [^{35}S]-radiolabeled GTPγS to initiate the reaction. Only two compounds did not significantly inhibit GPR56 7TM, MBI19 and MBI37 (**Figure 5.5A**). The other six compounds modestly decreased

G13 signaling to a level comparable or lower than when DHM was added. At 20 μM, MBI48 appeared the most efficacious, causing an approximate 35% decrease in signaling compared to vehicle control. The inhibition profile of GPR56 changed slightly when we instead pre-incubated our compounds with GPR56 ΔTA prior to addition of the agonist peptidomimetic GPR56-AP. When used in this manner, MBI43, MBI49, and MBI37 failed to inhibit GPR56-AP stimulation (**Figure 5.5**). The other five compounds reduced peptide stimulation by 20-25%, including MBI19 which failed to inhibit constitutively active GPR56 7TM.

5.3.5 MBI19 and MBI48 are Inhibitors of Platelet Aggregation

We recently established a novel role for GPR56 as a platelet collagen receptor that uses hemostatic shear force to initiate early-stage platelet aggregation [170]. As part of our characterization of this role, we identified that platelets were receptive to GPR56 modulatory compounds. When added to isolated human or mouse platelets, our previously identified partial agonist 3-α-DOG and full agonist GPR56-AP induced platelet shape change and aggregation in a manner that is consistent with G13-dependent Rho signaling. Additionally, low micromolar

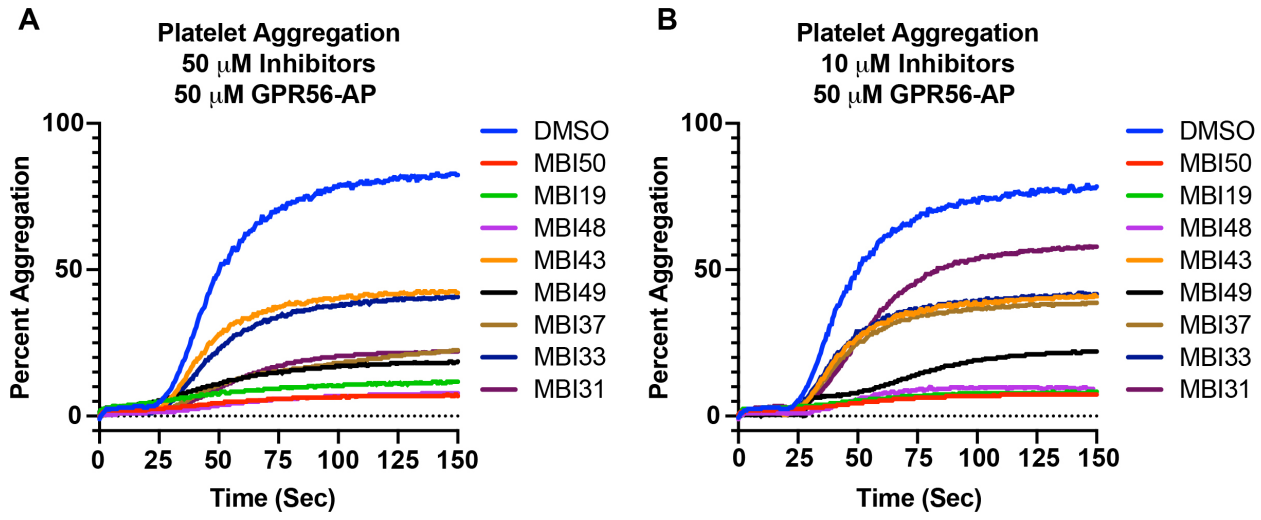

Figure 5.6 GPR56 Inhibitors Attenuate Platelet Aggregation. Washed human platelets were pre-incubated with either 50 μM (**A**) or 10 μM (**B**) GPR56 inhibitors for 5 minutes before being stimulated with 50 μM GPR56-AP and aggregation measurements were started. Data represent single traces of n=1 from one human donor.

concentrations of our GPR56 antagonist DHM inhibited GPR56-AP stimulation of platelets, but did not inhibit stimulation by PAR4-AP, a synthetic peptide agonist for the platelet PAR4 receptor. We used this platform to test whether our eight candidate inhibitors could abrogate platelet aggregation *ex vivo* in a manner similar to DHM. Washed human platelets were pre-incubated with 50 μM of each compound inside an aggregometer prior to stimulation by 50 μM of GPR56-AP. All compounds substantially inhibited platelet aggregation (**Figure 5.6A**). MBI43 and MBI33 were the least efficacious compounds, reducing aggregation by approximately 50% of vehicle control, while the remaining six reduced platelet aggregation by at least 75%.

When we lowered the concentration of inhibitors to 10 μM, three compounds were still capable of a near 90% inhibition of aggregation: MBI50, MBI19, and MBI48 (**Figure 5.6B**). We then tested these compounds in concentration response curves ranging from 0.1 μM to 40 μM using both GPR56-AP and PAR4-AP to acquire early estimates of potency *ex vivo*. MBI19 most potently inhibited aggregation with an estimated IC_{50} of 2.11 μM, while MBI50 and MBI48 had

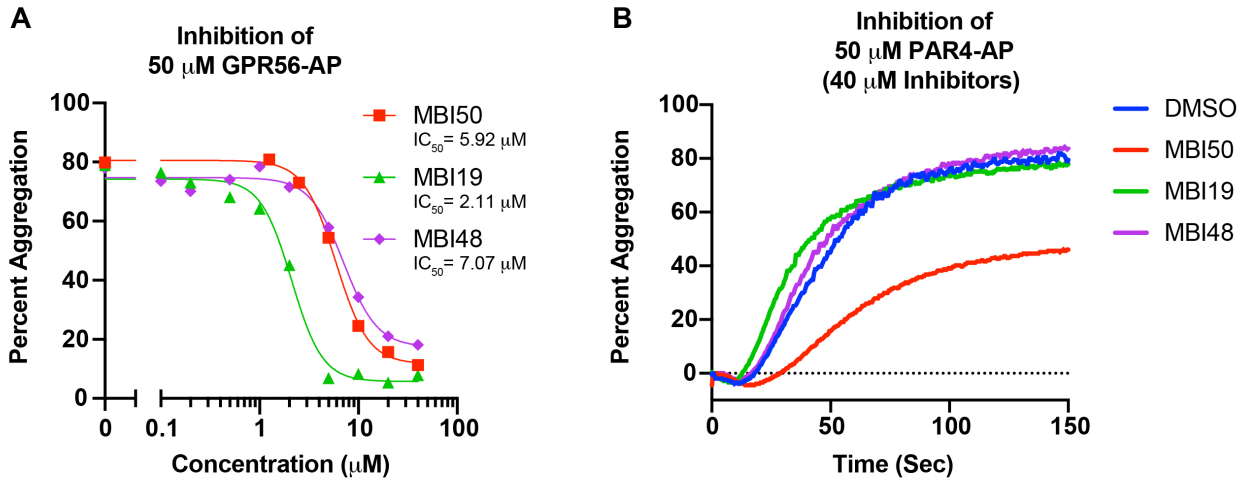

Figure 5.7 MBI19 and MBI48 are Potent Inhibitors of Platelet Aggregation. A. Dose responses of candidate GPR56 inhibitors with GPR56-AP. Human platelets were pre-incubated with increasing concentrations of MBI50, MBI19, or MBI 48 for 5 minutes prior to being stimulated with 50 μM GPR56-AP and platelet aggregation measurements were started. Shown are the aggregation plateaus after 5 minutes. **B**. Effect of GPR56 inhibitors on PAR4-AP stimulation. Human platelets were pre-incubated with 40 μM of MBI50, MBI19, or MBI48 for 5 minutes prior to being stimulated with 50 μM PAR4-AP. Data represent single traces of n=1 from a different human donor than the one for **Figure 5.6**.

estimated IC_{50}s of below 5.92 μM and 7.07 μM, respectively (**Figure 5.7A**). Notably, MBI19 and MBI48 were incapable of inhibiting platelet aggregation induced by PAR4-AP, as inhibitor concentrations of up to 40 μM did not alter the aggregation response (**Figure 5.7B**). On the other hand, 40 μM of MBI50 attenuated aggregation by approximately 50%, suggesting potential off-target effects or cytotoxicity.

5.4 Discussion

While much has been revealed about AGPCR biology and mechanisms within the last decade, research has been attenuated in part due to a lack of a pharmacological toolbox to study receptor activities both *in vitro* and *in vivo*. Few small molecules have been identified as agonists or antagonists for AGPCRs, and consequently there does not exist any AGPCR-targeted therapeutics. The most reliable pharmacological tools available are synthetic peptidomimetics that copy the sequence of the natural tethered agonist peptide. These full agonist peptides have seen moderate success in both *in vitro* and *in vivo* studies [33, 34, 56, 57, 59, 60]. However, AGPCR peptides make for poor therapeutic leads due to their hydrophobicity, large molecular weights, and low potencies. We previously identified the isoflavanoid antagonist DHM, which could robustly inhibit GPR56 both *in vitro* and *ex vivo*, but notably inhibited electron transport chain (ETC) Complex I, resulting in cytotoxicity above 10 μM and limiting its potential as a drug lead [114, 170]. For these reasons, there is a need to identify novel, potent GPR56 antagonists that may better serve as tool compounds or as therapeutic leads.

Herein we provide the early-stage identification of a small collection of GPR56 inhibitors from a high throughput screen of over 20,000 compounds. 50 unique inhibitor structures were identified following primary and counter screening, which was reduced to a collection of 15 after vetting compounds in concentration response curves. Of note, our primary screening workflow did

not eliminate any compounds that exhibited negative inhibition (*i.e.,* increased luminescence signal) in the Gα13-QL assay, resulting in many of the 50 initial hits having a substantial activation effect in the counter assay. These compounds likely have off target effects downstream of G13 signaling, as many of them exhibited poor activity curves in our robotically pipetted concentration response assays. Additionally, none of the 50 initial compounds were previously identified as primary hits in the agonist screen conducted in Chapter 4, ruling them out as potential Gα13 activators.

While we intend to conduct follow up characterization of all 15 compounds validated in our screen, we initially purchased a smaller batch of the eight most promising inhibitors. All eight compounds robustly inhibited signaling when reconstituted from fresh powders and added to cells freshly transfected with GPR56 7TM, but four additionally inhibited in the Gα13-QL counter assay at higher concentrations: MBI50, MBI19, MBI49, and MBI33. This raises the likelihood that these compounds have off target effects but doesn't necessarily rule them out as GPR56 7TM inhibitors. MBI19, for example, reduces the activity of GPR56 7TM by ~50% and has no effect in the counter assay at 3.125 μM. The exception to this pattern is MBI49 which substantially reduced signaling in both the primary and counter assay at all concentrations. Future work needs to be done to assess the cytotoxicity or off target binding of these compounds. Surprisingly, the activity of our inhibitors varied in the GPCR reconstitution assay depending on whether they were preincubated with GPR56 7TM or ΔTA. MBI19 failed to inhibit GPR56 7TM, but could significantly attenuate the activation of GPR56 ΔTA by GPR56-AP. Conversely, MBI43 and MBI49 substantially reduced GPR56 7TM signaling, but did not affect the activation of GPR56 ΔTA. These inconsistencies may be described by differences in binding mechanisms. MBI19 may bind to the orthosteric site and compete with the natural peptide, explaining why it only appears to

inhibit a receptor with an impaired TA, GPR56 ΔTA. On the other hand, MBI43 and MBI49 could bind allosterically at a site only available in the active conformation of the receptor, explaining an apparent selectivity for GPR56 7TM. However, these inconsistencies cannot be fully rationalized without kinetic curves showing the activation of G13 over time. Future work will be conducted to accurately evaluate the potencies of all inhibitors in our biochemical assays, and to evaluate their kinetic effects on GPR56.

When applied in an *ex vivo* platelet aggregation assay, we found that three of our compounds potently inhibited GPR56-AP-stimulated platelet aggregation across multiple human donors: MBI50, MBI19, and MBI48. MBI19 appeared the most potent of the three, with an approximate IC_{50} of 2.11 μM. Importantly, MBI19 and MBI48 failed to attenuate PAR4-AP-stimulated aggregation, suggesting their anti-platelet activity is GPR56 dependent. MBI50 attenuated PAR4-AP-stimulated platelet aggregation by approximately 50% at 40 μM, implying off target effects or cytotoxicity. These assays are a promising early look at the therapeutic properties of these compounds. MBI19 and MBI48 both appear to be ideal candidates as therapeutic leads for GPR56-targeted drugs as they appear to inhibit GPR56 both *in vitro* and *ex vivo*. However, much more work must be done to characterize these compounds before they can be tailored into GPR56 therapeutics. First, receptor selectivity must be evaluated by vetting these compounds against other adhesion or non-adhesion GPCRs. AGPCRs share a conserved activation mechanism, and consequently have similar orthosteric binding sites. If these compounds interact at the orthosteric site, it is likely that they would inhibit other AGPCRs. Additionally, the potential cytotoxicity of these compounds must be assessed in cell viability assays, as MBI19 modestly reduced activity in our counter assay, which implies an off-target effect or cytotoxicity. Finally, a more accurate profile of platelet activity must be conducted with our inhibitors. Aggregation is a

threshold-like response that only reports on the late stages of the platelet activation pathway. Earlier stages can be probed with a variety of other assays. Rho activation occurs downstream of G13 signaling and can be monitored via a Rho-GTP pulldown assay; platelet shape change occurs downstream of rho signaling and can be monitored by visualizing actin-stained platelets adhered to vitronectin-coated dishes; and finally, alpha granule secretion or $\alpha_{IIb}\beta_{III}$ integrin activation can be monitored in flow cytometric assays measuring anti-CD62P (P-selectin) or PAC-1 binding, respectively.

In sum, we present here an early look at a collection of eight novel, potent GPR56 inhibitors that have robust activity *in vitro* and *ex vivo*. We have recently purchased the remaining seven inhibitors identified in our primary screens and are also conducting early-stage SAR for both MBI19 and MBI48. These compounds have high potential for use as tool compounds to study AGPCR activity in endogenous tissue systems and may serve as leads for the first AGPCR-targeting drugs.

Chapter 6 Conclusions and Future Perspectives

Adhesion AGPCRs are a biologically relevent yet uniquely misunderstood family of GPCRs with few tools to study their activation *in vivo* or *in vitro*. More than half of the 33 receptors remain as orphans, and there are currently no form of AGPCR-targeted therapeutics. The work in this thesis uses GPR56 and a small subset of other AGPCRs as a model to understand the mechanism of tethered peptide agonsim, and as a screening platform to identify novel, small molecular activators and inhibitors. This work highlights the first cryo-EM structures of an activated AGPCR with its tethered agonist bound to the orthosteric site, and identifies highly potent and selective agonists and platelet-responsive antagonists for GPR56.

6.1 Low Resolution Structures of Holoreceptor GPR56 and LPHN3

We have highlighted here the first reported structures of AGPCRs in their holoreceptor form, albeit in low resolution maps. Although our structures are too low resolution to map individual residues, they illustrate an important feature of full-length AGPCRs: the NTF is a flexible region that is distal to the 7TM. This sheds light on the allosteric (*i.e.,* TA-independent) mechanism of activation, the details of which have mostly remained elusive. There have been many theories for how the NTF of an AGPCR can cause signaling changes in the CTF independently of the TA. Some have hypothesized that the NTF acts as an autoinhibitory domain that interacts with the 7TM to downregulate signaling, and the allosteric binding of ligands adjusts or alleviates inhibition [45, 46]. Other groups have suggested that the TA can decrypt itself from the NTF and interact with the orthosteric site without the NTF dissociating from the receptor [198,

208]. Our maps of holoreceptor GPR56 and LPHN3 demonstrate that these theories are unlikely, as the NTF is too far from the 7TM to act as an autoinhibitory domain, or for the tethered agonist to transiently interact with the orthosteric site. The exact details for allosteric modulation remain unknown and will likely be revealed as higher resolution structures for AGPCRs are solved.

6.2 Structures of Activated GPR56 and LPHN3

Structures for GPR56 and LPHN3 in their activated, TA-bound state were solved to a resolution of 2.7 Å and 2.9 Å, respectively. These high-resolution maps reveal a core 7TM structure that is not unlike the closely related family B1 hormone receptors. In the activated state, the tethered agonist is bent 180º into a partial helix conformation beneath ECL2, which is stabilized by a conserved disulfide bond between $C^{45.50}$ and $C^{3.29}$ on TM3. TA binding results in the breaking of TMs 6 and 7 about the pivot residues $G^{6.50}$ and $G^{7.50}$, respectively, which opens the intracellular side of the receptor to allow for G protein engagement. The hydrophobic core of the 7TM barrel near $G^{6.50}$ contains a highly conserved tryptophan, $W^{6.53}$, that appears to function similarly to the toggle switch of class A GPCRs. This residue is stabilized by electrostatic interactions with $Q^{7.49}$, and through coordination with $M389^{TA}$, $M487^{3.47}$, and $F637^{7.42}$ in GPR56, or $M848^{TA}$, $M945^{3.45}$ and $F1086^{7.42}$ in LPHN3.

Notably, the structures for GPR56 and LPHN3 shared a high degree of similarity despite the receptors being from distant families. These structures are also distinct from the recently published cryo-EM structure of the GPR97-miniGo complex bound to a glucocorticoid agonist [185]. In this structure, cortisol is bound within the orthosteric site but TMs 6 and 7 are not broken and thus the extracellular and intracellular faces of the receptor are in a more closed conformation. It is for this reason we believe that the cortisol and beclomethasone agonists identified for GPR97

are partial agonists that stabilize an intermediate state of the receptor, rather than a fully active conformation that is stabilized by the tethered agonist.

6.3 Tethered Agonist-7TM Interactions Reveal a Conserved Activation Mechanism

Our high-resolution structures of activated GPR56 and LPHN3 revealed for the first time how the tethered agonist interacts with the 7TM following NTF dissociation. Surprisingly, the TA exhibits a dramatic conformational shift from a β-strand within the GAIN domain, to a partial helix within the orthosteric site. Furthermore, the TA binds the orthosteric site through a narrow opening in the structurally stable ECL2 that occupies a majority of the extracellular space. These findings suggest that the TA is not a rigid element, and instead exhibits a high amount of conformational flexibility following fragment dissociation. Our structures also revealed the specific residue interactions that stabilize the active conformations of GPR56 and LPHN3. The P3, P6, and P7 residues of the TA (typically phenylalanine, methionine, and leucine) interact at the deepest point within the orthosteric site. P3 phenylalanine interacts with $F^{4.54}$ in the hydrophobic core of both GPR56 and LPHN3 via pi-pi interactions. P6 leucine interacts with $W^{45.52}$ on ECL2, which bends down into the orthosteric site in a conformation stabilized by a disulfide bond between $C^{45.50}$ and $C^{3.29}$. Finally, P7 methionine forms a critical interaction with the toggle switch $W^{6.53}$ deep within the hydrophobic core. Disrupting any of these interactions via alanine point mutations on either the 7TM or the tethered agonist resulted in a near complete loss in signaling, demonstrating their importance for TA engagement.

The P3, P6, and P7 residues of the TA are highly conserved across all AGPCRs and have been previously shown to be vital for AGPCR signaling [33]. Across all 33 receptors, EMR1 and GPR124 are the only receptors without a P3 phenylalanine or tyrosine capable of pi-pi interactions, and VLGR1 is the only receptor without a P6 leucine or isoleucine. The P7 methionine shows

slightly more variability between receptors, with eight receptors having a different hydrophobic residue (EMR4, GPR144, BAI1-3, GPR64, GPR97, and VLGR1). Thus, the interactions detailed here likely represent a uniform mechanism of activation across all AGPCRs. This was further proven by three other studies published simultaneously alongside ours that collectively highlight the active structures of GPR133, GPR114, GPR64, GPR112, and GPR110 [197-199]. Despite being from distantly related families, these structures all shared the same story: a flexible tethered agonist adopts a partial helix within the orthosteric site and interacts with the 7TM via its conserved hydrophobic residues.

6.4 Hexahydroquinoline Derivatives are Selective GPR56 Agonists

In search of novel, potent agonists for GPR56 that may better serve as tool compounds or leads for AGPCR-targeted therapeutics, we expanded our previous 2,000 compound cell-based screen 100-fold to screen over 200,000 compounds across three libraries. An expansion of this magnitude required a substantial optimization of cell handling to transfect upwards of two billion cells simultaneously with GPR56 ΔTA and our gene reporter. Ultimately, our cell pooling and cryopreservation methods allowed us to successfully complete the screen with a high degree of precision. From our primary and counter screens, we identified a collection of 155 compounds that was further narrowed to 74 structures following robotically pipetted concentration response curves. Surprisingly, a large number of these compounds failed to activate GPR56 ΔTA in our orthogonal GPCR reconstitution assay. Only 16 out of 74 compounds showed activity comparable or better than the GPR56-AP positive control. We rationalize this is because our biochemical assay is a much more direct validator of genuine GPR56 activators; Compounds used in these assays are reconstituted in a system that directly measures G protein activation, rather than indirectly via a gene reporter.

From our top hits, we noticed a structural cluster that showed far superior potency and efficacy compared to all other compounds. We identified these closely related analogs as hexahydroquinoline (HHQ) derivatives that share some similarities to L-type calcium channel blockers that have previously been marketed as drugs to treat hypertension (*e.g.,* nifedipine). The most potent of these compounds, which we have designated as Compound 36, activated GPR56 ΔTA with an EC_{50} of 2.95 μM ± 0.42 μM. This is over a ten-fold increase in potency compared to the GPR56-AP positive control. Furthermore, Compound 36 activated GPR56 ΔTA to a level equivalent to that of the constitutively active GPR56 7TM, suggesting that it acts as a full agonist. In contrast to our previously identified partial agonist 3-α-DOG, and nearly all other compounds identified in this study, Compound 36 robustly activated cleavage-deficient full-length GPR56 to near full efficacy. Compound 36 also appeared to be highly selective; it did not activate any other adhesion or non-adhesion GPCRs that we tested.

Following two rounds of SAR analysis, we were able to discover an optimized structure, Compound 36.40, that replaced a bromine and isopropyl group with a CF_3 and cyclopentyl group, respectively. Overall, we observed that increasing the general hydrophobicity of the compound correlated with an increase in potency. This is consistent with our *in silico* analysis that predicted both Compound 36 and 36.40 bind to a hydrophobic pocket within the orthosteric site of GPR56 and interact with several residues that also interact with the endogenous TA. Further derivatization of Compound 36.40 would likely extend the hydrophobic regions of the structure. I hypothesize that replacement of the cyclopentane ring with an aryl group would further improve its potency, as that would likely enable it to interact with the $F^{2.64}$ residue via pi-pi interactions. Our SAR efforts were nearly exhaustive towards the collection of commercially available analogs, meaning further analysis would require chemical derivatization. Nonetheless, Compound 36.40 has shown

to be an extremely capable AGPCR tool compound, and I predict that further derivatization could make it a promising candidate for a first-in-class AGPCR drug. I also predict that Compounds 36 and 36.40 will not have a significant hypotensive off target effect. During SAR, we observed that increases in hydrophobicity correlated with higher potencies towards GPR56, while the inverse of this is typically seen with the derivatization of L-type calcium channel antagonists; The most potent calcium channel blockers are often much more hydrophilic. Whether these compounds actually bind to calcium channels or other receptors *in vivo* remains to be tested.

6.5 Early Identification of Platelet-Responsive GPR56 Inhibitors

Our high throughput screening work has also revealed a small collection of promising GPR56 inhibitors. Using the same methodology as our previous HTS efforts, we screened ~23,000 compounds from the Maybridge library for their ability to inhibit constitutively active GPR56 7TM in the SRE-Luc assay. Surprisingly, the hit rate for inhibitors of GPR56 was substantially higher than that for activators of GPR56, even with a strict hit threshold of 85% inhibition. Our primary hit rate for activators (prior to counter screening) was 0.64%, whereas our hit rate for inhibitors was 12.3%. This necessitated running the entire screen in duplicate, once for the inhibition of GPR56 7TM, and once for the counter assay using cells transfected with $G_{\alpha 13}$-QL. This proved successful and lowered our hit rate to a much more manageable 0.61%. Following reconfirmation assays, we identified a collection of 50 candidate inhibitor structures (MBI1-50), which was further narrowed to 15 compounds following robotically pipetted concentration response curves. During our assays, we observed that many these candidates caused an *increase* in signaling in the counter assay, which we suspected to be a result off-target binding downstream of GPR56. Our screening workflow only removed compounds that inhibited in the counter assay, so it is not surprising that many of the compounds that survived validation had an activation effect.

We opted to include these compounds in our concentration response curves, and our suspicions were validated when they failed to show promising potency or efficacy.

We chose a small subset of eight compounds to purchase from fresh powder and found that all compounds recapitulated their activity in our directed dual-luciferase assays. Most of our compounds also modestly reduced $G_{\alpha 13}$ signaling in our GPCR reconstitution assay. When added to washed platelets, however, we noticed two compounds that stood above the rest in their ability to attenuate GPR56-AP stimulation: MBI19 and MBI48. Both compounds inhibited GPR56-AP-stimulated aggregation with low micromolar IC_{50}s, with MBI19 appearing the more potent of the two. Notably, both compounds did not affect platelet aggregation stimulated by the PAR4 peptide agonist, PAR4-AP, suggesting that their activity on platelets is GPR56-specific. These assays strongly suggest that these compounds are capable of inhibiting GPR56 in endogenous tissue systems and may serve as lead compounds for AGPCR therapeutics. There remains much work that must be done with MBI19 and MBI48 to establish them as bona fide GPR56 antagonists. First, their receptor selectivity has not been tested. Our counter screening assay suggests that these compounds are not pathway inhibitors, but it would not be unreasonable for them to bind to other AGPCRs, especially those within the same family that likely share similar orthosteric binding sites. DHM, a GPR56 antagonist we previously identified using the same screening approach, inhibited multiple receptors within the G subfamily of AGPCRs [114]. Consequently, I hypothesize that MBI19 and MBI48 may inhibit other G subfamily receptors, such as GPR114 or GPR97. Additionally, a more comprehensive investigation of platelet signaling must be done with our inhibitors. GPR56 couples to $G_{\alpha 13}$, which signals through Rho to initiate cytoskeletal rearrangements and cell shape change. This pathway can be investigated in platelets via the Rho-GTP pulldown assay, or by shape change assays of platelets adhered to a vitronectin matrix. This

work is ongoing, and we have recently purchased additional GPR56 inhibitors identified in our screens to vet their activity in platelets. With further characterization, these compounds have the potential to be developed into vital GPR56 tool compounds, or novel anti platelet drugs.

6.6 The Impact of Novel Structures and Pharmacological Tools

The work embodied here serves as a vital foundation for both a structural understanding of AGPCR mechanisms and AGPCR high throughput screening. Adhesion GPCRs play pivotal roles in numerous cell processes and their dysfunction has been implicated in the pathogenesis of neurological disorders, hearing loss, infertility, and several cancers. Prior to this work, the details of orthosteric activation of AGPCRs in these contexts have remained murky. While the tethered-peptide agonist theory of activation had been supported by the GAIN structure, urea fractionation experiments, and the use of synthetic peptides, the specific interactions within the orthosteric site were unknown and impeded our understanding of these receptors. With the newly solved structures of GPR56 and LPHN3 presented here, the binding mechanism of the tethered agonist is unambiguous, and an accurate model of the orthosteric site in the active state is now known. This model will prove instrumental in structure-based design of future AGPCR-targeted drugs; *in silico* docking and mutational analysis is now feasible for drug SAR to improve therapeutic properties, as shown in Chapter 4 with the docking of Compound 36 and 36.40. These models will additionally provide context for future structures of other receptors in different activation states; comparison of tethered agonist binding sites can now be accomplished to decipher the ambiguous differences in peptide specificity across receptors.

The high-potency compounds highlighted here – Compounds 4, 36, and 36.40 – provide some of the most promising leads to date for AGPCR-targeted therapeutics. All three compounds share two key properties that elevate them above the previously identified 3-α-DOG and DHM

molecules: they are highly selective and are capable of activating the full-length receptor. Receptor selectivity is a vital part of therapeutic development, as it helps mitigate unwanted side effects from off-target binding, and a capacity to activate the full-length receptor means the compound is much more likely to bind to the receptor in its resting, inactive state *in vivo*. Compound 36.40, being the most potent and selective compound, shows great promise for future development into a first-in-class drug targeting GPR56. A GPR56-activating drug would serve as a useful procoagulant, as the receptor was recently shown to regulate early activation of shear force-dependent platelet activation [209]. Procoagulant drugs are vital tools to aid in the treatment of blood loss in trauma patients [170]. Ideally, a more potent variant of Compound 36.40 could be applied topologically to stimulate platelet activation and blood clotting to stop bleeding. On the other hand, drugs developed from the inhibitors identified in Chapter 5 could serve as anti-thrombotic drugs by inhibiting platelet activation through GPR56. In either case, both sets of compounds require additional follow-up optimization before they can be assessed as potential drug leads. But even in the event that these compounds fail as therapeutic leads, the cell culturing and screening methods listed here provide a previously unavailable means to survey large libraries of chemicals for their ability to activate AGPCRs in cell-based assays. To our knowledge, this is the largest wet screen of any AGPCR to date, and the workflow is applicable to nearly every AGPCR. Indeed, this work may lead to future screens of other AGPCRs with disease relevance, such as LPHN3 or GPR110.

6.7 Concluding Remarks

While there is still mystery surrounding the allosteric activation of adhesion GPCRs, the work presented in this thesis highlights the conserved mechanism of orthosteric tethered agonist activation using the first cryo-EM structures of fully activated GPR56 and LPHN3. Through

mutational analysis, we have identified key TA-7TM interactions that enable the activation of AGPCRs following fragment dissociation. Our high-resolution structures will provide the framework for understanding the activation of other AGPCRs and their pharmacology *in vivo*. Furthermore, the potent GPR56 agonists and antagonists identified in our high throughput screens will serve as vital tool compounds to aid AGPCR research both *in vitro* and *in vivo,* and have a high potential to serve as lead structures for first-in-class GPR56 drugs.

Appendix A Contributions and Funding Sources

Chapter 1 Contributions

Maiya Yu helped organize and align the sequences used in **Figure 1.2**. Drs. Jennifer Yeung and Rashmi Adhikari assisted in the early-stage planning and literature search for the publication version of this chapter. Dr. Gregory Tall aided in the writing and figure making of the publication version of this chapter.

Chapter 3 Contributions

Drs. Gregory Tall and Luciana Rosselli-Murai designed and cloned the PAR-GPR56 and PAR-GPR114 fusion constructs used in **Figure 3.1**. Dr. Gregory Tall and Dr. Ximena Barros-Alvarez from Stanford University designed the GPR56, LPHN3, and G protein constructs used in structural studies. Dr. Ximena Barros-Alvarez from Stanford University and Dr. Moran Shalev-Benami from the Weizmann Institute of Science designed the LPHN3 constructs used in structural studies. Dr. Ximena Barros-Alvarez expressed and purified activated GPR56 and LPHN3 7TM complexes, prepared cryo-EM grids, oversaw cryo-EM data collection, processed data for complexes, modelled the structures, and analyzed the structural data for **Figure 3.2**, **Figure 3.3**, **Figure 3.4**, and **Figure 3.7**. Dr. Robert Nwokonko from Stanford University performed mutagenesis experiments for all mutants and conducted initial cloning into pFastBac1 vectors. Dr. Frank Kwarcinski and Dr. Gregory Tall assisted in follow-up baculovirus production and preparation of membrane homogenates. Dr. Donna Matzov from the Weizmann Institute of

Science expressed and purified NTF-bound LPHN3, prepared cryo-EM grids, and collected and processed cryo-EM data for **Figure 3.2C**. Dr. Feng He from Stanford University purified and processed cryo-EM data for full length GPR56 in **Figure 3.2C**. Dr. Gregory Tall performed the cell surface biotinylation-pulldown experiment for **Figure 3.6**. Dr. Frank Kwarcinski assisted in the western blotting of GPR56 membrane homogenates for **Figure 3.5**. Dr. Makaía M. Papasergi-Scott assembled the cartoon model used in **Figure 3.10**.

Chapter 4 Contributions

Dr. Gregory Tall and Maiya Yu helped design and clone constructs for heterotrimeric G proteins and GPCRs. Dr. Yukiko Maeda aided in the purification of G protein α subunits used in GPCR reconstitution assays. Dr. Nick Santoro and Renju Jacob from UM's Center for Chemical Genomics assisted in the methodology and analysis of GPR56 high throughput screens. Dr. Michael Robertson from Stanford University performed *in silico* docking analysis for **Figure 4.12**.

Chapter 5 Contributions

Dr. Nick Santoro from UM's Center for Chemical Genomics assisted in the methodology and analysis of GPR56 inhibitor screens. Frank Kwarcinski and Xinyi Yi assisted in the isolation of washed platelets and the aggregation assays conducted in **Figure 5.6** and **Figure 5.7**.

The student independently conducted all other work for this dissertation. This work was funded by National Institutes of Health (NIH) R01s GM120110 and NS103946 to Dr. Gregory Tall, and NHLBI, NIH, Grant F31 HL-152563-01 to Alexander Vizurraga. Alexander Vizurraga was additionally funded by the Cellular and Molecular Biology Training Grant T-32-GM007315.

Bibliography

1. Krogh, A., et al., *Predicting transmembrane protein topology with a hidden Markov model: application to complete genomes.* J Mol Biol, 2001. **305**(3): p. 567-80.
2. Sonnhammer, E.L., G. von Heijne, and A. Krogh, *A hidden Markov model for predicting transmembrane helices in protein sequences.* Proc Int Conf Intell Syst Mol Biol, 1998. **6**: p. 175-82.
3. Tu, Y.K., J.G. Duman, and K.F. Tolias, *The Adhesion-GPCR BAI1 Promotes Excitatory Synaptogenesis by Coordinating Bidirectional Trans-synaptic Signaling.* J Neurosci, 2018. **38**(39): p. 8388-8406.
4. Duman, J.G., et al., *The adhesion-GPCR BAI1 shapes dendritic arbors via Bcr-mediated RhoA activation causing late growth arrest.* Elife, 2019. **8**.
5. Chong, Z.-S., et al., *Pooled extracellular receptor-ligand interaction screening using CRISPR activation.* Genome Biology, 2018. **19**(1): p. 205-205.
6. O'Sullivan, M.L., et al., *FLRT proteins are endogenous latrophilin ligands and regulate excitatory synapse development.* Neuron, 2012. **73**(5): p. 903-10.
7. Ranaivoson, F.M., et al., *Structural and Mechanistic Insights into the Latrophilin3-FLRT3 Complex that Mediates Glutamatergic Synapse Development.* Structure (London, England : 1993), 2015. **23**(9): p. 1665-1677.
8. Li, J., et al., *Structural Basis for Teneurin Function in Circuit-Wiring: A Toxin Motif at the Synapse.* Cell, 2018. **173**(3): p. 735-748.e15.
9. T, A.K., *CFSSP: Chou and Fasman Secondary Structure Prediction server.* WIDE SPECTURM - Research Journal (ISSN 2250-2815), 2013. **1**: p. 15-19.
10. Araç, D., et al., *A novel evolutionarily conserved domain of cell-adhesion GPCRs mediates autoproteolysis.* The EMBO Journal, 2012. **31**(6): p. 1364-1378.
11. Kishore, A., et al., *Stalk-dependent and Stalk-independent Signaling by the Adhesion G Protein-coupled Receptors GPR56 (ADGRG1) and BAI1 (ADGRB1).* Journal of Biological Chemistry, 2016. **291**(7): p. 3385-3394.
12. Lelianova, V.G., et al., *Alpha-latrotoxin receptor, latrophilin, is a novel member of the secretin family of G protein-coupled receptors.* J Biol Chem, 1997. **272**(34): p. 21504-8.
13. Rahman, M.A., et al., *Norepinephrine exocytosis stimulated by alpha-latrotoxin requires both external and stored Ca2+ and is mediated by latrophilin, G proteins and phospholipase C.* Philos Trans R Soc Lond B Biol Sci, 1999. **354**(1381): p. 379-86.
14. Mathiasen, S., et al., *G12/13 is activated by acute tethered agonist exposure in the adhesion GPCR ADGRL3.* Nat Chem Biol, 2020. **16**(12): p. 1343-1350.
15. Vizurraga, A., et al., *Mechanisms of adhesion G protein-coupled receptor activation.* J Biol Chem, 2020. **295**(41): p. 14065-14083.
16. Rask-Andersen, M., S. Masuram, and H.B. Schioth, *The druggable genome: Evaluation of drug targets in clinical trials suggests major shifts in molecular class and indication.* Annu Rev Pharmacol Toxicol, 2014. **54**: p. 9-26.

17. Attwood, T.K. and J.B. Findlay, *Fingerprinting G-protein-coupled receptors.* Protein Eng, 1994. **7**(2): p. 195-203.
18. Krishnan, A., et al., *The origin of GPCRs: identification of mammalian like Rhodopsin, Adhesion, Glutamate and Frizzled GPCRs in fungi.* PLoS One, 2012. **7**(1): p. e29817.
19. Fredriksson, R., et al., *The G-protein-coupled receptors in the human genome form five main families. Phylogenetic analysis, paralogon groups, and fingerprints.* Mol Pharmacol, 2003. **63**(6): p. 1256-72.
20. Bjarnadottir, T.K., et al., *The human and mouse repertoire of the adhesion family of G-protein-coupled receptors.* Genomics, 2004. **84**(1): p. 23-33.
21. Hamann, J., et al., *International Union of Basic and Clinical Pharmacology. XCIV. Adhesion G Protein–Coupled Receptors.* Pharmacological Reviews, 2015. **67**(2): p. 338-367.
22. McKnight, A.J. and S. Gordon, *EGF-TM7: a novel subfamily of seven-transmembrane-region leukocyte cell-surface molecules.* Immunol Today, 1996. **17**(6): p. 283-7.
23. Lin, H.-H., et al., *Human EMR2, a Novel EGF-TM7 Molecule on Chromosome 19p13.1, Is Closely Related to CD97.* Genomics, 2000. **67**(2): p. 188-200.
24. Arac, D., N. Strater, and E. Seiradake, *Understanding the Structural Basis of Adhesion GPCR Functions.* Handb Exp Pharmacol, 2016. **234**: p. 67-82.
25. Lum, A.M., et al., *Orphan receptor GPR110, an oncogene overexpressed in lung and prostate cancer.* BMC Cancer, 2010. **10**: p. 40.
26. Abe, J., T. Fukuzawa, and S. Hirose, *Cleavage of Ig-Hepta at a "SEA" module and at a conserved G protein-coupled receptor proteolytic site.* J Biol Chem, 2002. **277**(26): p. 23391-8.
27. Leon, K., et al., *Structural basis for adhesion G protein-coupled receptor Gpr126 function.* Nat Commun, 2020. **11**(1): p. 194.
28. Nieberler, M., et al., *Control of Adhesion GPCR Function Through Proteolytic Processing.* Handb Exp Pharmacol, 2016. **234**: p. 83-109.
29. Lin, H.H., et al., *Autocatalytic cleavage of the EMR2 receptor occurs at a conserved G protein-coupled receptor proteolytic site motif.* J Biol Chem, 2004. **279**(30): p. 31823-32.
30. Krasnoperov, V., et al., *Post-translational proteolytic processing of the calcium-independent receptor of alpha-latrotoxin (CIRL), a natural chimera of the cell adhesion protein and the G protein-coupled receptor. Role of the G protein-coupled receptor proteolysis site (GPS) motif.* J Biol Chem, 2002. **277**(48): p. 46518-26.
31. Promel, S., T. Langenhan, and D. Arac, *Matching structure with function: the GAIN domain of adhesion-GPCR and PKD1-like proteins.* Trends Pharmacol Sci, 2013. **34**(8): p. 470-8.
32. Krasnoperov, V., et al., *Structural requirements for alpha-latrotoxin binding and alpha-latrotoxin-stimulated secretion. A study with calcium-independent receptor of alpha-latrotoxin (CIRL) deletion mutants.* J Biol Chem, 1999. **274**(6): p. 3590-6.
33. Stoveken, H.M., et al., *Adhesion G protein-coupled receptors are activated by exposure of a cryptic tethered agonist.* Proc Natl Acad Sci U S A, 2015. **112**(19): p. 6194-9.
34. Liebscher, I., et al., *A Tethered Agonist within the Ectodomain Activates the Adhesion G Protein-Coupled Receptors GPR126 and GPR133.* Cell Reports, 2014. **9**(6): p. 2018-2026.
35. Formstone, C.J., et al., *Basal enrichment within neuroepithelia suggests novel function(s) for Celsr1 protein.* Mol Cell Neurosci, 2010. **44**(3): p. 210-22.

36. Vallon, M. and M. Essler, *Proteolytically Processed Soluble Tumor Endothelial Marker (TEM) 5 Mediates Endothelial Cell Survival during Angiogenesis by Linking Integrin α _v β ₃ to Glycosaminoglycans.* Journal of Biological Chemistry, 2006. **281**(45): p. 34179-34188.
37. Prömel, S., et al., *Characterization and functional study of a cluster of four highly conserved orphan adhesion-GPCR in mouse.* Developmental Dynamics, 2012. **241**(10): p. 1591-1602.
38. Hsiao, C.C., et al., *Site-specific N-glycosylation regulates the GPS auto-proteolysis of CD97.* FEBS Lett, 2009. **583**(19): p. 3285-90.
39. Wei, W., et al., *Characterization of cis-autoproteolysis of polycystin-1, the product of human polycystic kidney disease 1 gene.* J Biol Chem, 2007. **282**(30): p. 21729-37.
40. Manglik, A. and B. Kobilka, *The role of protein dynamics in GPCR function: insights from the β2AR and rhodopsin.* Current Opinion in Cell Biology, 2014. **27**: p. 136-143.
41. Hilger, D., M. Masureel, and B.K. Kobilka, *Structure and dynamics of GPCR signaling complexes.* Nat Struct Mol Biol, 2018. **25**(1): p. 4-12.
42. Xu, J., et al., *Conformational Complexity and Dynamics in a Muscarinic Receptor Revealed by NMR Spectroscopy.* Mol Cell, 2019. **75**(1): p. 53-65 e7.
43. Purcell, R.H. and R.A. Hall, *Adhesion G Protein–Coupled Receptors as Drug Targets.* Annual Review of Pharmacology and Toxicology, 2018. **58**(1): p. 429-449.
44. Langenhan, T., *Adhesion G protein-coupled receptors-Candidate metabotropic mechanosensors and novel drug targets.* Basic Clin Pharmacol Toxicol, 2019.
45. Kishore, A. and R.A. Hall, *Versatile Signaling Activity of Adhesion GPCRs.* Handb Exp Pharmacol, 2016. **234**: p. 127-146.
46. Paavola, K.J. and R.A. Hall, *Adhesion G protein-coupled receptors: signaling, pharmacology, and mechanisms of activation.* Mol Pharmacol, 2012. **82**(5): p. 777-83.
47. Folts, C.J., et al., *Adhesion G Protein-Coupled Receptors as Drug Targets for Neurological Diseases.* Trends Pharmacol Sci, 2019. **40**(4): p. 278-293.
48. Liebscher, I. and T. Schoneberg, *Tethered Agonism: A Common Activation Mechanism of Adhesion GPCRs.* Handb Exp Pharmacol, 2016. **234**: p. 111-125.
49. Langenhan, T., G. Aust, and J. Hamann, *Sticky signaling--adhesion class G protein-coupled receptors take the stage.* Sci Signal, 2013. **6**(276): p. re3.
50. Paavola, K.J., et al., *The N Terminus of the Adhesion G Protein-coupled Receptor GPR56 Controls Receptor Signaling Activity.* Journal of Biological Chemistry, 2011. **286**(33): p. 28914-28921.
51. Okajima, D., G. Kudo, and H. Yokota, *Brain-specific angiogenesis inhibitor 2 (BAI2) may be activated by proteolytic processing.* J Recept Signal Transduct Res, 2010. **30**(3): p. 143-53.
52. Ward, Y., et al., *LPA Receptor Heterodimerizes with CD97 to Amplify LPA-Initiated RHO-Dependent Signaling and Invasion in Prostate Cancer Cells.* Cancer Research, 2011. **71**(23): p. 7301-7311.
53. Paavola, K.J., et al., *Type IV collagen is an activating ligand for the adhesion G protein-coupled receptor GPR126.* Science Signaling, 2014. **7**(338): p. ra76-ra76.
54. Azimzadeh, P., et al., *Spatial regulation of GPR64/ADGRG2 signaling by beta-arrestins and GPCR kinases.* Ann N Y Acad Sci, 2019. **1456**(1): p. 26-43.
55. Monk, K.R., et al., *A G protein-coupled receptor is essential for Schwann cells to initiate myelination.* Science, 2009. **325**(5946): p. 1402-5.

56. Brown, K., et al., *Epithelial Gpr116 regulates pulmonary alveolar homeostasis via Gq/11 signaling.* JCI Insight, 2017. **2**(11).
57. Wilde, C., et al., *The constitutive activity of the adhesion GPCR GPR114/ADGRG5 is mediated by its tethered agonist.* FASEB J, 2016. **30**(2): p. 666-73.
58. Salzman, G.S., et al., *Stachel-independent modulation of GPR56/ADGRG1 signaling by synthetic ligands directed to its extracellular region.* Proceedings of the National Academy of Sciences, 2017. **114**(38): p. 10095-10100.
59. Demberg, L.M., et al., *Activation of Adhesion G Protein-coupled Receptors: AGONIST SPECIFICITY OF STACHEL SEQUENCE-DERIVED PEPTIDES.* J Biol Chem, 2017. **292**(11): p. 4383-4394.
60. Demberg, L.M., et al., *Identification of the tethered peptide agonist of the adhesion G protein-coupled receptor GPR64/ADGRG2.* Biochem Biophys Res Commun, 2015. **464**(3): p. 743-7.
61. Stoveken, H.M., et al., *Gedunin- and Khivorin-Derivatives Are Small-Molecule Partial Agonists for Adhesion G Protein-Coupled Receptors GPR56/ADGRG1 and GPR114/ADGRG5.* Mol Pharmacol, 2018. **93**(5): p. 477-488.
62. Vu, T.K., et al., *Molecular cloning of a functional thrombin receptor reveals a novel proteolytic mechanism of receptor activation.* Cell, 1991. **64**(6): p. 1057-68.
63. Gerszten, R.E., et al., *Specificity of the thrombin receptor for agonist peptide is defined by its extracellular surface.* Nature, 1994. **368**(6472): p. 648-51.
64. Lerner, D.J., et al., *Agonist recognition by proteinase-activated receptor 2 and thrombin receptor. Importance of extracellular loop interactions for receptor function.* J Biol Chem, 1996. **271**(24): p. 13943-7.
65. Chiang, N.Y., et al., *Heparin interacts with the adhesion GPCR GPR56, reduces receptor shedding, and promotes cell adhesion and motility.* J Cell Sci, 2016. **129**(11): p. 2156-69.
66. Kaur, B., et al., *Vasculostatin, a proteolytic fragment of brain angiogenesis inhibitor 1, is an antiangiogenic and antitumorigenic factor.* Oncogene, 2005. **24**(22): p. 3632-42.
67. de Groot, D.M., et al., *Therapeutic antibody targeting of CD97 in experimental arthritis: the role of antigen expression, shedding, and internalization on the pharmacokinetics of anti-CD97 monoclonal antibody 1B2.* J Immunol, 2009. **183**(6): p. 4127-34.
68. Chiang, N.Y., et al., *Disease-associated GPR56 mutations cause bilateral frontoparietal polymicrogyria via multiple mechanisms.* J Biol Chem, 2011. **286**(16): p. 14215-25.
69. Luo, R., et al., *Mechanism for adhesion G protein-coupled receptor GPR56-mediated RhoA activation induced by collagen III stimulation.* PLoS One, 2014. **9**(6): p. e100043.
70. Scholz, N., et al., *Mechano-dependent signaling by Latrophilin/CIRL quenches cAMP in proprioceptive neurons.* eLife, 2017. **6**: p. e28360.
71. Scholz, N., et al., *Adhesion GPCRs as a Putative Class of Metabotropic Mechanosensors.* Handb Exp Pharmacol, 2016. **234**: p. 221-247.
72. Scholz, N., et al., *The adhesion GPCR latrophilin/CIRL shapes mechanosensation.* Cell Rep, 2015. **11**(6): p. 866-874.
73. Promel, S., et al., *The GPS motif is a molecular switch for bimodal activities of adhesion class G protein-coupled receptors.* Cell Rep, 2012. **2**(2): p. 321-31.
74. Zhu, B., et al., *GAIN domain-mediated cleavage is required for activation of G protein-coupled receptor 56 (GPR56) by its natural ligands and a small-molecule agonist.* J Biol Chem, 2019. **294**(50): p. 19246-19254.

75. Stephenson, J.R., et al., *Brain-specific Angiogenesis Inhibitor-1 Signaling, Regulation, and Enrichment in the Postsynaptic Density.* Journal of Biological Chemistry, 2013. **288**(31): p. 22248-22256.
76. Jin, Z., et al., *Disease-associated mutations affect GPR56 protein trafficking and cell surface expression.* Hum Mol Genet, 2007. **16**(16): p. 1972-85.
77. Kishore, A. and R.A. Hall, *Disease-associated extracellular loop mutations in the adhesion G protein-coupled receptor G1 (ADGRG1; GPR56) differentially regulate downstream signaling.* Journal of Biological Chemistry, 2017. **292**(23): p. 9711-9720.
78. Silva, J.P., et al., *Functional cross-interaction of the fragments produced by the cleavage of distinct adhesion G-protein-coupled receptors.* J Biol Chem, 2009. **284**(10): p. 6495-506.
79. Kim, H.-Y. and A.A. Spector, *N-Docosahexaenoylethanolamine: A neurotrophic and neuroprotective metabolite of docosahexaenoic acid.* Molecular Aspects of Medicine, 2018. **64**: p. 34-44.
80. Huang, B.X., et al., *Synaptamide activates the adhesion GPCR GPR110 (ADGRF1) through GAIN domain binding.* Commun Biol, 2020. **3**(1): p. 109.
81. Lee, J.W., et al., *Orphan GPR110 (ADGRF1) targeted by N-docosahexaenoylethanolamine in development of neurons and cognitive function.* Nat Commun, 2016. **7**: p. 13123.
82. Iguchi, T., et al., *Orphan G protein-coupled receptor GPR56 regulates neural progenitor cell migration via a G alpha 12/13 and Rho pathway.* J Biol Chem, 2008. **283**(21): p. 14469-78.
83. Salzman, Gabriel S., et al., *Structural Basis for Regulation of GPR56/ADGRG1 by Its Alternatively Spliced Extracellular Domains.* Neuron, 2016. **91**(6): p. 1292-1304.
84. Cho, C., P.M. Smallwood, and J. Nathans, *Reck and Gpr124 Are Essential Receptor Cofactors for Wnt7a/Wnt7b-Specific Signaling in Mammalian CNS Angiogenesis and Blood-Brain Barrier Regulation.* Neuron, 2017. **95**(5): p. 1221-1225.
85. Vallon, M., et al., *A RECK-WNT7 Receptor-Ligand Interaction Enables Isoform-Specific Regulation of Wnt Bioavailability.* Cell reports, 2018. **25**(2): p. 339-349.e9.
86. Hamoud, N., et al., *Spatiotemporal regulation of the GPCR activity of BAI3 by C1qL4 and Stabilin-2 controls myoblast fusion.* Nat Commun, 2018. **9**(1): p. 4470.
87. Devenport, D., et al., *Mitotic internalization of planar cell polarity proteins preserves tissue polarity.* Nat Cell Biol, 2011. **13**(8): p. 893-902.
88. Zuko, A., et al., *Association of Cell Adhesion Molecules Contactin-6 and Latrophilin-1 Regulates Neuronal Apoptosis.* Front Mol Neurosci, 2016. **9**: p. 143.
89. Boucard, A.A., S. Maxeiner, and T.C. Sudhof, *Latrophilins function as heterophilic cell-adhesion molecules by binding to teneurins: regulation by alternative splicing.* J Biol Chem, 2014. **289**(1): p. 387-402.
90. Sando, R., X. Jiang, and T.C. Sudhof, *Latrophilin GPCRs direct synapse specificity by coincident binding of FLRTs and teneurins.* Science, 2019. **363**(6429).
91. Wacker, D., R.C. Stevens, and B.L. Roth, *How Ligands Illuminate GPCR Molecular Pharmacology.* Cell, 2017. **170**(3): p. 414-427.
92. Moreno-Salinas, A.L., et al., *Latrophilins: A Neuro-Centric View of an Evolutionary Conserved Adhesion G Protein-Coupled Receptor Subfamily.* Front Neurosci, 2019. **13**: p. 700.

93. Park, D., et al., *BAI1 is an engulfment receptor for apoptotic cells upstream of the ELMO/Dock180/Rac module.* Nature, 2007. **450**(7168): p. 430-434.
94. Koh, J.T., et al., *Extracellular fragment of brain-specific angiogenesis inhibitor 1 suppresses endothelial cell proliferation by blocking alphavbeta5 integrin.* Exp Cell Res, 2004. **294**(1): p. 172-84.
95. Das, S., et al., *Brain angiogenesis inhibitor 1 (BAI1) is a pattern recognition receptor that mediates macrophage binding and engulfment of Gram-negative bacteria.* Proc Natl Acad Sci U S A, 2011. **108**(5): p. 2136-41.
96. Kaur, B., et al., *Vasculostatin inhibits intracranial glioma growth and negatively regulates in vivo angiogenesis through a CD36-dependent mechanism.* Cancer Res, 2009. **69**(3): p. 1212-20.
97. Zencir, S., et al., *Identification of brain-specific angiogenesis inhibitor 2 as an interaction partner of glutaminase interacting protein.* Biochemical and Biophysical Research Communications, 2011. **411**(4): p. 792-797.
98. Bolliger, M.F., D.C. Martinelli, and T.C. Sudhof, *The cell-adhesion G protein-coupled receptor BAI3 is a high-affinity receptor for C1q-like proteins.* Proceedings of the National Academy of Sciences, 2011. **108**(6): p. 2534-2539.
99. Sigoillot, S.M., et al., *The Secreted Protein C1QL1 and Its Receptor BAI3 Control the Synaptic Connectivity of Excitatory Inputs Converging on Cerebellar Purkinje Cells.* Cell Rep, 2015. **10**(5): p. 820-832.
100. Lindenmaier, L.B., et al., *Dystroglycan is a scaffold for extracellular axon guidance decisions.* eLife, 2019. **8**: p. e42143-e42143.
101. Warschkau, H. and A.F. Kiderlen, *A monoclonal antibody directed against the murine macrophage surface molecule F4/80 modulates natural immune response to Listeria monocytogenes.* Journal of immunology (Baltimore, Md. : 1950), 1999. **163**(6): p. 3409-16.
102. Stacey, M., et al., *The epidermal growth factor-like domains of the human EMR2 receptor mediate cell attachment through chondroitin sulfate glycosaminoglycans.* Blood, 2003. **102**(8): p. 2916-2924.
103. Stacey, M., et al., *Human Epidermal Growth Factor (EGF) Module-containing Mucin-like Hormone Receptor 3 Is a New Member of the EGF-TM7 Family That Recognizes a Ligand on Human Macrophages and Activated Neutrophils.* Journal of Biological Chemistry, 2001. **276**(22): p. 18863-18870.
104. Stacey, M., et al., *EMR4, a Novel Epidermal Growth Factor (EGF)-TM7 Molecule Up-regulated in Activated Mouse Macrophages, Binds to a Putative Cellular Ligand on B Lymphoma Cell Line A20.* Journal of Biological Chemistry, 2002. **277**(32): p. 29283-29293.
105. Wang, T., et al., *CD97, an adhesion receptor on inflammatory cells, stimulates angiogenesis through binding integrin counterreceptors on endothelial cells.* Blood, 2005. **105**(7): p. 2836-2844.
106. Wandel, E., et al., *Thy-1 (CD90) Is an Interacting Partner for CD97 on Activated Endothelial Cells.* The Journal of Immunology, 2012. **188**(3): p. 1442-1450.
107. Hamann, J., et al., *The seven-span transmembrane receptor CD97 has a cellular ligand (CD55, DAF).* J Exp Med, 1996. **184**(3): p. 1185-9.

108. Schneberger, D., et al., *Organic barn dust inhibits surfactant protein D production through protein kinase-c alpha dependent increase of GPR116.* PLOS ONE, 2018. **13**(12): p. e0208597-e0208597.
109. Fukuzawa, T., et al., *Lung Surfactant Levels are Regulated by Ig-Hepta/GPR116 by Monitoring Surfactant Protein D.* PLoS ONE, 2013. **8**(7): p. e69451-e69451.
110. Giera, S., et al., *Microglial transglutaminase-2 drives myelination and myelin repair via GPR56/ADGRG1 in oligodendrocyte precursor cells.* eLife, 2018. **7**: p. e33385.
111. Xu, L., et al., *GPR56, an atypical G protein-coupled receptor, binds tissue transglutaminase, TG2, and inhibits melanoma tumor growth and metastasis.* Proceedings of the National Academy of Sciences, 2006. **103**(24): p. 9023-9028.
112. Jin, G., et al., *The G-protein coupled receptor 56, expressed in colonic stem and cancer cells, binds progastrin to promote proliferation and carcinogenesis.* Oncotarget, 2017. **8**(25): p. 40606-40619.
113. Ackerman, S.D., et al., *GPR56/ADGRG1 regulates development and maintenance of peripheral myelin.* J Exp Med, 2018. **215**(3): p. 941-961.
114. Stoveken, H.M., et al., *Dihydromunduletone Is a Small-Molecule Selective Adhesion G Protein-Coupled Receptor Antagonist.* Mol Pharmacol, 2016. **90**(3): p. 214-24.
115. Luo, R., et al., *G protein-coupled receptor 56 and collagen III, a receptor-ligand pair, regulates cortical development and lamination.* Proceedings of the National Academy of Sciences, 2011. **108**(31): p. 12925.
116. Huang, K.Y. and H.H. Lin, *The Activation and Signaling Mechanisms of GPR56/ADGRG1 in Melanoma Cell.* Front Oncol, 2018. **8**: p. 304.
117. Petersen, Sarah C., et al., *The Adhesion GPCR GPR126 Has Distinct, Domain-Dependent Functions in Schwann Cell Development Mediated by Interaction with Laminin-211.* Neuron, 2015. **85**(4): p. 755-769.
118. Kuffer, A., et al., *The prion protein is an agonistic ligand of the G protein-coupled receptor Adgrg6.* Nature, 2016. **536**(7617): p. 464-8.
119. Krasnoperov, V.G., et al., *alpha-Latrotoxin stimulates exocytosis by the interaction with a neuronal G-protein-coupled receptor.* Neuron, 1997. **18**(6): p. 925-37.
120. Silva, J.P., et al., *Latrophilin 1 and its endogenous ligand Lasso/teneurin-2 form a high-affinity transsynaptic receptor pair with signaling capabilities.* Proc Natl Acad Sci U S A, 2011. **108**(29): p. 12113-8.
121. Boucard, A.A., J. Ko, and T.C. Sudhof, *High affinity neurexin binding to cell adhesion G-protein-coupled receptor CIRL1/latrophilin-1 produces an intercellular adhesion complex.* J Biol Chem, 2012. **287**(12): p. 9399-413.
122. Jackson, V.A., et al., *Structures of Teneurin adhesion receptors reveal an ancient fold for cell-cell interaction.* Nat Commun, 2018. **9**(1): p. 1079.
123. Jackson, V.A., et al., *Super-complexes of adhesion GPCRs and neural guidance receptors.* Nat Commun, 2016. **7**: p. 11184.
124. Arcos-Burgos, M., et al., *A common variant of the latrophilin 3 gene, LPHN3, confers susceptibility to ADHD and predicts effectiveness of stimulant medication.* Mol Psychiatry, 2010. **15**(11): p. 1053-66.
125. Ribases, M., et al., *Contribution of LPHN3 to the genetic susceptibility to ADHD in adulthood: a replication study.* Genes Brain Behav, 2011. **10**(2): p. 149-57.
126. Domene, S., et al., *Screening of human LPHN3 for variants with a potential impact on ADHD susceptibility.* Am J Med Genet B Neuropsychiatr Genet, 2011. **156B**(1): p. 11-8.

127. Chen, C.H., et al., *High resolution analysis of rare copy number variants in patients with autism spectrum disorder from Taiwan.* Sci Rep, 2017. **7**(1): p. 11919.
128. Legge, S.E., et al., *Genome-wide common and rare variant analysis provides novel insights into clozapine-associated neutropenia.* Mol Psychiatry, 2017. **22**(10): p. 1502-1508.
129. Vezain, M., et al., *A de novo variant in ADGRL2 suggests a novel mechanism underlying the previously undescribed association of extreme microcephaly with severely reduced sulcation and rhombencephalosynapsis.* Acta Neuropathol Commun, 2018. **6**(1): p. 109.
130. Li, J., et al., *Alternative splicing controls teneurin-latrophilin interaction and synapse specificity by a shape-shifting mechanism.* Nat Commun, 2020. **11**(1): p. 2140.
131. Del Toro, D., et al., *Structural Basis of Teneurin-Latrophilin Interaction in Repulsive Guidance of Migrating Neurons.* Cell, 2020. **180**(2): p. 323-339 e19.
132. Moers, A., et al., *Galpha12/Galpha13 deficiency causes localized overmigration of neurons in the developing cerebral and cerebellar cortices.* Mol Cell Biol, 2008. **28**(5): p. 1480-8.
133. Kranenburg, O., et al., *Activation of RhoA by lysophosphatidic acid and Galpha12/13 subunits in neuronal cells: induction of neurite retraction.* Mol Biol Cell, 1999. **10**(6): p. 1851-7.
134. Katoh, H., et al., *Constitutively active Galpha12, Galpha13, and Galphaq induce Rho-dependent neurite retraction through different signaling pathways.* J Biol Chem, 1998. **273**(44): p. 28700-7.
135. Barrett, K., M. Leptin, and J. Settleman, *The Rho GTPase and a putative RhoGEF mediate a signaling pathway for the cell shape changes in Drosophila gastrulation.* Cell, 1997. **91**(7): p. 905-15.
136. Suzuki, N., N. Hajicek, and T. Kozasa, *Regulation and physiological functions of G12/13-mediated signaling pathways.* Neurosignals, 2009. **17**(1): p. 55-70.
137. Cruz-Ortega, J.S. and A.A. Boucard, *Actin cytoskeleton remodeling defines a distinct cellular function for adhesion G protein-coupled receptors ADGRL/latrophilins 1, 2 and 3.* Biol Open, 2019. **8**(4).
138. Muller, A., et al., *Oriented Cell Division in the C. elegans Embryo Is Coordinated by G-Protein Signaling Dependent on the Adhesion GPCR LAT-1.* PLoS Genet, 2015. **11**(10): p. e1005624.
139. Tojima, T., et al., *Second messengers and membrane trafficking direct and organize growth cone steering.* Nat Rev Neurosci, 2011. **12**(4): p. 191-203.
140. Rothe, J., et al., *Involvement of the Adhesion GPCRs Latrophilins in the Regulation of Insulin Release.* Cell Rep, 2019. **26**(6): p. 1573-1584 e5.
141. Perry-Hauser, N.A., et al., *Disentangling autoproteolytic cleavage from tethered agonist-dependent activation of the adhesion receptor ADGRL3.* J Biol Chem, 2022. **298**(12): p. 102594.
142. Vysokov, N.V., et al., *Proteolytically released Lasso/teneurin-2 induces axonal attraction by interacting with latrophilin-1 on axonal growth cones.* Elife, 2018. **7**.
143. Stephenson, J.R., R.H. Purcell, and R.A. Hall, *The BAI subfamily of adhesion GPCRs: synaptic regulation and beyond.* Trends Pharmacol Sci, 2014. **35**(4): p. 208-15.
144. Koh, J.T., et al., *Characterization of mouse brain-specific angiogenesis inhibitor 1 (BAI1) and phytanoyl-CoA alpha-hydroxylase-associated protein 1, a novel BAI1-binding protein.* Brain Res Mol Brain Res, 2001. **87**(2): p. 223-37.

145. Sokolowski, J.D., et al., *Brain-specific angiogenesis inhibitor-1 expression in astrocytes and neurons: implications for its dual function as an apoptotic engulfment receptor.* Brain Behav Immun, 2011. **25**(5): p. 915-21.
146. Mori, K., et al., *Brain-specific angiogenesis inhibitor 1 (BAI1) is expressed in human cerebral neuronal cells.* Neurosci Res, 2002. **43**(1): p. 69-74.
147. Liu, B.P., et al., *Myelin-associated glycoprotein as a functional ligand for the Nogo-66 receptor.* Science, 2002. **297**(5584): p. 1190-3.
148. Ressl, S., et al., *Structures of C1q-like proteins reveal unique features among the C1q/TNF superfamily.* Structure, 2015. **23**(4): p. 688-99.
149. White, J.P., et al., *G protein-coupled receptor 56 regulates mechanical overload-induced muscle hypertrophy.* Proceedings of the National Academy of Sciences, 2014. **111**(44): p. 15756.
150. Giera, S., et al., *The adhesion G protein-coupled receptor GPR56 is a cell-autonomous regulator of oligodendrocyte development.* Nature Communications, 2015. **6**: p. 6121.
151. Mogha, A., et al., *Gpr126 functions in Schwann cells to control differentiation and myelination via G-protein activation.* J Neurosci, 2013. **33**(46): p. 17976-85.
152. Hawgood, S. and J.A. Clements, *Pulmonary surfactant and its apoproteins.* J Clin Invest, 1990. **86**(1): p. 1-6.
153. Fisher, J.H., et al., *Pulmonary-specific expression of SP-D corrects pulmonary lipid accumulation in SP-D gene-targeted mice.* Am J Physiol Lung Cell Mol Physiol, 2000. **278**(2): p. L365-73.
154. Liu, Z., et al., *Clinical Significance of G Protein-Coupled Receptor 110 (GPR110) as a Novel Prognostic Biomarker in Osteosarcoma.* Med Sci Monit, 2018. **24**: p. 5216-5224.
155. Shi, H. and S. Zhang, *Expression and prognostic role of orphan receptor GPR110 in glioma.* Biochem Biophys Res Commun, 2017. **491**(2): p. 349-354.
156. Gupte, J., et al., *Signaling property study of adhesion G-protein-coupled receptors.* FEBS Lett, 2012. **586**(8): p. 1214-9.
157. Bradley, E.C., et al., *In vivo identification of small molecules mediating Gpr126/Adgrg6 signaling during Schwann cell development.* Ann N Y Acad Sci, 2019. **1456**(1): p. 44-63.
158. Lipinski, C.A., et al., *Experimental and computational approaches to estimate solubility and permeability in drug discovery and development settings.* Adv Drug Deliv Rev, 2001. **46**(1-3): p. 3-26.
159. Kozasa, T., *Purification of G protein subunits from Sf9 insect cells using hexahistidine-tagged alpha and beta gamma subunits.* Methods Mol Biol, 2004. **237**: p. 21-38.
160. Kozasa, T. and A.G. Gilman, *Purification of recombinant G proteins from Sf9 cells by hexahistidine tagging of associated subunits. Characterization of alpha 12 and inhibition of adenylyl cyclase by alpha z.* J Biol Chem, 1995. **270**(4): p. 1734-41.
161. Kozasa, T., *Purification of Recombinant G Protein α and βγ Subunits from Sf9 Cells*, in *G Proteins: Techniques of Analysis*, D. Manning, Editor. 1999, CRC Press. p. 23-38.
162. Kozasa, T., *Expression and Purification of G-Protein α Subunits in Escherichia coli*, in *G Proteins: Techniques of Analysis*, D. Manning, Editor. 1999, CRC Press. p. 1-21.
163. Barros-Alvarez, X., et al., *The tethered peptide activation mechanism of adhesion GPCRs.* Nature, 2022. **604**(7907): p. 757-762.
164. Zhang, J.H., T.D. Chung, and K.R. Oldenburg, *A Simple Statistical Parameter for Use in Evaluation and Validation of High Throughput Screening Assays.* J Biomol Screen, 1999. **4**(2): p. 67-73.

165. Leemans, J.C., et al., *The epidermal growth factor-seven transmembrane (EGF-TM7) receptor CD97 is required for neutrophil migration and host defense.* J Immunol, 2004. **172**(2): p. 1125-31.
166. Wansleeben, C. and F. Meijlink, *The planar cell polarity pathway in vertebrate development.* Dev Dyn, 2011. **240**(3): p. 616-26.
167. Li, X., et al., *Gpr125 modulates Dishevelled distribution and planar cell polarity signaling.* Development, 2013. **140**(14): p. 3028-3039.
168. Gray, J.X., et al., *CD97 is a processed, seven-transmembrane, heterodimeric receptor associated with inflammation.* J Immunol, 1996. **157**(12): p. 5438-47.
169. Chen, G., et al., *GPR56 is essential for testis development and male fertility in mice.* Dev Dyn, 2010. **239**(12): p. 3358-67.
170. Yeung, J., et al., *GPR56/ADGRG1 is a platelet collagen-responsive GPCR and hemostatic sensor of shear force.* Proc Natl Acad Sci U S A, 2020. **117**(45): p. 28275-28286.
171. Chang, G.-W., et al., *The Adhesion G Protein-Coupled Receptor GPR56/ADGRG1 Is an Inhibitory Receptor on Human NK Cells.* Cell Reports, 2016. **15**(8): p. 1757-1770.
172. Ackerman, S.D., et al., *The adhesion GPCR Gpr56 regulates oligodendrocyte development via interactions with Gα12/13 and RhoA.* Nature Communications, 2015. **6**: p. 6122.
173. Wu, M.P., et al., *G-protein coupled receptor 56 promotes myoblast fusion through serum response factor- and nuclear factor of activated T-cell-mediated signalling but is not essential for muscle development in vivo.* FEBS J, 2013. **280**(23): p. 6097-113.
174. Salzman, G.S., et al., *Specific and direct modulation of the interaction between adhesion GPCR GPR56/ADGRG1 and tissue transglutaminase 2 using synthetic ligands.* Sci Rep, 2020. **10**(1): p. 16912.
175. Yang, L., et al., *GPR56 inhibits melanoma growth by internalizing and degrading its ligand TG2.* Cancer Res, 2014. **74**(4): p. 1022-31.
176. Shashidhar, S., et al., *GPR56 is a GPCR that is overexpressed in gliomas and functions in tumor cell adhesion.* Oncogene, 2005. **24**(10): p. 1673-82.
177. Chiang, N.Y., et al., *GPR56/ADGRG1 Activation Promotes Melanoma Cell Migration via NTF Dissociation and CTF-Mediated Galpha12/13/RhoA Signaling.* J Invest Dermatol, 2017. **137**(3): p. 727-736.
178. Yang, L., et al., *GPR56 Regulates VEGF production and angiogenesis during melanoma progression.* Cancer Res, 2011. **71**(16): p. 5558-68.
179. Ji, B., et al., *GPR56 promotes proliferation of colorectal cancer cells and enhances metastasis via epithelial-mesenchymal transition through PI3K/AKT signaling activation.* Oncol Rep, 2018. **40**(4): p. 1885-1896.
180. Zhang, S., et al., *GPR56 Drives Colorectal Tumor Growth and Promotes Drug Resistance through Upregulation of MDR1 Expression via a RhoA-Mediated Mechanism.* Mol Cancer Res, 2019. **17**(11): p. 2196-2207.
181. Ke, N., et al., *Orphan G protein-coupled receptor GPR56 plays a role in cell transformation and tumorigenesis involving the cell adhesion pathway.* Mol Cancer Ther, 2007. **6**(6): p. 1840-50.
182. Piao, X., et al., *G protein-coupled receptor-dependent development of human frontal cortex.* Science, 2004. **303**(5666): p. 2033-6.

183. Regan, S.L., M.T. Williams, and C.V. Vorhees, *Latrophilin-3 disruption: Effects on brain and behavior.* Neurosci Biobehav Rev, 2021. **127**: p. 619-629.
184. Wallis, D., et al., *Initial characterization of mice null for Lphn3, a gene implicated in ADHD and addiction.* Brain Res, 2012. **1463**: p. 85-92.
185. Ping, Y.Q., et al., *Structures of the glucocorticoid-bound adhesion receptor GPR97-Go complex.* Nature, 2021. **589**(7843): p. 620-626.
186. Nehme, R., et al., *Mini-G proteins: Novel tools for studying GPCRs in their active conformation.* PLoS One, 2017. **12**(4): p. e0175642.
187. Wootten, D., et al., *Polar transmembrane interactions drive formation of ligand-specific and signal pathway-biased family B G protein-coupled receptor conformations.* Proc Natl Acad Sci U S A, 2013. **110**(13): p. 5211-6.
188. Ballesteros, J.A. and H. Weinstein, *[19] Integrated methods for the construction of three-dimensional models and computational probing of structure-function relations in G protein-coupled receptors*, in *Methods in neurosciences*. 1995, Elsevier. p. 366-428.
189. Weis, W.I. and B.K. Kobilka, *The Molecular Basis of G Protein-Coupled Receptor Activation.* Annu Rev Biochem, 2018. **87**: p. 897-919.
190. Zhang, Y., et al., *Cryo-EM structure of the activated GLP-1 receptor in complex with a G protein.* Nature, 2017. **546**(7657): p. 248-253.
191. Hilger, D., et al., *Structural insights into differences in G protein activation by family A and family B GPCRs.* Science, 2020. **369**(6503).
192. Liang, Y.L., et al., *Phase-plate cryo-EM structure of a class B GPCR-G-protein complex.* Nature, 2017. **546**(7656): p. 118-123.
193. Lin, H.H., et al., *The macrophage F4/80 receptor is required for the induction of antigen-specific efferent regulatory T cells in peripheral tolerance.* J Exp Med, 2005. **201**(10): p. 1615-25.
194. Wang, J.J., et al., *Gpr97 is essential for the follicular versus marginal zone B-lymphocyte fate decision.* Cell Death Dis, 2013. **4**(10): p. e853.
195. Arac, D., et al., *A novel evolutionarily conserved domain of cell-adhesion GPCRs mediates autoproteolysis.* EMBO J, 2012. **31**(6): p. 1364-78.
196. Liebscher, I., et al., *A tethered agonist within the ectodomain activates the adhesion G protein-coupled receptors GPR126 and GPR133.* Cell Rep, 2014. **9**(6): p. 2018-26.
197. Qu, X., et al., *Structural basis of tethered agonism of the adhesion GPCRs ADGRD1 and ADGRF1.* Nature, 2022. **604**(7907): p. 779-785.
198. Ping, Y.Q., et al., *Structural basis for the tethered peptide activation of adhesion GPCRs.* Nature, 2022. **604**(7907): p. 763-770.
199. Xiao, P., et al., *Tethered peptide activation mechanism of the adhesion GPCRs ADGRG2 and ADGRG4.* Nature, 2022. **604**(7907): p. 771-778.
200. Mehta, P. and X. Piao, *Adhesion G-protein coupled receptors and extracellular matrix proteins: Roles in myelination and glial cell development.* Dev Dyn, 2017. **246**(4): p. 275-284.
201. Brown, K., et al., *Epithelial Gpr116 regulates pulmonary alveolar homeostasis via Gq/11 signaling.* JCI Insight, 2017. **2**(11).
202. Zhao, C., et al., *Pharmaceutical and medicinal significance of sulfur (S(VI))-Containing motifs for drug discovery: A critical review.* Eur J Med Chem, 2019. **162**: p. 679-734.
203. Bladen, C., et al., *Synthesis and evaluation of 1,4-dihydropyridine derivatives with calcium channel blocking activity.* Pflugers Arch, 2014. **466**(7): p. 1355-63.

204. Liu, X., et al., *Molecular simulations study of novel 1,4-dihydropyridines derivatives with a high selectivity for Cav3.1 calcium channel.* Protein Sci, 2015. **24**(11): p. 1737-47.
205. Epstein, B.J., K. Vogel, and B.F. Palmer, *Dihydropyridine calcium channel antagonists in the management of hypertension.* Drugs, 2007. **67**(9): p. 1309-27.
206. Murakami, M., et al., *Antihypertensive effect of (4-2'-nitrophenyl)-2,6-dimethyl-1,4-dihydropyridine-3,5-dicarbonic acid dimethylester (Nifedipine, Bay-a 1040), a new coronary dilator.* Jpn Heart J, 1972. **13**(2): p. 128-35.
207. Takahashi, D., et al., *Structure-activity relationships of receptor binding of 1,4-dihydropyridine derivatives.* Biol Pharm Bull, 2008. **31**(3): p. 473-9.
208. Beliu, G., et al., *Tethered agonist exposure in intact adhesion/class B2 GPCRs through intrinsic structural flexibility of the GAIN domain.* Mol Cell, 2021. **81**(5): p. 905-921 e5.
209. James, S.H., *Hematology pharmacology: anticoagulant, antiplatelet, and procoagulant agents in practice.* AACN Adv Crit Care, 2009. **20**(2): p. 177-92.